Measurement of the t[bar over t] production cross-section as a function of jet multiplicity and jet transverse momentum in 7 TeV proton-proton collisions with the ATLAS detector

Published for SISSA by Springer

Received: *July 4, 2014*
Revised: *November 16, 2014*
Accepted: *December 12, 2014*
Published: *January 8, 2015*

Measurement of the $t\bar{t}$ production cross-section as a function of jet multiplicity and jet transverse momentum in 7 TeV proton-proton collisions with the ATLAS detector

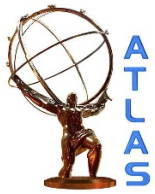

The ATLAS collaboration

E-mail: atlas.publications@cern.ch

Abstract: The $t\bar{t}$ production cross-section dependence on jet multiplicity and jet transverse momentum is reported for proton-proton collisions at a centre-of-mass energy of 7 TeV in the single-lepton channel. The data were collected with the ATLAS detector at the CERN Large Hadron Collider and comprise the full 2011 data sample corresponding to an integrated luminosity of 4.6 fb^{-1}. Differential cross-sections are presented as a function of the jet multiplicity for up to eight jets using jet transverse momentum thresholds of 25, 40, 60, and 80 GeV, and as a function of jet transverse momentum up to the fifth jet. The results are shown after background subtraction and corrections for all known detector effects, within a kinematic range closely matched to the experimental acceptance. Several QCD-based Monte Carlo models are compared with the results. Sensitivity to the parton shower modelling is found at the higher jet multiplicities, at high transverse momentum of the leading jet and in the transverse momentum spectrum of the fifth leading jet. The MC@NLO+HERWIG MC is found to predict too few events at higher jet multiplicities.

Keywords: Hadron-Hadron Scattering

ArXiv ePrint: 1407.0891

doi:10.1007/JHEP01(2015)020

Contents

JHEP01(2015)020

1 Introduction

Final states of proton-proton (pp) collisions at the Large Hadron Collider (LHC) [1] often include jets arising from QCD bremsstrahlung due to the strongly interacting partons in the initial state and the high centre-of-mass energy of the scattering process that allows for radiation in a large kinematic phase space. In this paper, an inclusive measurement of jets in top-antitop ($t\bar{t}$) final states is presented, which is sensitive to the production mechanism

of additional jets in these events. The events studied have a high partonic-system centre-of-mass energy and are complex final states consisting of several coloured partons, with sensitivity to various hard scales.

The production of additional jets in $t\bar{t}$ events is sensitive to higher-order perturbative QCD effects. The uncertainties associated with these processes are a significant source of uncertainty in precision measurements, such as the measurement of the top-quark mass [2] or the inclusive $t\bar{t}$ production cross-section at the LHC [18]. Several theoretical approaches are available to model $t\bar{t}$ processes, including NLO QCD calculations, parton-shower models and methods matching fixed-order QCD with the parton shower. The aim of this paper is to test these theoretical approaches by making a direct measurement of jet activity in $t\bar{t}$ events. Furthermore, $t\bar{t}$ production with additional jets is a dominant background in certain Higgs boson production processes and decay modes and to many searches for new physics phenomena [3, 4].

Tests similar to those presented in this paper have been performed at lower energies, using measurements of jets associated with colour-singlet vector-boson production at the LHC [5, 6] and at the Tevatron [7–10]. The CMS collaboration recently measured the cross-section of additional jets normalised to the inclusive $t\bar{t}$ production cross-section [11]. The present measurement is complementary to the measurement of $t\bar{t}$ production with a veto on additional jet activity [12], which is mostly sensitive to the first perturbative QCD emission.

In the Standard Model (SM), a top-quark[1] decays almost exclusively to a W boson and a b quark. The W boson decays into a pair of leptons ($e\overline{\nu}_e$, $\mu\overline{\nu}_\mu$, $\tau\overline{\nu}_\tau$) or into a pair of quark-jets. τ leptons produced by W boson decays can also decay into leptons ($e\overline{\nu}_e\nu_\tau$, $\mu\overline{\nu}_\mu\nu_\tau$). Selected events are classified by the decay of one or both of the W bosons into leptons, as either single-lepton or dilepton channel, respectively.

In this paper, the $t\bar{t}$ production cross-section is measured differentially in jet multiplicity and in jet transverse momentum (p_{T}) in the single-lepton channel, without explicit separation between jets related to $t\bar{t}$ decays and additional jets. The jet multiplicity is measured for several different jet p_{T} thresholds in order to probe the p_{T} dependence of the hard emission. The jet multiplicity, especially for values greater than four, is closely related to the number of hard emissions in QCD bremsstrahlung processes.

In addition, the differential cross-section with respect to the jet p_{T} is presented separately for the five highest p_{T} jets. These differential cross-sections are particularly sensitive to the modelling of higher-order QCD effects in Monte Carlo (MC) generators [13, 14]. Therefore, a precise measurement can be used to discriminate between different models and to determine their free parameters. Furthermore, a precise measurement of the leading jet p_{T} could be used to determine the p_{T} of the $t\bar{t}$ system above approximately[2] 130 GeV, since for large transverse momenta the leading jet p_{T} is correlated with the p_{T} of the $t\bar{t}$ system as illustrated in figure 1. Therefore, measurements of the leading jet p_{T} provide complementary information with respect to existing differential production cross-section measurements of the top-quark [15, 16].

[1] Charge conjugate states are equally considered unless noted otherwise.

[2] Units in the paper are reported with $c = 1$.

JHEP01(2015)020

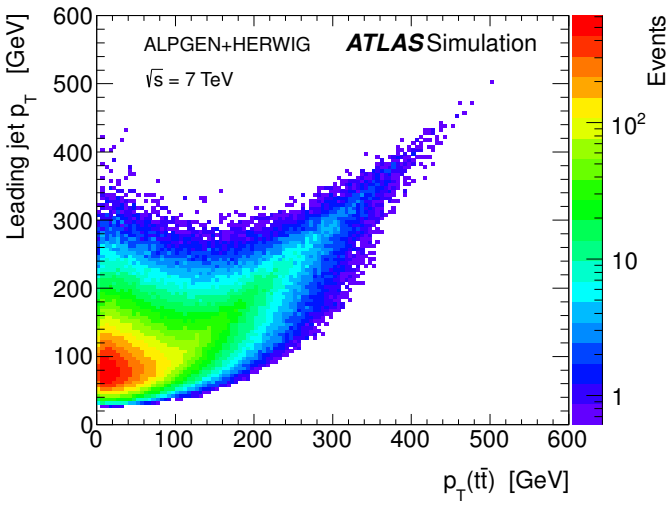

Figure 1. The relationship between the p_{T} of the $t\bar{t}$ system in the single-lepton channel and the p_{T} of the highest p_{T} jet in $t\bar{t}$ events generated with ALPGEN+HERWIG. The p_{T} of the $t\bar{t}$ system is taken at parton level and the leading jet is constructed at particle level.

The present analysis uses pp data collected during 2011 corresponding to an integrated luminosity of 4.59 ± 0.08 fb^{-1} [17]. The measurements are corrected for all known detector effects and are presented in the form of differential cross-sections, defined within the detector acceptance ("fiducial" cross-sections) in order to avoid model-dependent extrapolations and to facilitate comparisons with theoretical predictions. The fiducial volume definition follows previous kinematic definitions of cross-section measurements involving top quarks [18]. In addition, the objects used to define the fiducial volume at particle level were reconstructed such that they closely match the reconstructed objects in data.

2 The ATLAS detector

The ATLAS detector [19] covers nearly the entire solid angle around the LHC-beam collision point. Due to the complexity of the final state in the selected events, the present analysis relies on all main ATLAS detector subsystems.

The ATLAS reference system is a Cartesian right-handed coordinate system, where the nominal collision point is at the origin. The anti-clockwise beam direction defines the positive z-axis, while the positive x-axis is defined as pointing from the collision point to the centre of the LHC ring and the positive y-axis points upwards. The azimuthal angle ϕ is measured around the beam axis, and the polar angle θ is measured with respect to the z-axis. The pseudorapidity is defined as $\eta = -\ln\tan(\theta/2)$.

The ATLAS detector consists of an inner tracking detector (ID), comprising a silicon pixel detector, a silicon microstrip detector (SCT), and a transition radiation tracker (TRT). The ID is surrounded by a superconducting solenoid that provides a 2 T magnetic field. The ID is used for reconstruction of tracks and primary vertices and plays a crucial role in b-quark jet identification. It is surrounded by high-granularity liquid-argon (LAr) electromagnetic (EM) sampling calorimeters with lead absorbers. An iron absorber and

JHEP01(2015)020

scintillating tile calorimeter provides hadronic energy measurements in the central pseudorapidity range of $|\eta| < 1.7$. The end-cap and forward regions are instrumented with LAr calorimeters for both electromagnetic and hadronic energy measurements up to $|\eta| = 4.9$. The calorimeter system is surrounded by a muon spectrometer (MS) that incorporates a system of air-core superconducting toroid magnets arranged with an eight-fold azimuthal coil symmetry around the calorimeters, and a system of three stations of chambers for triggering and for precise track measurements.

The online event selection relies on a three-level trigger system. A hardware-based first-level trigger is used to initially reduce the event rate by $\mathcal{O}(300)$. The detector readout is available for two stages of software-based (higher-level) triggers. In the second level, partial object reconstruction is carried out to improve the selection and reduce the rate of soft pp interactions recorded. At the last level, the event filter, the full online event reconstruction is used, which reduced the rate to approximately 300 Hz during the 2011 run period.

3 Data sample and event selection

Data were selected from the full 2011 data-taking period using the pp LHC running periods during which all ATLAS sub-detectors were fully operational, corresponding to an integrated luminosity of 4.59 ± 0.08 fb^{-1}.

During this data-taking period, the peak luminosity delivered by the LHC was high enough to produce multiple pp collisions from one pp bunch crossing. The LHC bunch structure and high luminosity also produced pp collisions in immediately adjacent pp bunch crossings. The average number of pp collisions, over all bunch crossings and all data analysed, was measured and is referred to as $\langle\mu\rangle$. At the beginning of the data-taking period $\langle\mu\rangle$ was around five, whereas by the end of period it was approximately eighteen. The effects of particles created in additional collisions are mitigated by the object and event selections used in this analysis.

3.1 Object reconstruction

Primary vertices were reconstructed from tracks within the ID. The selected primary vertex was required to have at least five tracks and to be consistent with the beam-collision region in the x-y plane. If more than one primary vertex candidate was found, then the vertex with the highest $\sum p_{\mathrm{T}}^2$ of associated tracks was chosen to be associated with the hard scattering process.

Electron candidates were identified [20] as energy deposits (clusters) in the electromagnetic calorimeters, with a matching reconstructed track in the ID. These electrons were selected within the pseudorapidity range $|\eta| < 2.47$, excluding the barrel/end-cap transition region of $1.37 < |\eta| < 1.52$. The energy cluster in the calorimeter was required to be isolated. The isolation requirement was formed by calculating the total transverse energy within a cone of size $\Delta R = 0.2$ around the electron direction, where $\Delta R = \sqrt{(\Delta\phi)^2 + (\Delta\eta)^2}$ and $\Delta\phi$ and $\Delta\eta$ are the difference of azimuthal angle and pseudorapidity, respectively. This

JHEP01(2015)020

calculation was performed after the exclusion of calorimeter cells associated with the electron cluster. The electron was considered isolated if this energy sum was below 10% of the electron energy. Similarly, the summed p_{T} of additional tracks within a cone of size $\Delta R = 0.3$ around the electron direction was required to be below 10% of the electron candidate track p_{T}. The electron was required to have a longitudinal impact parameter with respect to the selected primary vertex of less than 2 mm. The reconstructed p_{T} of electrons used in the event selection was required to be greater than 25 GeV, but electrons with $p_{\mathrm{T}} > 15$ GeV were considered when removing jets that overlap with electrons and when applying a veto on events with additional leptons.

Muon candidates were required to have a reconstructed track in the MS matched with a track reconstructed in the ID, a reconstructed $p_{\mathrm{T}} > 25$ GeV and $|\eta| < 2.5$ [21]. The selected muons were required to be isolated in the calorimeter and tracking volume. The calorimeter isolation was constructed from the sum of transverse energy components within a cone of $\Delta R = 0.2$ around the direction of the muon and was required to be less than 4 GeV. The isolation within the ID was formed using a p_{T} sum of additional tracks within a cone of $\Delta R = 0.3$ around the direction of the muon and was required to be less than 2.5 GeV. To reduce the effects of additional primary vertices, the muon was required to have a longitudinal impact parameter with respect to the selected primary vertex of less than 2 mm. In the same manner as the electron selection, muons with p_{T} as low as 15 GeV were used to veto events with additional leptons.

Topological clusters [22] were formed from calorimeter energy deposits. These clusters were used as input to the anti-k_t [23] jet algorithm, which was run with a radius parameter of 0.4. The jets were calibrated using the EM+JES scheme described in [24, 25] to correct the jet energy, which was calibrated for electromagnetic particles to the response for hadrons, based on the jet energy and η. In a first step, the calibration procedure corrected the jet energy relative to jets built from stable particles in MC simulations (see section 7.1 for details). In a second step, differences between data and MC simulation were evaluated using in situ techniques exploiting the p_{T} balance between high-p_{T} jets and well measured physics objects. The calibrated jets are required to have $p_{\mathrm{T}} > 25$ GeV and $|\eta| < 2.5$. To suppress jets from additional pp interactions, the sum of the p_{T} of the tracks originating from the selected primary vertex and associated with the jet was required to be at least 75% of the p_{T} sum of all tracks associated with the jet. This quantity is referred to as the jet vertex fraction (JVF). Jets with no associated tracks were also accepted.

The identification of the electron, muon and jet objects was performed independently of other object identifications, using clusters and tracks. In particular, no distinction was made between clusters arising from electron energy deposits or from hadrons within a jet. In order to optimise the object identification for the event selection of this analysis and to avoid double counting of energy deposits, the overlap between these identified objects was resolved as described below.

In order to remove jets that were reconstructed from energy deposits associated with prompt electrons, jets were removed from an event if they were within $\Delta R = 0.2$ of an electron with $p_{\mathrm{T}} > 15$ GeV. To remove residual muons from heavy-flavour decays, muons that were within $\Delta R = 0.4$ of any jet were removed. To apply a similar constraint on the

JHEP01(2015)020

electrons, electrons that were within $\Delta R = 0.4$ of any jet were removed from the events. For this condition, the only jets considered were those remaining after the removal of jets associated with electrons as previously described.

The missing transverse momentum azimuthal angle and magnitude ($E_{\mathrm{T}}^{\mathrm{miss}}$) were reconstructed from the vector sum of the transverse momenta of the reconstructed objects (electrons, muons, jets) as well as the transverse-energy deposited in calorimeter cells not associated with these objects, within the range $|\eta| < 4.9$. The object classification scheme for the electrons, muons and jets used to calculate $E_{\mathrm{T}}^{\mathrm{miss}}$ was chosen to be the same as the definitions given above. Calorimeter cells not associated with an object were calibrated at the electromagnetic (EM) scale before being added to $E_{\mathrm{T}}^{\mathrm{miss}}$. This calibration scheme is similar to the one described in [26].

Jets were identified as "b-jets" by detecting b-hadron decays within the jet. These b-jets were identified using the MV1 algorithm [27], which combines several tagging algorithms into a single neural-network-based discriminant, taking into account jet p_{T} and η distributions. The selection efficiency is approximately 70% for $p_{\mathrm{T}} > 20$ GeV in simulated $t\bar{t}$ events. The rejection factor for jets initiated by light quarks was found to be approximately 130.

3.2 Event selection

Data used in this measurement were collected by triggering on either a high-p_{T} electron, based on calorimeter energy deposits, shower shape and track quality constraints; or a high-p_{T} muon, comprising a reconstructed track in the MS matched with a reconstructed track in the ID. The p_{T} threshold for the muon trigger was 18 GeV, whereas the electron trigger threshold was 20 GeV or 22 GeV according to the data-taking period. The reconstructed lepton object was required to be within $\Delta R < 0.15$ of the lepton reconstructed by the high-level trigger.

The selected events were required to contain at least one reconstructed primary vertex. To avoid events with bad detector components or reconstruction performance, events were rejected that contained any jet with $p_{\mathrm{T}} > 20$ GeV that was identified as arising from calorimeter noise or out-of-time activity with respect to the primary pp collision [24]. Furthermore, events in which an electron and a muon shared the same track were removed.

Events were selected if they contain exactly one reconstructed electron (e) or muon (μ) and at least three jets with $p_{\mathrm{T}} > 25$ GeV and $|\eta| < 2.5$. One of the jets was required to be b-tagged. In addition, $E_{\mathrm{T}}^{\mathrm{miss}} > 30$ GeV and a transverse W mass[3] $m_{\mathrm{T}}(W) > 35$ GeV were required. To reduce the contribution of dilepton $t\bar{t}$ final states, events with additional leptons (electrons or muons) with $p_{\mathrm{T}} > 15$ GeV were excluded. Events with jet-jet pairs with $\Delta R < 0.5$ were excluded to reduce jet p_{T} migrations between particle and reconstructed jets.

In addition to this event selection, events for the jet p_{T} measurement were required to have a leading jet with $p_{\mathrm{T}} > 50$ GeV and a 2$^{\mathrm{nd}}$-leading jet $p_{\mathrm{T}} > 35$ GeV. Measurements of

[3]The variable $m_{\mathrm{T}}(W)$ is defined as $\sqrt{2p_{\mathrm{T}}^{\ell}p_{\mathrm{T}}^{\nu}(1-\cos(\phi^{\ell}-\phi^{\nu}))}$, where ℓ and ν refer to the charged lepton (e or μ) and $E_{\mathrm{T}}^{\mathrm{miss}}$ respectively.

JHEP01(2015)020

the jet multiplicity were also performed by selecting events with the jet p_{T} threshold raised from 25 GeV to 40 GeV, 60 GeV and 80 GeV in both channels, where the rest of the event selection was as described before.

The numbers of selected events are shown in tables 1 and 2 for the electron and muon channel, respectively.

3.3 Estimation of backgrounds

The dominant background in this measurement is the associated production of W bosons with jets (including those arising from charm and bottom quarks), followed by single-top-quark production and multijet production. Smaller backgrounds arise from Z/γ^*+jets and diboson production (WW, WZ, ZZ).

The normalisation of the W+jets contribution was extracted from a lepton charge asymmetry measurement from data. The method uses the fact that the production of W bosons at the LHC is charge asymmetric, and the theoretical prediction of the ratio $r_{\mathrm{MC}} \equiv \frac{\sigma(pp\to W^+)}{\sigma(pp\to W^-)}$ has an uncertainty of only a few percent. Most processes other than W production are either mostly or completely charge symmetric. The number of events in data with a positively (negatively) charged-lepton was measured and is referred to as D^+ (D^-). Therefore, $N_{W^+} - N_{W^-} \approx D^+ - D^-$, where N_{W^+} (N_{W^-}) is the number of W^+ (W^-) events. The W+jets estimate then comes from:

$$N_{W^+} + N_{W^-} = \frac{r_{\mathrm{MC}} + 1}{r_{\mathrm{MC}} - 1}(D^+ - D^-) \tag{3.1}$$

The normalisation was determined in W+jets events before any b-tagging requirement, separately for the W+3 jet, W+4 jet and $W+\geq 5$ jet events.

The flavour composition was derived from a W+2 jets measurement from data. The number of $W+2$ jet events before and after b-tagging was measured using the charge-asymmetry technique. The number of $W+2$ jet events after b-tagging can be expressed in terms of the number of $W+2$ jet events before b-tagging, the flavour fractions and b-tagging probabilities. The flavour fractions were adjusted to ensure that the derived number of W+2 jet events after b-tagging matched the data. The overall charge-asymmetry normalisation was fixed, and a fit procedure was used to extract the normalisation of the bottom and charm-quark fractions ($Wb\bar{b}$+jets, $Wc\bar{c}$+jets, and Wc+jets). The heavy-flavour components were then extrapolated to events with higher jet multiplicities.

In the e + jets channel, either jets or electrons originating from photon conversions can mimic an isolated electron from a W boson decay and are referred to as the multijet background. In the μ + jets channel, the multijet background arises mostly from leptonic decays of heavy-flavour quarks. The shape and normalisation of the multijet background in the e + jets channel was obtained using a matrix method [28] with looser electron identification cuts and no isolation requirement. The $E_{\mathrm{T}}^{\mathrm{miss}} < 20$ GeV region was used as the control region for this method. The multijet background in the μ + jets channel was determined using the mean of two matrix method estimates, which differ in their choice of normalisation region. The first method uses a low-$m_{\mathrm{T}}(W)$ region, whereas the second method uses a region where the selected muon has a large impact parameter with respect to

JHEP01(2015)020

		Reconstructed jet multiplicity					
Source	Yield	3	4	5	6	7	$\geq$8
$t\bar{t}$	25660	10060	9068	4335	1567	472	158
W+jets	7238	5257	1525	367	70	13	6
Multijet	2150	1409	498	166	58	12	7
Single-top-quark	2935	1904	760	215	45	9	1
Z/γ^*+jets	925	578	239	85	18	5	1
Diboson	180	140	32	6	1	0	0
Expectation	39087	19347	12123	5174	1759	512	172
Data (4.59 ± 0.08 fb^{-1})	38318	19471	11791	4964	1544	424	124

Table 1. The numbers of selected data, MC simulation and background events in the electron channel, for the 25 GeV jet p_{T} threshold. The yield column shows the total number of events passing the full event selection, which requires three or more selected jets. The POWHEG+PYTHIA MC simulation sample was used for the $t\bar{t}$ prediction. The numbers of $t\bar{t}$, single-top-quark, Z/γ^*+jets and diboson events were normalised to the integrated luminosity of the data. The other yields were determined from fits to data distributions.

		Reconstructed jet multiplicity					
Source	Yield	3	4	5	6	7	$\geq$8
$t\bar{t}$	30741	11953	10884	5220	1903	580	200
W+jets	10424	7514	2261	510	104	28	7
Multijet	1063	737	227	68	23	7	3
Single-top-quark	3498	2274	901	252	57	11	3
Z/γ^*+jets	546	368	126	40	10	1	0
Diboson	211	166	38	7	1	0	0
Expectation	46482	23013	14436	6096	2098	627	213
Data (4.59 ± 0.08 fb^{-1})	46192	23447	14170	5851	1977	568	179

Table 2. The numbers of selected data, MC simulation and background events in the muon channel, for the 25 GeV jet p_{T} threshold. The yield column shows the total number of events passing the full event selection, which requires three or more selected jets. The POWHEG+PYTHIA MC simulation sample was used for the $t\bar{t}$ prediction. The numbers of $t\bar{t}$, single-top-quark, Z/γ^*+jets and diboson events were normalised to the integrated luminosity of the data. The other yields were determined from fits to data distributions.

the primary vertex. The low-$m_{\mathrm{T}}(W)$ region includes events that do not contain W bosons, whereas the high impact parameter region includes muons from heavy-flavour decays.

Contributions from single-top-quark, Z/γ^*+jets, and diboson production were evaluated using the corresponding MC samples and theoretical cross-sections for these processes.

4 Monte Carlo simulation

MC simulations were used to correct the measurement for detector effects and to estimate some of the background contributions.

JHEP01(2015)020

To derive corrections for detector effects, a good description of the $t\bar{t}$ signal process is important. Signal predictions rely on matrix-element calculations for short distance physics processes and on parton shower, fragmentation and proton remnant modelling for long-range effects. The potential bias of the final result due to a particular model chosen was estimated by generating MC samples using alternative models for each of these components.

In modern MC generators, there are mainly two different approaches used to provide predictions of $t\bar{t}$ final states and their multijet topology. The first approach focuses on a precise prediction using merged leading-order (LO) matrix elements for a given number of hard partons supplemented with parton-shower emissions in the soft-collinear region. The second approach focuses on the most accurate prediction of the inclusive rates of $t\bar{t}$ production by calculating the matrix elements at next-to-leading order (NLO). Programs implementing this approach also provide an accurate description at leading order of the $t\bar{t}$+1 jet final state, and leading-logarithmic accuracy for additional jet production. In this analysis, the first approach was used in the form of the ALPGEN [29] MC generator. This sample was compared with the alternative approach implemented in the MC@NLO [30] and POWHEG [31] MC generators. In both cases, the matrix-element calculation was matched to separate programs for the simulation of the long-range effects.

The ALPGEN sample was generated using version 2.13, with the CTEQ6L1 parton distribution functions (PDFs) and the associated value of the strong coupling constant $\alpha_{\mathrm{S}}(m_{\mathrm{Z}}) = 0.129$ [32]. The factorisation and renormalisation scales were set to the default values of the program, i.e. $\mu_{\mathrm{F}}^2 = \mu_{\mathrm{R}}^2 = \sum \left(m^2 + p_{\mathrm{T}}^2\right)$, where the sum was calculated over top, heavy quarks and light quarks with mass m and transverse momentum p_{T}. ALPGEN was used to calculate LO matrix elements for up to five hard partons. Parton showering and fragmentation were performed using HERWIG [33] v6.520 together with JIMMY [34] for the multiple-parton interaction model using the AUET1 tune [35]. The MLM parton-jet matching scheme [29] was applied,[4] to avoid double counting configurations generated by both the parton shower and the matrix-element calculation. This resulted in samples with up to four hard partons exclusively and five hard partons inclusively, where the inclusive five parton sample includes jets produced by the parton shower. The processes $t\bar{t} + b\bar{b}$ and $t\bar{t}$+$c\bar{c}$ were generated separately using the same programs and algorithm as described above. The exclusive heavy-flavour samples were combined with the $t\bar{t}$ inclusive samples, after the removal of overlapping events. The overlapping events were rejected if the p_{T} of the b or c-quarks was above 25 GeV and they were matched to jets within a cone of $\Delta R = 0.4$. This sample is referred to as "ALPGEN+HERWIG" in the following discussion.

Further $t\bar{t}$ samples were generated following the alternative approach with NLO perturbative QCD calculations. A MC@NLO sample was produced with the CT10 [36] PDF set and using the default values of the program for renormalisation and factorisation scales, i.e. $\mu_{\mathrm{F}}^2 = \mu_{\mathrm{R}}^2 = (p_{\mathrm{T,t}}^2 + p_{\mathrm{T,\bar{t}}}^2)/2 + m_{\mathrm{t}}^2$, where $p_{\mathrm{T,t}}$ ($p_{\mathrm{T,\bar{t}}}$) refers to the p_{T} of the top (antitop) quark and m_{t} is the top mass. MC@NLO was also interfaced to HERWIG/JIMMY with the AUET1 tune. POWHEG (POWHEG-hvq, patch4) samples were produced with the CT10 PDF set, using the default setting of the hard-process scales $\mu_{\mathrm{F}}^2 = \mu_{\mathrm{R}}^2 = p_{\mathrm{T}}^2 + m_{\mathrm{t}}^2$,

[4] using matching scale *ETCLUS* of 20 GeV and a matching radius of 0.7.

JHEP01(2015)020

where p_{T} corresponds to the parton-level top-quark transverse momentum. POWHEG was used to produce the matrix-element calculation and top-quark decay. To assess the effect of different fragmentation, multi-parton interaction and parton-shower models, the same POWHEG sample was matched to two different multi-purpose generators. One sample was produced by matching with PYTHIA6 [37], using the "C" variant of the Perugia 2011 tune family [38] that uses the CTEQ6L1 PDF. Another sample was produced by matching to HERWIG+JIMMY with the AUET1 tune. These samples are referred to as "POWHEG+PYTHIA" and "POWHEG+HERWIG", respectively, in the following text. The POWHEG+PYTHIA sample was used as the nominal $t\bar{t}$ sample for the correction of detector effects.

The uncertainty on the predictions due to modelling of initial-state radiation (ISR) and final-state radiation (FSR) was estimated using ALPGEN v2.14 with the PYTHIA6 parton-shower, the CTEQ5L PDF [39], and the Perugia 2011 family of tunes. For these variations, the same $\alpha_{\mathrm{S}}(m_{\mathrm{Z}})$ value was used for the calculation of the matrix elements and for the parton shower as suggested in ref. [40]. For the ALPGEN+PYTHIA central sample, the Perugia 2011 central tune which employs $\lambda_{\mathrm{QCD}} = 0.26$ was used. Uncertainties due to ISR/FSR-modelling choices were estimated by varying the ALPGEN renormalisation scale associated with α_{S} up and down at each local vertex in the matrix element relative to the original scale. A factor of 2.0 (0.5) was applied, resulting in lower (higher) α_{S} values, respectively. The effective α_{S} value in the parton shower was varied by the same factors as the matrix-element calculation and the corresponding PYTHIA6 tunes "Perugia 2011 radHi" and "Perugia 2011 radLo" [38] were used. In this paper, these samples are referred to as "α_{S} down" and "α_{S} up". These settings were shown to produce variations that are similar to the uncertainty bands on the distributions of the additional jet-veto variables $f(Q_0)$ and $f(Q_{\mathrm{sum}})$ that are described in ref. [41].

To estimate radiation uncertainties in the POWHEG predictions, the model parameter h_{damp}, which effectively regulates the high-p_{T} radiation in POWHEG, was set to 172.5 GeV (value used for m_{t}) following a similar strategy as in ref. [42] while all other POWHEG samples used the default value $h_{\mathrm{damp}} \sim \infty$. This sample was generated using POWHEG-BOX (revision 2330, version 1.0) and is referred to as "POWHEG(h_{damp})+PYTHIA" in the following discussion.

The effect of colour reconnection was estimated by generating a POWHEG+PYTHIA6 sample in which no colour reconnection was allowed within PYTHIA6, using the "noCR" Perugia 2011 tune [38].

The $t\bar{t}$ cross-section for pp collisions at a centre-of-mass energy of $\sqrt{s} = 7$ TeV was calculated to be $\sigma_{\mathrm{t\bar{t}}} = 177^{+10}_{-11}$ pb for $m_{\mathrm{t}} = 172.5$ GeV. This calculation was carried out at next-to-next-to-leading order (NNLO) in QCD including resummation of next-to-next-to-leading logarithmic (NNLL) soft gluon terms [43–47] with Top++2.0 [48]. The PDF and α_{S} uncertainties were calculated using the PDF4LHC prescription [49] with the MSTW2008 68CL NNLO [50, 51], CT10 NNLO [36, 52] and NNPDF2.3 5f FFN [53] PDF sets, and added in quadrature to the scale uncertainty. The NNLO+NNLL value is about 3% larger than the exact NNLO prediction, as implemented in HATHOR 1.5 [54]. All $t\bar{t}$-MC samples were generated with $m_{\mathrm{t}} = 172.5$ GeV and were normalised to the NNLO+NNLL theoretical cross-section.

JHEP01(2015)020

For the simulation of the background processes, samples of W and Z bosons with additional jets were generated using ALPGEN v2.13, with the CTEQ6L1 PDF, HERWIG and JIMMY with the AUET1 tune. Separate configurations were used for each partonic final-state with one to four associated partons. Parton multiplicities of five or more were generated inclusively. Since this analysis selects events based on identified b-jets, specific predictions of $Wb\bar{b}$+jets, $Wc\bar{c}$+jets, Wc+jets and $Zb\bar{b}$+jets events are necessary. Therefore, these processes were generated using LO matrix-element calculations and the overlap between these samples and the respective inclusive jet-flavour samples was removed using the same method as previously described for the $t\bar{t}$ samples. In the case of W+jets, the normalisation was determined from data as described in section 3.3, whereas the MC simulation was used to provide the information on the shape of the multiplicity spectrum.

The t-channel single-top-quark sample was generated with the AcerMC generator [55], whereas MC@NLO was used to generate the Wt and s-channel single-top-quark production processes. The single-top-quark samples were each normalised according to a calculation of the inclusive production cross-section at NLO accuracy complemented with an approximate NNLO calculation for the t-channel [56], s-channel [57] and Wt-channel [58]. Diboson events (WW, WZ, ZZ) were produced using HERWIG normalised to the cross-section obtained from a NLO calculation with MCFM [59] using the MSTW2008NLO PDF.

To properly simulate the LHC environment, additional inelastic pp interactions were generated with PYTHIA6 using the AMBT1 tune and then overlaid on top of the hard-processes. The MC events were re-weighted such that the predicted $\langle\mu\rangle$ distribution matched that of the data run period. The particles from additional interactions were added before the detector simulation, but were not used within the particle-level definition described in section 7.1.

The POWHEG+PYTHIA, ALPGEN+HERWIG, MC@NLO+HERWIG and the central ALPGEN+PYTHIA MC samples were passed through a full Geant4 [60] simulation of the ATLAS detector [61]. The ISR/FSR variations, colour reconnection and POWHEG+HERWIG MC samples were passed through a parameterised simulation of the detector response [61].

5 Systematic uncertainties

This section describes the sources of systematic uncertainties and how they were estimated for the signal and background yields. The sources of these uncertainties include the object reconstruction and identification, the jet energy scale (JES) calibration, the jet energy resolution (JER), the b-tagging calibration, the multijet-background normalisation, and MC generator modelling. Uncertainties relating to MC simulation modelling were evaluated for both signal and background MC samples. The resulting uncertainty on the final measurement is reported separately for each source in appendix C.

Jet energy scale. The JES uncertainty was evaluated using 21 effective nuisance parameters, which describe the p_{T} and η dependence of the JES uncertainty. The effective nuisance parameters were derived for inclusive jet samples. They include eleven parameters for the effective uncertainties of in situ measurements covering detector and modelling

JHEP01(2015)020

related uncertainties and uncertainties where the two components can not be separated ("mixed"). In addition, there are statistical uncertainties, two parameters to model $\langle\mu\rangle$ and N_{PV} dependence, one parameter for close-by jets, i.e. jet-jet pairs with a separation of $\Delta R < 1.0$, one parameter for the calibration of b-jets and two parameters for η-intercalibration, i.e. the uncertainty of the η dependence of the calibration. Uncertainties due to different detector-simulation configurations used in the analysis and in the calibration were added as one additional uncertainty parameter ("relative non-closure").

Since details of the fragmentation differ between jets initiated by quarks and those initiated by gluons [24], the respective jet energy scale also differs slightly. However, the in situ techniques mainly rely on processes that produce jets initiated by quarks. Therefore, an additional uncertainty was assigned to cover potential differences resulting from the different quark/gluon flavour composition of the analysed sample ("flavour composition") and the jet response dependence on the jet flavour ("flavour response"). The quark and gluon fractions in the analysed sample were evaluated as a function of jet multiplicity, jet p_{T} and jet η, using the ALPGEN+HERWIG and MC@NLO $t\bar{t}$ signal samples. Depending on the jet multiplicity, gluon fractions between 10% and 60% were predicted within the acceptance of this measurement. The predictions of the two MC models were found to agree within 10% over the majority of the acceptance range. The uncertainty on the predicted gluon-fractions was taken as the difference between the two MC models, where 10% was assigned as a conservative estimate when the difference between the two models was less than this. For events with more than seven jets, the uncertainty estimate for seven jet events was used. The gluon-fraction and its associated uncertainty, together with the quark and gluon-response uncertainties, were used to determine the resulting JES uncertainty, which was found to vary in the range 1.5–8% depending on jet p_{T}, η, and the jet multiplicity in the event. An additional p_{T}-dependent uncertainty of up to 2.5% was applied to jets matched to b-hadrons, to account for neutrino and muon energy losses. This was added in quadrature to the inclusive JES uncertainty resulting in a total JES uncertainty in the analysed sample between about 5% at low p_{T} and about 1% at high p_{T} in the central region.

Jet energy resolution. The measurements of the jet energy resolution from MC simulation and data were found to agree within their uncertainties [25]. The resulting uncertainties on the measurement were evaluated by additionally smearing the jet energies by the systematic uncertainties on the jet energy measurement. This resulted in an uncertainty of 2–20%, depending on p_{T} and η.

Jet reconstruction efficiency. The jet reconstruction efficiency was derived from MC simulation and the uncertainty on the efficiency was estimated in situ with jets reconstructed from tracks in the ID that were matched to a jet reconstructed using calorimeter information. Data and MC simulation were found to agree within the uncertainties of the in situ method. For $p_{\mathrm{T}} < 30$ GeV the in situ measurement suffers from relatively large uncertainties. Therefore a 2% uncertainty corresponding to the shift between data and the MC simulation [25] was assigned in this range. The uncertainty at higher jet p_{T} is negligible.

JHEP01(2015)020

***b*-tagging.** The efficiency of the b-tagging algorithm was evaluated using MC samples. The differences between the efficiency in data and MC simulation were evaluated using jets containing a muon within a multijet sample. The p_{T} of the muon relative to the jet axis, $p_{\mathrm{T}}^{\mathrm{rel}}$, is in general harder for muons originating from b-hadron decays than from muons in c-jets and light-flavour jets. The b-tagging efficiency was extracted using template fits to the $p_{\mathrm{T}}^{\mathrm{rel}}$ spectrum. The difference between data and MC simulation efficiencies was expressed as a function of p_{T} and η and was applied to the MC simulation events used in this analysis. The uncertainties on this difference were derived from the statistical and systematic uncertainties on the efficiency measurements and ranges from 5% at low p_{T} to 19% at $p_{\mathrm{T}} > 140\,\mathrm{GeV}$ [62].

The mis-tag scale factors for light-flavour jets were measured using a vertex-mass method [63]. The vertex-mass was defined as the invariant mass of the charged particles associated with the secondary vertex. Templates were derived from simulations and fitted to the vertex-mass distribution obtained from data to determine the number of light and c-jets. The fits were performed on samples before and after applying b-tagging and the ratio of the results is taken as the mistag rate which is between 1 and 3%. A p_{T} dependent scale factor corrects for the different mistag rate in data and simulation. The uncertainty on the scale factor ranges from 18% in the intermediate p_{T} range for central jets to as much as 49% in the high p_{T} region for forward jets. This uncertainty is caused dominantly by the efficiency to reconstruct the secondary vertex.

Jet vertex fraction. The efficiency to separate hard scatter jets from pile-up jets with the JVF > 0.75 requirement was measured using $Z \to \ell^+\ell^-$ events, with exactly one additional jet after the suppression of jets from additional primary interactions. This suppression was achieved by selecting events where the jet was produced with p_{T} balancing the Z boson and an azimuthal opening angle close to π. The efficiency to identify a hard scatter jet is about 90% for jets with p_{T} of 25 GeV and close to 100% for jets with $p_{\mathrm{T}} > 100\,\mathrm{GeV}$. Up to 10% of the pile-up jets are misidentified as hard scatter jets in particular at low p_{T} . The ratio between the efficiencies derived in data and in MC is used as a scale factor. The systematic uncertainty on the scale factor was estimated by varying the selection parameters used to define the $Z+1$ jet region and by applying the results from $Z \to \ell^+\ell^-$ events on events with $t\bar{t}$-decay topology. The uncertainty is about 1% for the efficiency to select hard scatter jets and about 10% for the mis-identification of pile-up jets.

Leptons. The mis-modelling of lepton trigger, reconstruction and selection efficiencies in the simulation were corrected for by calculating data/MC correction factors derived from measurements of these efficiencies in data. Z boson and W boson decays ($Z \to \mu\mu$, $Z \to ee$, and $W \to e\nu$) were used to obtain data/MC correction factors as functions of the lepton kinematic distributions. The uncertainties were evaluated by varying each of the lepton trigger, reconstruction and selection efficiencies within their associated one standard deviation errors, where each contribution was evaluated separately. The uncertainty is within 2.5-3.2%.

The energy scale and resolution of reconstructed electromagnetic energy clusters were calibrated from resonance decays such as $Z \to ee$, $J/\psi \to ee$, or from studies of the en-

JHEP01(2015)020

ergy/momentum ratio using isolated electrons from $W \to e\nu$. Uncertainties on the scale and resolution were independently evaluated by fluctuating the scale or resolution correction applied to the MC events by the associated calibration factor uncertainty. In a similar manner, the scale and resolution of the reconstructed p_{T} of muons were calibrated from $Z \to \mu\mu$ and $J/\psi \to \mu\mu$ decays. The uncertainties on these calibrations were independently evaluated by smearing the correction applied to MC events by the associated calibration factor uncertainty.

The systematic uncertainties related to the lepton energy scale and resolution are within 1–1.5%.

Missing transverse momentum. Energy scale and p_{T} resolution corrections for e, μ and jets were included in the $E_{\mathrm{T}}^{\mathrm{miss}}$ calculation. For the calorimeter cells not associated with a reconstructed electron or jet with p_{T} greater than 20 GeV, an uncertainty dependent on the total transverse energy in the calorimeter (ΣE_{T}) was assigned to their energy. This is approximately 13% and is referred to as the "Cell Out uncertainty". The uncertainty on $E_{\mathrm{T}}^{\mathrm{miss}}$ due to additional pp interactions is about 10% and was estimated by varying the contributions from the cells associated with soft jets (with $7 < p_{\mathrm{T}} < 20$ GeV) and Cell Out components of $E_{\mathrm{T}}^{\mathrm{miss}}$ within their calibration uncertainty. This procedure was chosen following studies of the dependence of energy resolution on the number of additional interactions.

PDF uncertainties. The uncertainty from using the selected PDF for MC event production was evaluated by re-weighting the $t\bar{t}$ ALPGEN+HERWIG MC sample generated with the CTEQ6L1 PDF to the nominal and eigenvector sets of the MSTW2008lo68cl PDF [50]. The CTEQ6L1 PDF does not provide associated eigenvector sets that can be used for this purpose. Therefore, the systematic uncertainty was determined from the differences obtained using the MSTW2008lo68cl PDF eigenvector sets, as well as the difference between the results based on the best-fit PDF sets of MSTW2008lo68cl and CTEQ6L1. The total PDF uncertainty was then evaluated by summing each of these orthogonal components in quadrature.

Generator model dependencies. Systematic uncertainties associated with generator modelling were evaluated from the bias observed after corrections for all known detector effects, where the nominal POWHEG+PYTHIA correction factors were used to correct the reconstructed spectra of the different MC samples to particle-level distributions.

The uncertainty due to fragmentation modelling was estimated by comparing ALPGEN+PYTHIA and ALPGEN+HERWIG $t\bar{t}$ samples. The difference between the biases on the fully corrected spectra was taken as the uncertainty on the final spectra. The ISR/FSR-modelling uncertainty was evaluated using the ALPGEN+PYTHIA $t\bar{t}$ sample and the corresponding ISR/FSR MC samples α_{S}-up and α_{S}-down. The maximum difference between the bias for the fully corrected spectra of ALPGEN+PYTHIA and the bias for the ISR/FSR samples was taken as the uncertainty.

The difference between fixed-order matrix-element calculations and associated matching schemes ("MC generator") was estimated by comparing the POWHEG+PYTHIA and

JHEP01(2015)020

ALPGEN+PYTHIA $t\bar{t}$ samples. This combination was chosen in preference to a combination with MC@NLO+HERWIG, since MC@NLO+HERWIG was found not to describe the reconstructed jet multiplicity observed in data for events with ≥ 6 jets.

W + jets background modelling. The reconstruction, charge-misidentification rate, backgrounds, MC generator uncertainties and PDF eigenvector sets were all varied to provide uncertainties on the W+jets normalisation scale factors derived from the charge-asymmetry technique. In total, these uncertainties were found to vary from 7% in 3-jet events up to 15% in $\geq$ 5-jet events. The uncertainty on each of the heavy-flavour fractions was determined by reconstruction, background and MC generator variations within their uncertainties and an additional uncertainty of 25% for scaling from the 2-jet bin to any higher jet multiplicity. The additional 25% uncertainty was chosen to cover the variations of different MC predictions. The uncertainty on the modelling of the kinematic distributions of the W+jets MC samples was estimated by varying the factorisation and renormalisation scales and the generator cuts in ALPGEN.[5]

Multijet background modelling. The shape uncertainty on the multijet background in the electron channel was estimated by varying the maximum $E_{\mathrm{T}}^{\mathrm{miss}}$ requirement for the background selection region between 15 and 25 GeV. The shape uncertainty in the muon channel was taken from the difference between the mean and individual shapes of the two different matrix methods. A 20% normalisation uncertainty was derived for the muon channel from the comparison of the two background selection regions. For the electron channel an uncertainty of 50% was chosen to cover the difference between MC predictions and data in the relevant control distributions.

Other theoretical uncertainties. The theoretical uncertainty on the single-top-quark cross-section was taken from the approximate NNLO cross-section uncertainties to be 4% for the t-channel, 4% for the s-channel and 8% for the Wt-channel. The theoretical uncertainty on the diboson cross-section was estimated to be 5% by varying PDFs and comparing NLO calculations of MCFM [59] and MC@NLO. For Z/γ^*+jets a normalisation uncertainty of 4% was used for samples with no additional jet and 24% for each additional jet was added in quadrature to cover the model uncertainties of this prediction.

Luminosity. The integrated luminosity was measured from interaction rates in symmetric forward and backward facing detectors that were calibrated using van der Meer scans [17]. The systematic uncertainty on this measurement was estimated to be 1.8%. The integrated luminosity of the data and its uncertainty were used to normalise all MC simulation signal and background samples, with the exception of the W+jets and multijet-background estimates that were extracted from fits to the data.

6 Reconstructed yields and distributions

The predicted and observed reconstructed jet multiplicity yields for the jet p_{T} threshold of 25 GeV are presented in figure 2. The uncertainty bands shown correspond to the

[5] using the ALPGEN parameters `iqopt3` and `ptjmin`.

JHEP01(2015)020

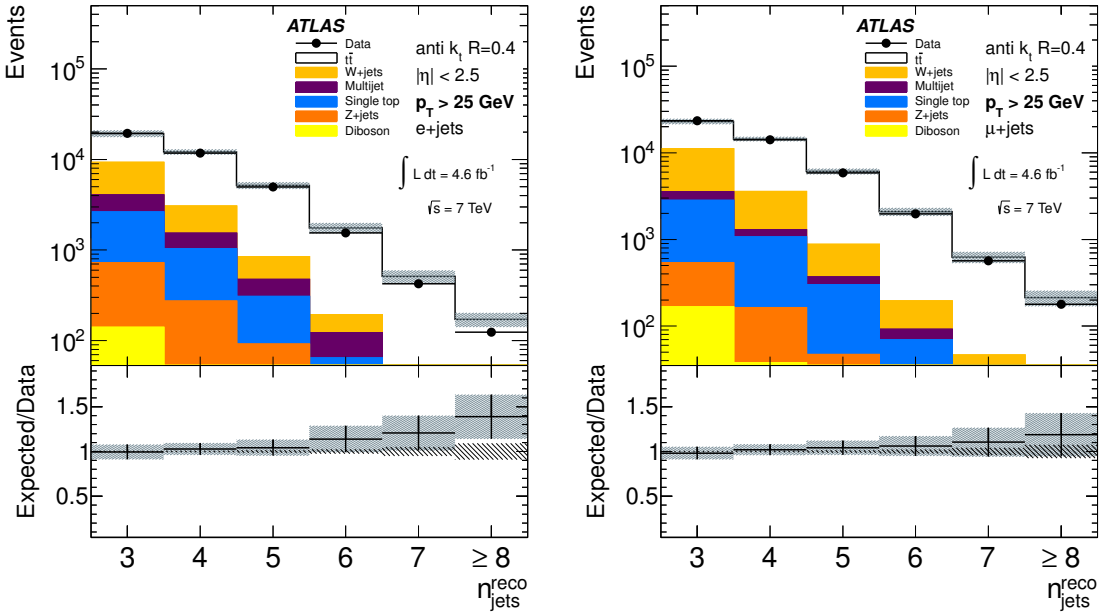

(a) $e+\text{jets}$, $p_{\mathrm{T}} > 25$ GeV (b) $\mu+\text{jets}$, $p_{\mathrm{T}} > 25$ GeV

Figure 2. The reconstructed jet multiplicities for the jet p_{T} threshold of 25 GeV, in the (a) electron ($e+\text{jets}$) and (b) muon ($\mu+\text{jets}$) channel. The data are compared to the sum of the $t\bar{t}$ POWHEG+PYTHIA MC signal prediction and the background models. The shaded bands show the total systematic and statistical uncertainties on the combined signal and background estimate. The errors bar on the black points and the hatched area in the ratio, show the statistical uncertainty on the data measurements.

combination of the uncertainty sources listed in section 5. The jet multiplicity distributions with jet p_{T} thresholds of 40, 60 and 80 GeV are shown in appendix A. The comparison of predicted and observed jet p_{T} spectra for the leading and 5^{th} jet is shown in figure 3 for events with three or more selected jets. The bin sizes of the jet p_{T} spectra correspond to approximately one standard deviation of the jet energy resolution at low jet p_{T}. At high jet p_{T}, the highest-p_{T} bin is larger to limit the effect of statistical fluctuations. In a similar manner, the inclusive bin of the jet multiplicity spectra limits the effects of statistical fluctuations. The predictions from the POWHEG+PYTHIA $t\bar{t}$ simulation and background estimates agree with the observed jet multiplicity and jet p_{T} spectra within the total uncertainty on the prediction and the statistical uncertainties on the observed data. The jet p_{T} spectra of the $2^{\mathrm{nd}}, 3^{\mathrm{rd}}$ and 4^{th} leading jet are shown in appendix A.

7 Corrections for detector effects and channel combinations

Each reconstructed spectrum was corrected to the corresponding spectrum at particle level, within the selected kinematic range, by accounting for detector efficiencies and resolution effects. To minimise the corrections of the measured data to particle level, the particles and particle jets were defined in a similar manner as the observable experimental objects and in a kinematic phase-space close to the experimental selection, as described in section 7.1.

JHEP01(2015)020

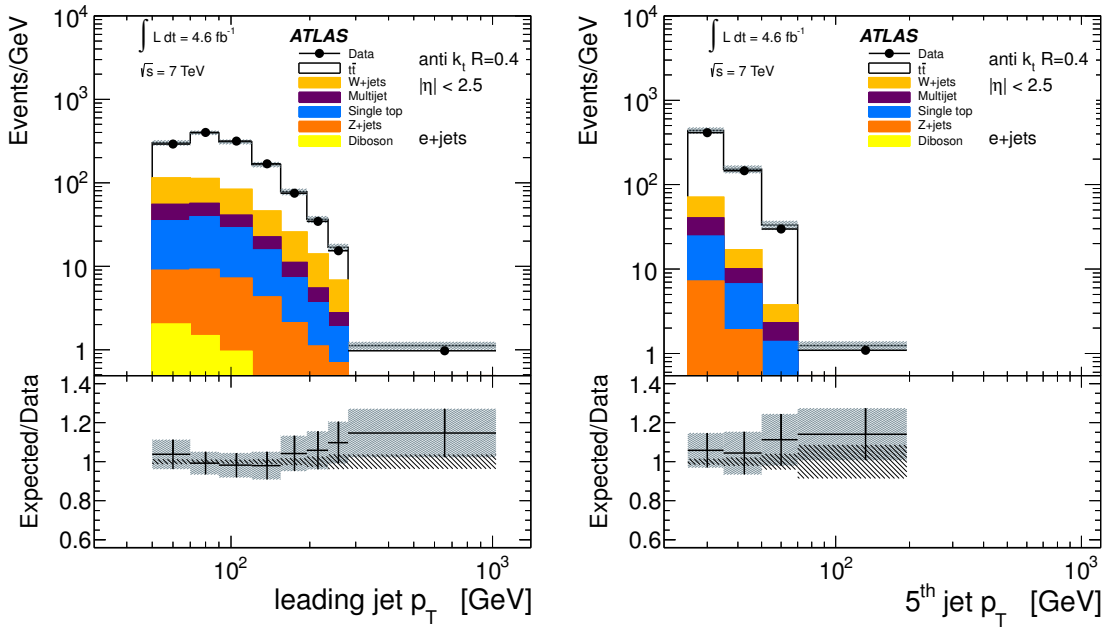

(a) $e+$jets, $p_{\mathrm{T}} > 25$ GeV, leading jet

(b) $e+$jets, $p_{\mathrm{T}} > 25$ GeV, 5th jet

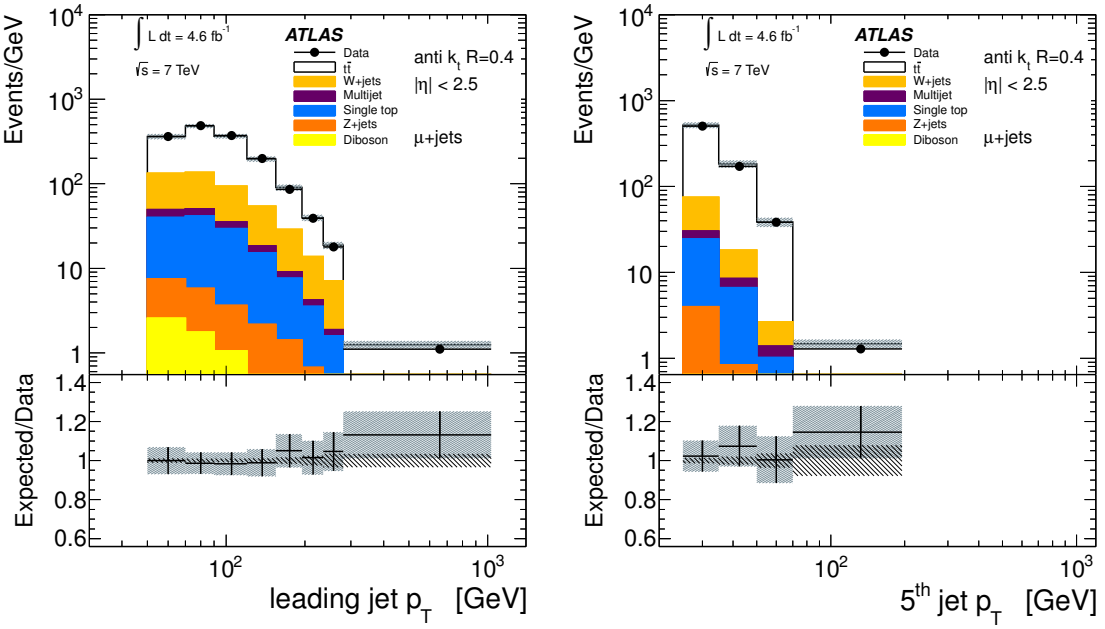

(c) $\mu+$jets, $p_{\mathrm{T}} > 25$ GeV, 5th jet

(d) $\mu+$jets, $p_{\mathrm{T}} > 25$ GeV, 5th jet

Figure 3. The reconstructed jet p_{T} for the electron ($e+$jets) channel (a) leading and (b) fifth jet and muon channel ($\mu+$jets) (c) leading and (d) fifth jet. The data are compared to the sum of the $t\bar{t}$ POWHEG+PYTHIA MC signal prediction and the background models. The shaded bands show the total systematic and statistical uncertainties on the combined signal and background estimate. The error bars on the black points and the hatched area in the ratio, show the statistical uncertainty on the data measurements.

JHEP01(2015)020

The details of the correction procedure are described in section 7.2. The propagation of measurement uncertainties through the correction procedure and additional uncertainties from the correction terms are discussed in section 7.3. Finally, the combination of the results of the electron and muon channels is described in section 7.4.

7.1 Definition of the fiducial cross-section measurement

The data were corrected by comparing to leptons and jets from MC generators that were defined using particles with a mean lifetime greater than 0.3×10^{-10} s, directly produced in pp interactions or from subsequent decays of particles with a shorter lifetime. To select the leptons from W boson decay, all leptons (e, μ, ν_e, ν_μ, ν_τ) for the cross-section definition were required not to be hadron decay products. Electron and muon four-vectors were calculated after the addition of photon four-vectors within a cone of $\Delta R = 0.1$ around their original directions. The $E_{\mathrm{T}}^{\mathrm{miss}}$ was calculated from the four-vector sum of neutrinos from W boson decays. Jets were defined using the anti-k_t algorithm with a radius parameter of 0.4. All particles were considered for jet clustering, except for leptons as defined above (i.e. neutrinos from hadron decays are included in jets) and any photons associated with the selected electrons or muons. Jets initiated by b-quarks were identified as such i.e. "b-tagged" if one or more b-hadrons was clustered within the given jet.

The cross-section was defined using events with exactly one electron or muon and at least three jets, each with $p_{\mathrm{T}} > 25$ GeV and $|\eta| < 2.5$. One of the jets was required to be b-tagged. In addition, $E_{\mathrm{T}}^{\mathrm{miss}} > 30$ GeV and $m_{\mathrm{T}}(W) > 35$ GeV were required.

To reduce the contribution from dilepton $t\bar{t}$ final states, events with additional leptons (electrons or muons) with $p_{\mathrm{T}} > 15$ GeV were excluded. Following the reconstructed object selection, events with jet-electron pairs or jet-muon pairs with $\Delta R < 0.4$ or jet-jet pairs with $\Delta R < 0.5$ were excluded.

The differential production cross-section in jet p_{T} was defined using the basic selection with three or more jets with $p_{\mathrm{T}} > 25$ GeV and the additional requirement of $p_{\mathrm{T}} > 50$ GeV and $p_{\mathrm{T}} > 35$ GeV on the leading and 2^{nd}-leading jet, respectively. This additional selection was applied to reduce uncertainties that can arise due to a different ordering of the measured jets with respect to the reference jets used in the correction procedure discussed in section 7.2. The two phase-space definitions are summarised in tables 3 and 4.

Additional cross-sections as a function of jet multiplicity were defined by increasing the jet p_{T} thresholds from 25 GeV to 40 GeV, 60 GeV and 80 GeV in both channels, where the rest of the fiducial-volume definition is as described before.

7.2 Correction procedure

The reconstructed jet multiplicity and momentum spectra were corrected to particle-level spectra, within the selected kinematic range defined in tables 3 and 4. The kinematic range of the measurement was chosen to be the same for particle-level and reconstruction-level objects. However, due to limited efficiencies and detector resolutions, differences between reconstructed and particle-level distributions exist and were corrected for. Jet related resolutions and efficiencies that potentially lead to migration effects and bin-to-bin correlations were taken into account within an iterative Bayesian unfolding [64].

JHEP01(2015)020

$E_{\mathrm{T}}^{\mathrm{miss}} > 30$ GeV & $m_{\mathrm{T}}(W) > 35$ GeV
One or more b-jets
Three or more jets with $p_{\mathrm{T}} > 25$ GeV & $\lvert\eta\rvert < 2.5$
e (μ) with $p_{\mathrm{T}} > 25$ GeV & $\lvert\eta\rvert < 2.5$
No additional e (μ) with $p_{\mathrm{T}} > 15$ GeV & $\lvert\eta\rvert < 2.5$
No μ (e) with $p_{\mathrm{T}} > 15$ GeV & $\lvert\eta\rvert < 2.5$
No jet-jet pair with $\Delta R < 0.5$
No jet-electron or jet-muon pair with $\Delta R < 0.4$

Table 3. Fiducial-volume definition for the electron (muon) channel of the $t\bar{t}$+jets cross-section measurement with the jet p_{T} threshold of 25 GeV. These conditions were applied on reconstruction-level and particle-level objects, with the exception of the electron where a veto on the η-region corresponding to the barrel-endcap transition region was applied on the reconstruction level (as described in section 3.1), but not included in the fiducial-volume definition. The jet p_{T} threshold in the jet multiplicity distributions was increased to 40, 60 and 80 GeV, for the corresponding cross-section measurements.

Leading jet with $p_{\mathrm{T}} > 50$ GeV & $\lvert\eta\rvert < 2.5$
2^{nd} leading jet with $p_{\mathrm{T}} > 35$ GeV & $\lvert\eta\rvert < 2.5$

Table 4. Additional fiducial-volume requirements implemented for the $t\bar{t}$ cross-section with respect to the jet p_{T}. These requirements were made in addition to those given in table 3 and were applied to the electron and the muon channel.

The reconstructed jet multiplicity measurements were corrected according to

$$N_{\mathrm{part}}^{\mathrm{i}} = f_{\mathrm{part!reco}}^{\mathrm{i}} \cdot \sum_{\mathrm{j}} M_{\mathrm{reco,j}}^{\mathrm{part,i}} \cdot f_{\mathrm{reco!part}}^{\mathrm{j}} \cdot f_{\mathrm{accpt}}^{\mathrm{j}} \cdot (N_{\mathrm{reco}}^{\mathrm{j}} - N_{\mathrm{bgnd}}^{\mathrm{j}}) \tag{7.1}$$

where $N_{\mathrm{part}}^{\mathrm{i}}$ is the total number of fully corrected events, i indicates the particle-jet multiplicity and $f_{\mathrm{part!reco}}^{\mathrm{i}}$ is an efficiency factor to correct for events that fulfil the jet multiplicity requirement at particle-level but not at reconstruction level.

$N_{\mathrm{reco}}^{\mathrm{j}}$ is the total number of reconstructed events in data, $N_{\mathrm{bgnd}}^{\mathrm{j}}$ is the background contribution discussed in section 3.3 and j indicates the reconstructed jet multiplicity. The factor $f_{\mathrm{accpt}}^{\mathrm{j}}$ corrects for all non-jet related efficiencies, such as those stemming from b-tagging, trigger and lepton-reconstruction efficiencies. It is defined as the ratio of the number of reconstructed jets, where the denominator includes the complete reconstruction-level event selection and the numerator is defined with particle-level objects for all terms other than the jet multiplicity. The reconstructed jet multiplicity of the numerator of $f_{\mathrm{accpt}}^{\mathrm{j}}$ is defined using the same jet-electron overlap removal algorithm as described in section 3.1, with the exception of the electron object where the particle-level electron from the W boson decay was used instead.

The factor $f_{\mathrm{reco!part}}^{\mathrm{j}}$ is a correction for events passing the jet multiplicity requirement at the reconstruction level, but not at the particle level. $M_{\mathrm{reco,j}}^{\mathrm{part,i}}$ is a response matrix applied iteratively as part of Bayesian unfolding. The correction factor $f_{\mathrm{reco!part}}^{\mathrm{j}}$ and the matrix $M_{\mathrm{reco,j}}^{\mathrm{part,i}}$ are defined for the reconstructed jet multiplicity after the correction for all non-jet

JHEP01(2015)020

acceptance effects. They were calculated using the reconstructed jet multiplicity, within the particle-level acceptance as defined in table 3.

The corrected spectra were found to converge after four iterations of the Bayesian unfolding algorithm. The resulting jet multiplicity for all events that passed particle-level lepton and b-tagging requirements was used for one axis of $M^{\mathrm{part,i}}_{\mathrm{reco,j}}$, and the $f^{\mathrm{j}}_{\mathrm{accpt}}$ numerator. The $f^{\mathrm{i}}_{\mathrm{part!reco}}$ factor was derived from the $t\bar{t}$ MC sample, in a similar fashion as $f^{\mathrm{j}}_{\mathrm{reco!part}}$.

The correction factors are shown as a function of jet multiplicity (for $p_{\mathrm{T}} > 25\,\mathrm{GeV}$) in figure 4. In the electron (muon) channel, $f^{\mathrm{j}}_{\mathrm{accpt}}$ is around 1.9 (1.6) and rises with increasing jet multiplicity by about 40% (20%) in the eight-jet inclusive bin. Higher values of $f^{\mathrm{j}}_{\mathrm{accpt}}$ in the electron channel arise from the electron identification efficiency being lower than that of the muon identification. The electron channel $f^{\mathrm{j}}_{\mathrm{accpt}}$ also includes an interpolation across the η regions of the calorimeter barrel-endcap transition. These η regions were excluded in the reconstructed electron selection, but not from the definition of the fiducial cross-section. The factors $f^{\mathrm{j}}_{\mathrm{accpt}}$ for the p_{T} thresholds of 40–80 GeV are significantly less dependent on the number of jets, as shown in appendix B.

All other correction factors are approximately the same for the electron and muon channel and close to unity for jet multiplicities larger than four. Events with three or four jets are affected by migrations into or out of the fiducial volume, which is visible in the distributions of $f^{\mathrm{j}}_{\mathrm{reco!part}}$ and $f^{\mathrm{i}}_{\mathrm{part!reco}}$.

The transverse momentum distribution of each of the p_{T}-ordered jets was corrected in a similar manner as the jet multiplicity measurements. Jet p_{T} migrations were separated into migrations between jet p_{T}-ordering and migrations for the same p_{T}-ordering. Reconstructed jets were matched with jets of stable particles within $\Delta R < 0.35$. Then a bin-by-bin correction ($f^{\mathrm{j}}_{\mathrm{misassign}}$) was defined as the ratio of the number of events with matching p_{T}-ordering over all matched jets. The p_{T} distribution for each jet was then corrected according to

$$N^{\mathrm{i}}_{\mathrm{part}} = f^{\mathrm{i}}_{\mathrm{part!reco}} \cdot \sum_{\mathrm{j}} M^{\mathrm{part,i}}_{\mathrm{reco,j}} \cdot f^{\mathrm{j}}_{\mathrm{misassign}} \cdot f^{\mathrm{j}}_{\mathrm{reco!part}} \cdot f^{\mathrm{j}}_{\mathrm{accpt}} \cdot (N^{\mathrm{j}}_{\mathrm{reco}} - N^{\mathrm{j}}_{\mathrm{bgnd}}) \tag{7.2}$$

where the correction terms $M^{\mathrm{part,i}}_{\mathrm{reco,j}}, f^{\mathrm{j}}_{\mathrm{misassign}}, f^{\mathrm{j}}_{\mathrm{reco!part}}, f^{\mathrm{j}}_{\mathrm{accpt}}$ and $N^{\mathrm{j}}_{\mathrm{bgnd}}$ are functions of the reconstructed jet p_{T}, $f^{\mathrm{i}}_{\mathrm{part!reco}}$ and $M^{\mathrm{part,i}}_{\mathrm{reco,j}}$ are functions of the particle-jet p_{T}, and j (i) indicates the bin of reconstructed (particle) jet p_{T} distribution. Correction factors were derived and applied individually to the p_{T} distributions of the leading, 2$^{\mathrm{nd}}$, 3$^{\mathrm{rd}}$ and 4$^{\mathrm{th}}$ jets. As demonstrated in figure 5, for jet p_{T} above 100 GeV no correction for missing jets on particle or reconstruction level is needed. Softer jets are more likely to fail the reconstruction-level requirements and hence the larger associated correction factor of up to 1.5. However, this is compensated by a factor up to 0.7 for soft reconstructed jets that do not have a matching jet at particle level. The acceptance factor ($f^{\mathrm{j}}_{\mathrm{accpt}}$) is almost independent of jet p_{T}; only at low p_{T} can a slight rise be observed as p_{T} decreases. The factor $f^{\mathrm{j}}_{\mathrm{misassign}}$ rises with jet number and with p_{T}, which follows from the number of jets that can potentially be wrongly assigned and the possible p_{T} difference between the misassigned and the correct matching jet. The $f^{\mathrm{j}}_{\mathrm{misassign}}$ correction is very close to unity for the leading jet and within 10% for the 2$^{\mathrm{nd}}$ jet.

JHEP01(2015)020

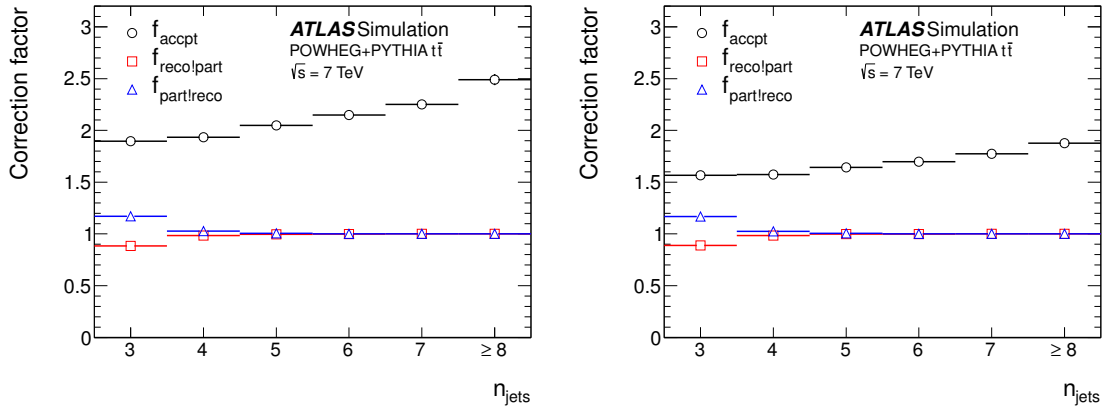

Figure 4. Global correction factors for the acceptance (f_{accpt}) and particle-level and reconstruction-level inefficiencies ($f_{\text{part!reco}}$, $f_{\text{reco!part}}$) to correct the jet multiplicity distribution with $p_{\text{T}} > 25$ GeV to particle level (a) in the electron and (b) in the muon channel as described in the text and in eq. (7.1). The symbol n_{jet} refers to the number of particle-level jets for $f_{\text{part!reco}}$ and to the number of reconstructed jets in case of $f_{\text{reco!part}}$ and f_{accpt}. The distributions are shown with statistical uncertainties only, which are too small to be visible.

7.3 Propagation of uncertainties

This section describes how the uncertainties listed in section 5 were taken into account in the unfolding and which additional uncertainties appear due to the unfolding procedure.

The response matrix ($M^{\text{part,i}}_{\text{reco,j}}$) and the correction factors ($f^{\text{i}}_{\text{part!reco}}$, $f^{\text{j}}_{\text{misassign}}$, $f^{\text{j}}_{\text{reco!part}}$ and $f^{\text{j}}_{\text{accpt}}$) were determined using the nominal POWHEG+PYTHIA $t\bar{t}$ MC sample. The statistical uncertainty on the size of the MC sample used to derive these factors was estimated by smearing the response matrix according to a Poisson distribution and the correction factors according to a normal distribution. A Poisson probability density function was chosen for the response matrix, since the matrix contains a number of events in each bin. The response matrix is also sparsely populated in bins that are far from the diagonal. Therefore, using a normal distribution is not a valid approximation. For the correction factor ratios ($f^{\text{i}}_{\text{part!reco}}$, $f^{\text{j}}_{\text{misassign}}$, $f^{\text{j}}_{\text{reco!part}}$ and $f^{\text{j}}_{\text{accpt}}$), the statistical uncertainty for the ratio does not correspond to an integer number of events and the number of events in each bin of the ratio is large. Therefore, a normal probability distribution was used as an approximation for the ratio of the two Poisson distributions. The statistical uncertainties were propagated by performing 1000 pseudo-experiments, smearing all terms simultaneously. The difference between the mean of all 1000 unfolded distributions and the true POWHEG+PYTHIA $t\bar{t}$ distribution was taken to be the systematic deviation or bias, whereas the standard deviation was taken to be the statistical uncertainty on the response matrix and the correction factors.

The statistical uncertainty on the reconstructed spectra ($N^{\text{j}}_{\text{reco}}$) was propagated by performing 1000 pseudo-experiments, following a Poisson distribution corresponding to the number of events in each bin (j), where the number of events in each bin of the reconstructed spectra was independently varied.

JHEP01(2015)020

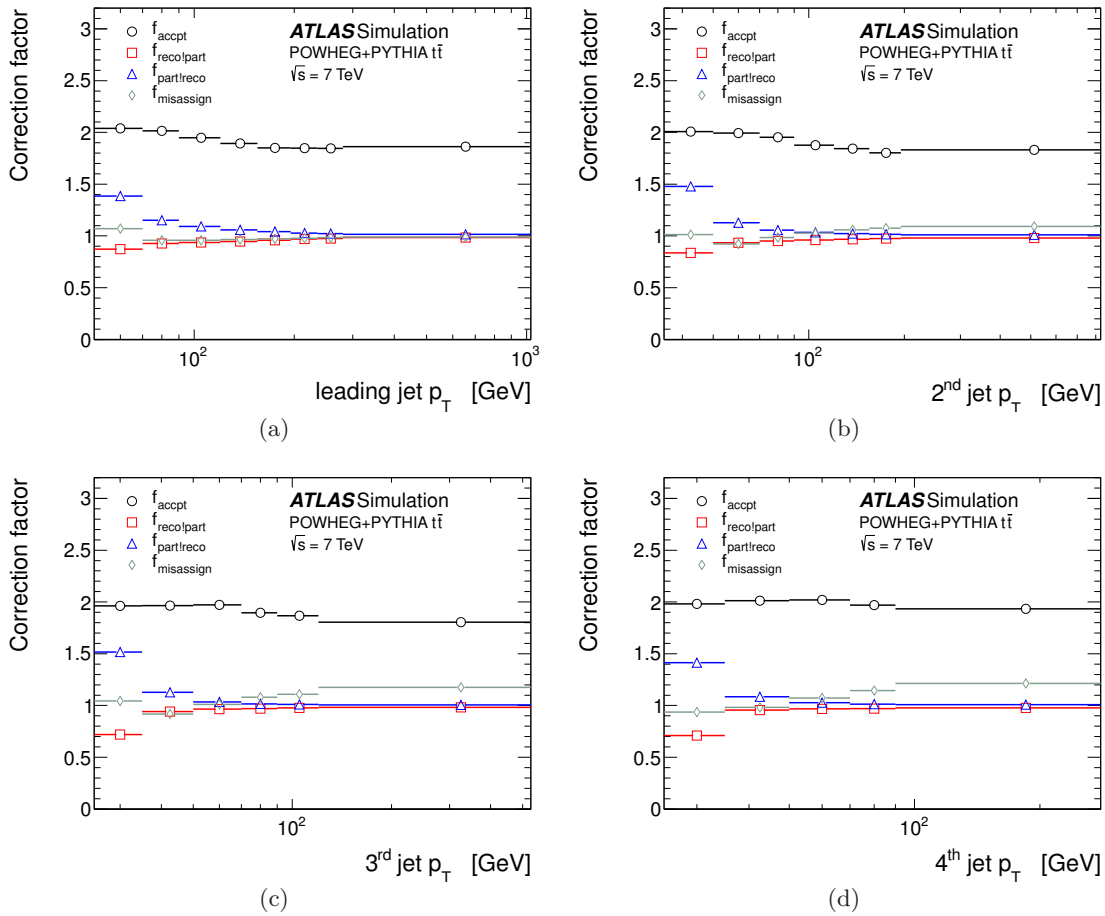

Figure 5. Global correction factors for the acceptance (f_{accpt}), particle-level and reconstruction-level inefficiencies ($f_{\text{part!reco}}$, $f_{\text{reco!part}}$) and misassignment in the p_{T} ordering of the jets ($f_{\text{misassign}}$), used to correct the jet p_{T} distributions to the particle level as described in the text and in eq. (7.2). The muon-channel correction factors are shown as an example. However, the corresponding distributions of the electron channel (not shown) are similar. The distributions are shown with statistical uncertainties only, which are too small to be visible.

The uncertainty on $N^{\text{j}}_{\text{bgnd}}$ was determined at the reconstruction level. The uncertainties related to the $W+$jets and multijet shapes and normalisations were propagated by forming background subtracted spectra for each of the background-uncertainty terms. The resulting difference between the nominal and shifted unfolded distributions was taken as the uncertainty. The statistical significance of this systematic uncertainty was evaluated by performing 1000 pseudo-experiments, following a normal distribution with a width matching the statistical uncertainty on the shifted input spectrum. If the root mean square of the variance of the pseudo-experiments was greater than 10% of the measured value then the systematic uncertainty estimate from the neighbouring measurement point was used. The value of 10% was established by studying all the systematic uncertainty variations as a function of the statistical uncertainty on the unfolded spectra. Above a statistical uncertainty of 10%, discontinuous predictions were observed for some systematic uncertainty

JHEP01(2015)020

variations. This procedure has a minimal effect on the highest jet-multiplicity bins of a subset of the corrected spectra.

To avoid enlarged uncertainties due to statistical fluctuations of the small background components, all other background uncertainty terms were combined according to their correlations and then propagated through the corrections by smearing the background subtracted spectra. The systematic uncertainty on the unfolded spectra from the background was evaluated by performing 1000 pseudo-experiments, following a normal distribution with a width matching the total uncertainty band. The square root of the variance of the unfolded spectra of the pseudo-experiments was taken as the uncertainty on the small background terms.

Systematic uncertainties affecting the $t\bar{t}$ sample used to unfold the jet multiplicity spectrum were each evaluated as a relative bias, i.e. deviations were determined from differences between the bias of the nominal sample and the systematically varied sample. For each variation, a pair of particle and reconstruction-level spectra was generated. The bias was evaluated by performing 1000 pseudo-experiments, fluctuating the reconstructed input-spectrum within its statistical uncertainty. Each pseudo-experiment was unfolded (using the response matrix derived from the nominal POWHEG+PYTHIA $t\bar{t}$ sample) and the bias was calculated from the difference between the mean corrected distribution and the true distribution. The systematic uncertainty estimation was taken from the relative bias, the difference between the bias evaluated with the nominal POWHEG+PYTHIA $t\bar{t}$ sample and the bias evaluated using each reconstructed and true systematic uncertainty variation sample. This applies to all cases except the ALPGEN+PYTHIA α_{S} variations, where the relative bias between the ALPGEN+PYTHIA central and shifted samples was used. The uncertainty on the fixed-order matrix-element calculation and matching scheme (the generator uncertainty) was estimated from the relative bias of unfolding ALPGEN+HERWIG with respect to the POWHEG+PYTHIA nominal $t\bar{t}$ sample. The MC@NLO sample was not used for this uncertainty, since it does not describe reconstructed data well at higher jet multiplicities. Each of the $t\bar{t}$ model uncertainties was propagated individually and symmetrised before being combined.

The effect on the measured multiplicity spectra due to the JES uncertainty rises with the jet multiplicity from 3% to 40% for the 25 GeV jet p_{T} threshold. This uncertainty decreases in the higher jet multiplicity bins for the higher jet p_{T} thresholds, to values of around 15%. For the 25 GeV jet p_{T} threshold, the background uncertainty is 18%(3%) for events with low (high) jet multiplicities. The effect of the ISR/FSR-modelling uncertainty varies from 1–6%. The next most significant uncertainties are the matrix-element generator and b-tagging uncertainties. These are of a similar magnitude as the ISR/FSR uncertainty. The systematic uncertainty from the MC statistical uncertainties of each of the correction fractions is within the range 1–11% (25 GeV p_{T} threshold) and becomes significant (40%) in events with 7(6) jets for the 60 (80) GeV p_{T} thresholds. Statistical uncertainties from the data are not dominant in any region.

The systematic uncertainties on the jet p_{T} spectra are 10–16% and increase with p_{T} except for the lowest jet p_{T} bin. There are many sources of uncertainties of approximately 2–7% depending on jet p_{T}. For example, there are uncertainties from the b-jet related

JHEP01(2015)020

systematic uncertainties, i.e. uncertainty on the b-jet energy scale (2–5%) and the b-tagging efficiency (4–7%), the uncertainty on the W+jets background (2–8% each for normalisation and flavour composition), and the uncertainty components of the jet energy calibration related to the detector, the close-by jet correction and the intercalibration (each 1–3%). The statistical error rises with jet p_{T} and with the order of the jet for a given jet p_{T} bin. The lowest values are 1.5% and the highest are 14%, which is only slightly smaller than the systematic uncertainty.

7.4 Combination of lepton channels

The particle-level jet multiplicity and jet p_{T} spectra were combined by using the Best Linear Unbiased Estimate (BLUE) method [65, 66] to build the average cross section of the two channels. The BLUE method determines the coefficients (weights) to be used in a linear combination of the input measurements by minimising the total uncertainty of the combined result. All uncertainties were assumed to be distributed according to a Gaussian probability density function. The algorithm takes both statistical and systematic uncertainties and their correlations into account. The BLUE combination was cross-checked against an average performed using the algorithm discussed in [67]. The two methods were found to agree within their uncertainties. The averaging procedure was also used to probe the compatibility of the electron and the muon channel, resulting in a $\chi^2/dof \approx 1$.

The systematic uncertainties related to the measurements of the leptons, the multijet-background normalisation and the overall W+jets background normalisation were treated as uncorrelated between the two channels, but bin-to-bin correlated within one channel. The data selected with the two different lepton event selections constitute independent samples, for which the multijet and overall W+jets normalisation were determined separately. The MC statistical uncertainties on the correction factors for the two samples were also assumed to be uncorrelated. All other systematic uncertainties were treated as fully correlated.

The uncertainty of the combined jet multiplicity measurement at low values is dominated by the uncorrelated background sources that are smaller in the muon channel than in the electron channel, due to the smaller multijet background in the muon channel (see section 7.3). The uncertainty of the combined result is therefore similar to the uncertainty of the muon channel result itself. At high multiplicity, the uncertainty is dominated by correlated sources, such as the uncertainty on the jet energy scale and model uncertainties of fragmentation and colour reconnection. The combined cross-section measurement has a 3% uncertainty improvement with respect to the muon channel result and approximately a 20% improvement with respect to the electron channel result.

The uncertainty of the cross-section measurements as a function of jet p_{T} are about 20% smaller in the muon channel measurement than in the electron-channel measurement, because of the significantly smaller uncertainty on the muon identification and energy scale compared to electrons. Therefore, the data selected in the muon channel have a statistically higher impact on the combined results. The uncertainty on the combined jet p_{T} measurements is 7–14% for the leading jet and up to 17% for the highest p_{T} region of the other jets. This corresponds to an uncertainty improvement of 15–30%, compared to the

JHEP01(2015)020

uncertainty on the electron channel measurement and 4–7% compared to the uncertainty on the muon-channel measurement.

A summary of systematic uncertainty components, statistical uncertainty and the total uncertainty after the channel combination is given in appendix C.

8 Results

The result of the combinations of the fully-corrected distributions for jet multiplicity and p_{T} were converted into fiducial cross-section measurements using $\sigma^{\mathrm{fid}}(n_{\mathrm{jet}}) = \frac{N(n_{\mathrm{jet,part}})}{\int L\mathrm{d}t}$ and $\sigma^{\mathrm{fid}}(p_{\mathrm{T}}) = \frac{N(p_{\mathrm{T,part}})}{\int L\mathrm{d}t}$, where $\int L\mathrm{d}t$ is the integrated luminosity, $N(n_{\mathrm{jet,part}})$ represents the fully-corrected distributions for the number of particle jets, $N(p_{\mathrm{T,part}})$ is the fully-corrected distribution of the number of jets as a function of p_{T} for each p_{T}-ordered distribution, and $\sigma^{\mathrm{fid}}(n_{\mathrm{jet}})$ and $\sigma^{\mathrm{fid}}(p_{\mathrm{T}})$ are the differential fiducial cross-sections.

The fully corrected fiducial $t\bar{t}$ production cross-section is shown as a function of jet multiplicity for the jet p_{T} thresholds of 25, 40, 60, and 80 GeV in figures 6 and 7 and as a function of the jet p_{T} in figures 8–10. Tabulated results with systematic uncertainties are given in appendix C. In these figures, the data are compared to predictions from POWHEG+PYTHIA, POWHEG(h_{damp})+PYTHIA with varied amount of hard radiation, ALPGEN+HERWIG and ALPGEN+PYTHIA with α_{S} variations, MC@NLO +HERWIG and the POWHEG+PYTHIA MC models.

The MC@NLO+HERWIG model is seen to be disfavoured by the jet-multiplicity spectra, since it predicts too few events with six or more $p_{\mathrm{T}} > 25$ GeV jets. This disagreement is visible for the higher jet p_{T} thresholds for events with five or more jets, although with less significance due to the larger uncertainty in these measurements. The ALPGEN+PYTHIA α_{S}-down variation is seen to best describe the data. The ALPGEN+HERWIG curve produces up to 20% more jets than the observed jet multiplicity which is slightly above the experimental uncertainty band.

The ALPGEN+PYTHIA α_{S}-up variation and the central tune are found to be disfavoured by the jet-multiplicity measurements. The ALPGEN+PYTHIA α_{S}-up variation deviates from data with five or more jets with $p_{\mathrm{T}} > 25$ GeV in the final state, whereas the ALPGEN+PYTHIA central sample deviates in the case of events with six or more jets with $p_{\mathrm{T}} > 25$ GeV. Similar disagreements are seen at higher jet p_{T} thresholds. The MC@NLO+HERWIG predictions underestimate the cross-section for six jets in the $t\bar{t}$ final state. The underestimate of the higher jet multiplicity bins for MC@NLO compared to ALPGEN is also observed in [13], where the difference is explained by a significantly smaller contribution of the $t\bar{t}+q(g)$ hard matrix-element calculation to the multijet final-states and a higher fraction of additional jets from the parton shower [13].

In contrast to MC@NLO, the prediction from POWHEG+PYTHIA is in reasonable agreement with the data for all jet p_{T} thresholds and jet multiplicities. POWHEG(h_{damp}) +PYTHIA provides the best description of the leading-jet p_{T} and the higher jet multiplicities. However, due to the damping of the hardest emissions, POWHEG(h_{damp})+PYTHIA predicts a softer 5^{th} jet p_{T} spectrum and a correspondingly slightly lower jet multiplicity spectrum for the 80 GeV threshold.

JHEP01(2015)020

As shown in figures 8 to 10, all models predict a similar cross-section as a function of jet p_{T} below approximately 100 GeV for the four leading jets. However, the ISR/FSR model variations differ significantly for higher jet p_{T} and for the full p_{T} spectrum of the 5$^{\mathrm{th}}$ leading jet. The conclusions drawn from the 5$^{\mathrm{th}}$ jet comparisons of data versus predictions are similar to the ones from the jet multiplicity measurements: the MC@NLO+HERWIG MC program generates a p_{T} spectrum that is softer than the observed data. The detailed study of POWHEG+PYTHIA in [14] shows that the probability of the emission at high p_{T} largely depends on the modelling of the ISR evolution and its upper limit of the virtuality on the ISR parton. The setting used in this analysis yields slightly higher predictions than the observed data, which could potentially be improved by tuning the free parameters of the ISR model. The ALPGEN+PYTHIA α_{S} variations demonstrate the sensitivity of the predictions to the value of α_{S} used in the calculation of the hard matrix element and the parton shower. All ISR variations are higher than the data, where α_{S}-down provides the best description.

9 Conclusions

The fiducial $t\bar{t}$ production cross-section in pp collisions at 7 TeV is presented as a function of the jet multiplicity for up to eight jets with jet p_{T} thresholds of 25, 40, 60, and 80 GeV using 4.6 fb^{-1} of data. The precision of the measurement is between approximately 10% and 30%, with the largest uncertainty at highest jet multiplicity. The fiducial $t\bar{t}$ production cross-section is shown as a function of the jet p_{T} separately for each jet up to the fifth jet. The measured jet p_{T} spectra have a precision between approximately 10% and 16%. The measurement precision is limited in most kinematic regions by systematic uncertainties, from background modelling (at lower jet multiplicities) to jet energy scale (at higher jet multiplicities).

The conclusions drawn from the comparisons of data versus theory predictions are similar at high jet multiplicity, high leading jet p_{T} and in the full spectrum of the 5$^{\mathrm{th}}$ jet. The presented measurements have discriminating power for MC model predictions. At high jet multiplicities, which are dominated by parton-shower emissions, MC@NLO is disfavoured by the data. A similar finding applies to the additional jet p_{T} distributions, which are too soft at high p_{T}. In contrast, predictions from POWHEG showered with PYTHIA are consistent with the data within the total uncertainties of the measurements. This agreement can be further improved by limiting the hard radiations in POWHEG using free model parameters.

The comparison to different α_{S} settings using the ALPGEN+PYTHIA sample indicates that the data prefer a softer parton-shower, i.e. a smaller value of α_{S}. The prediction of ALPGEN+HERWIG that uses a similar α_{S} in the matrix-element calculation as the lower α_{S} ALPGEN+PYTHIA configuration also yields a similar good agreement with the data. For the lowest jet p_{T} threshold the multiplicity distribution of the lower α_{S} ALPGEN+PYTHIA configuration is closest to the data. However, at high leading jet p_{T} the model predictions that describe the higher jet multiplicities well are at the upper limit

JHEP01(2015)020

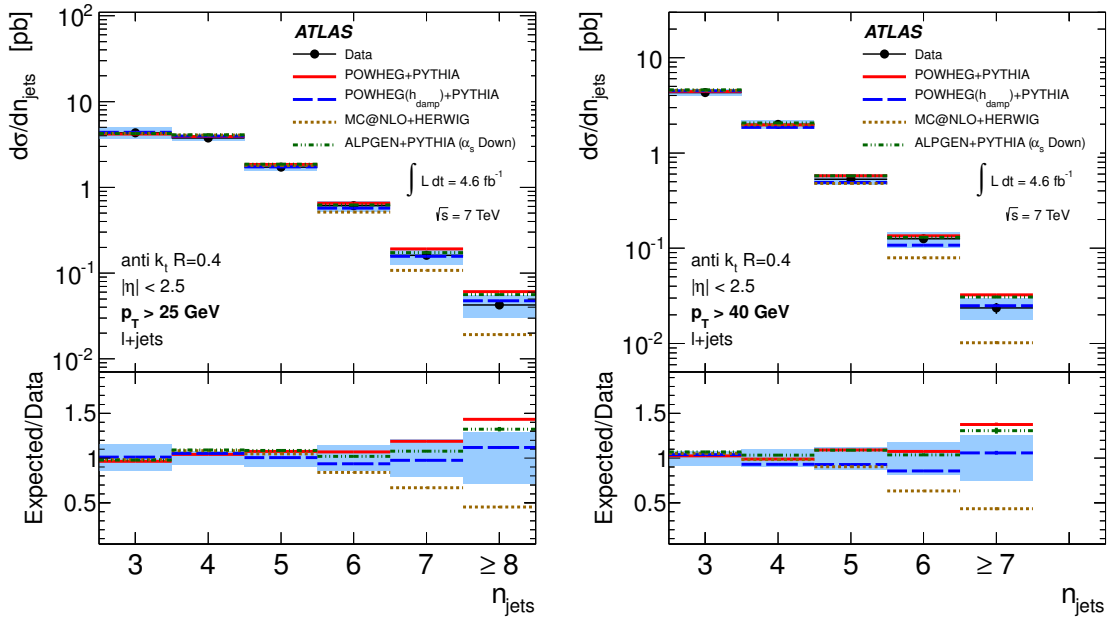

(a) $p_{\mathrm{T}} > 25$ GeV

(b) $p_{\mathrm{T}} > 40$ GeV

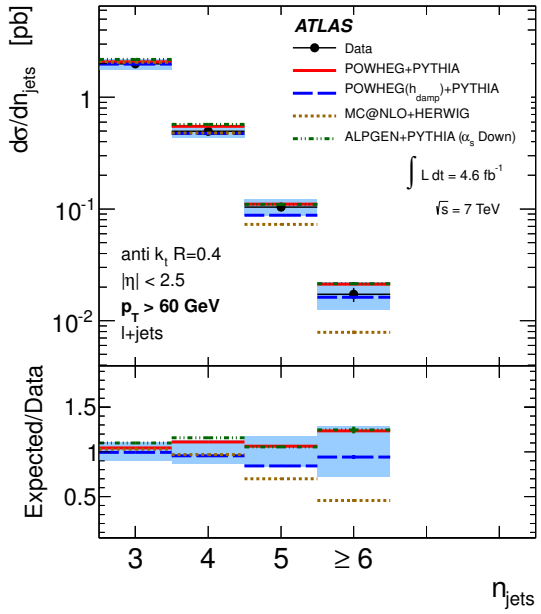

(c) $p_{\mathrm{T}} > 60$ GeV

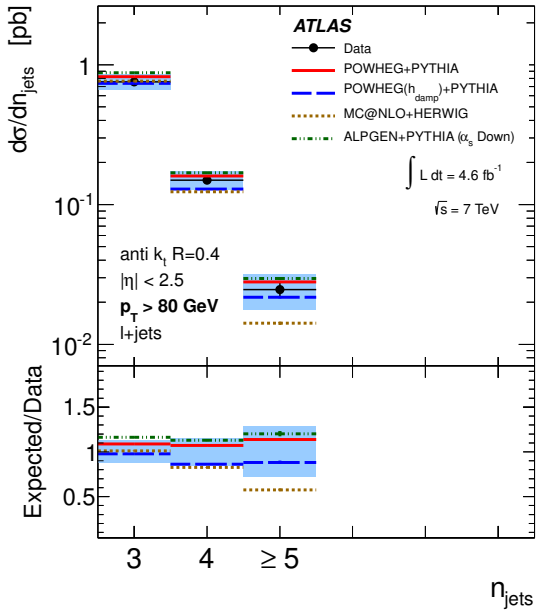

(d) $p_{\mathrm{T}} > 80$ GeV

Figure 6. The $t\bar{t}$ cross-section as a function of the jet multiplicity for the average of the electron and muon channels for the jet p_{T} thresholds (a) 25, (b) 40, (c) 60, and (d) 80 GeV. The data are shown in comparison to different NLO ME generators POWHEG+PYTHIA, POWHEG(h_{damp})+PYTHIA, MC@NLO+HERWIG and to the best predictions of the LO multi-leg generators, ALPGEN+PYTHIA (α_{S} down). The data points and their corresponding total statistical and systematic uncertainties added in quadrature is shown as a shaded band. The MC predictions are shown with their statistical uncertainty.

JHEP01(2015)020

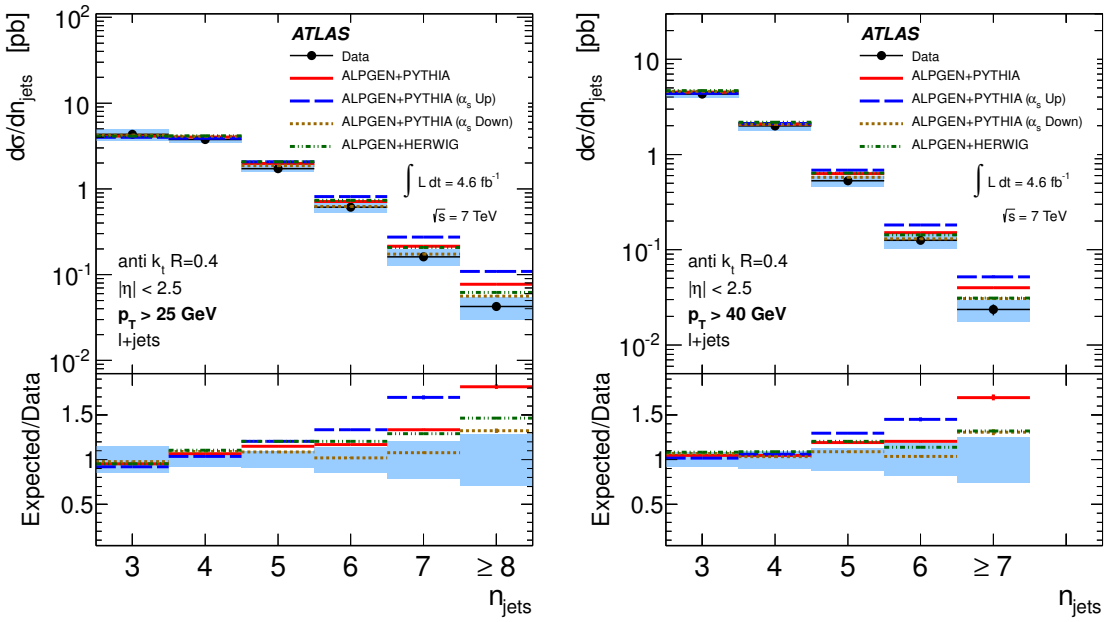

(a) $p_{\mathrm{T}} > 25$ GeV

(b) $p_{\mathrm{T}} > 40$ GeV

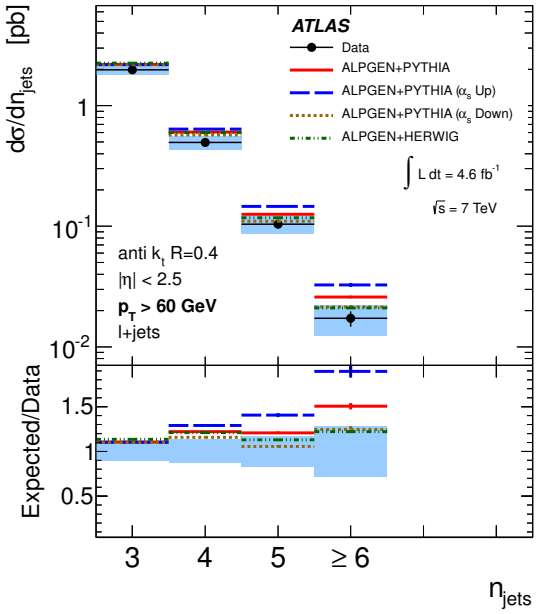

(c) $p_{\mathrm{T}} > 60$ GeV

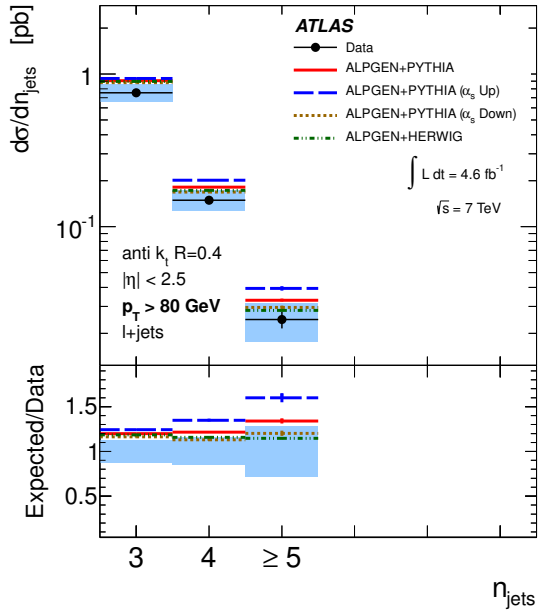

(d) $p_{\mathrm{T}} > 80$ GeV

Figure 7. The $t\bar{t}$ cross-section as a function of the jet multiplicity for the average of the electron and muon channels for the jet p_{T} thresholds (a) 25, (b) 40, (c) 60, and (d) 80 GeV. The data are shown in comparison to the ALPGEN+PYTHIA, ALPGEN+PYTHIA ISR/FSR scale variations and ALPGEN+HERWIG. The data points and their corresponding total statistical and systematic uncertainties added in quadrature is shown as a shaded band. The MC predictions are shown with their statistical uncertainty.

JHEP01(2015)020

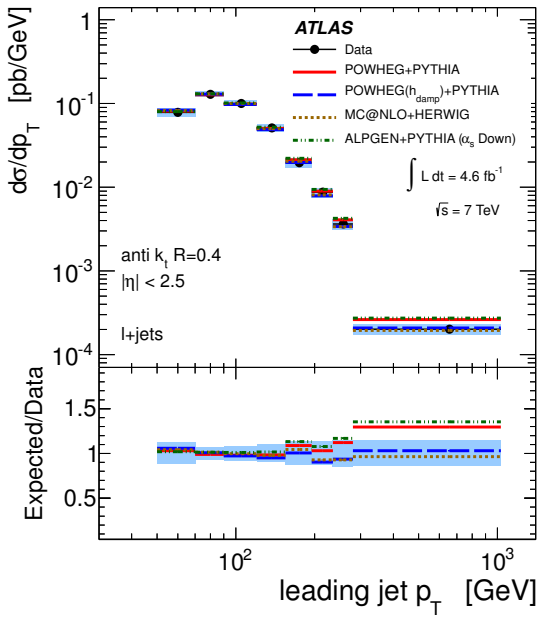

(a) $p_{\mathrm{T}} > 25$ GeV, leading jet

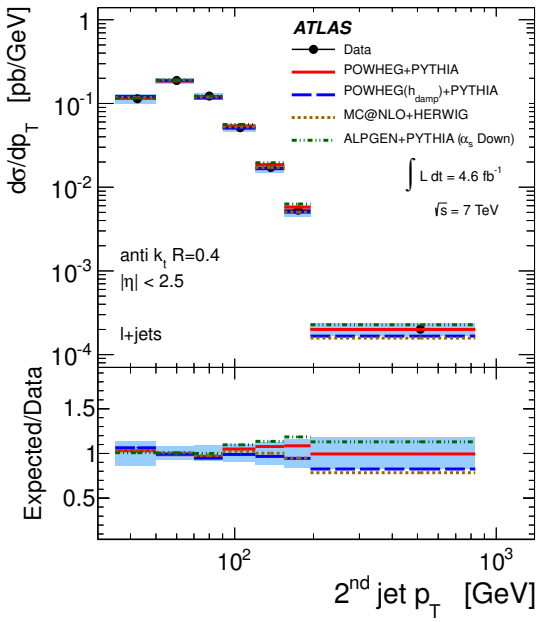

(b) $p_{\mathrm{T}} > 25$ GeV, 2nd jet

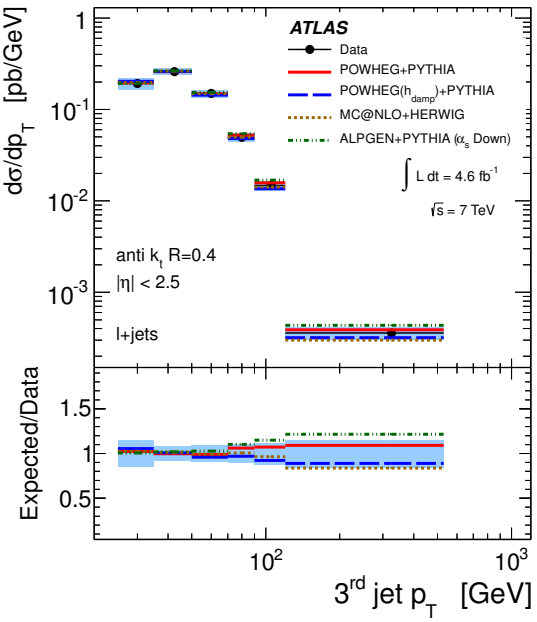

(c) $p_{\mathrm{T}} > 25$ GeV, 3rd jet

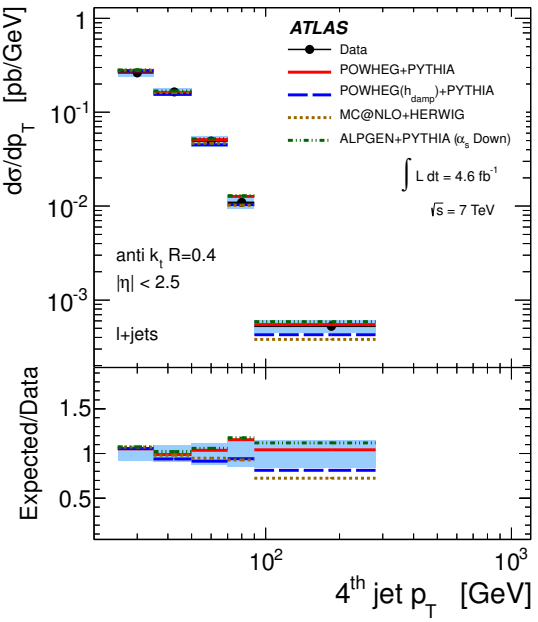

(d) $p_{\mathrm{T}} > 25$ GeV, 4th jet

Figure 8. The $t\bar{t}$ cross-section as a function of the jet p_{T} for the average of the electron and muon channels for the (a) leading, (b) 2nd, (c) 3rd, and (d) 4th jet. The data are shown in comparison to different NLO ME generators POWHEG+PYTHIA, POWHEG(h_{damp})+PYTHIA, MC@NLO+HERWIG and to the best predictions of the LO multi-leg generators, ALPGEN+PYTHIA (α_{S} down). The data points and their corresponding total statistical and systematic uncertainties added in quadrature is shown as a shaded band. The MC predictions are shown with their statistical uncertainty.

JHEP01(2015)020

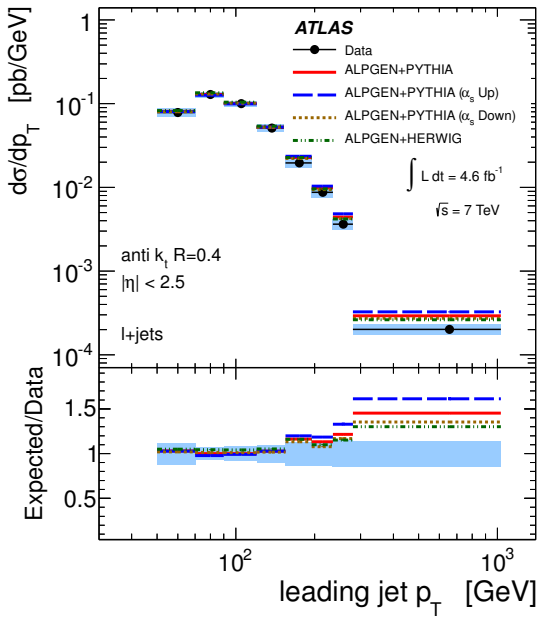

(a) $p_{\mathrm{T}} > 25$ GeV, leading jet

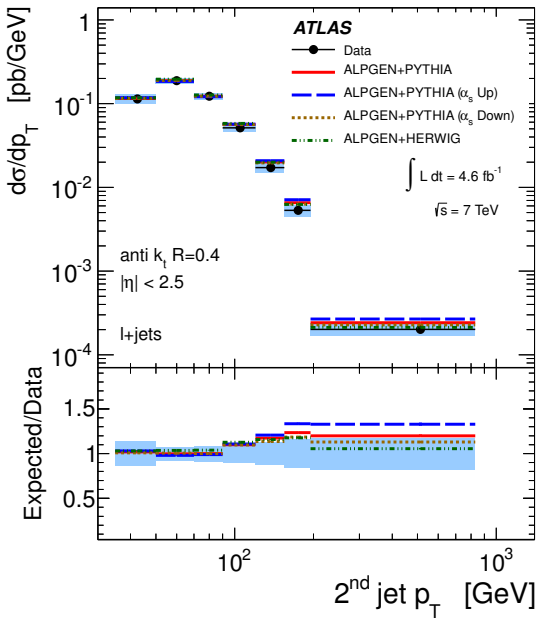

(b) $p_{\mathrm{T}} > 25$ GeV, 2nd jet

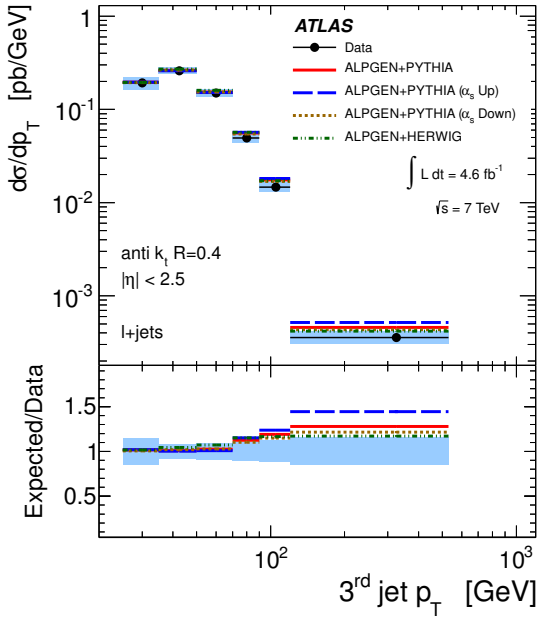

(c) $p_{\mathrm{T}} > 25$ GeV, 3rd jet

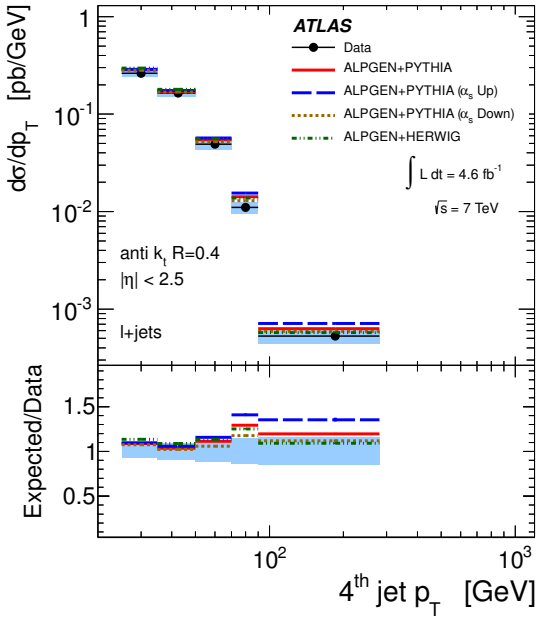

(d) $p_{\mathrm{T}} > 25$ GeV, 4th jet

Figure 9. The $t\bar{t}$ cross-section as a function of the jet p_{T} for the average of the electron and muon channels for the (a) leading, (b) 2nd, (c) 3rd, and (d) 4th jet. The data are shown in comparison to the ALPGEN+PYTHIA, ALPGEN+PYTHIA ISR/FSR scale variations and ALPGEN+HERWIG. The data points and their corresponding total statistical and systematic uncertainties added in quadrature is shown as a shaded band. The MC predictions are shown with their statistical uncertainty.

JHEP01(2015)020

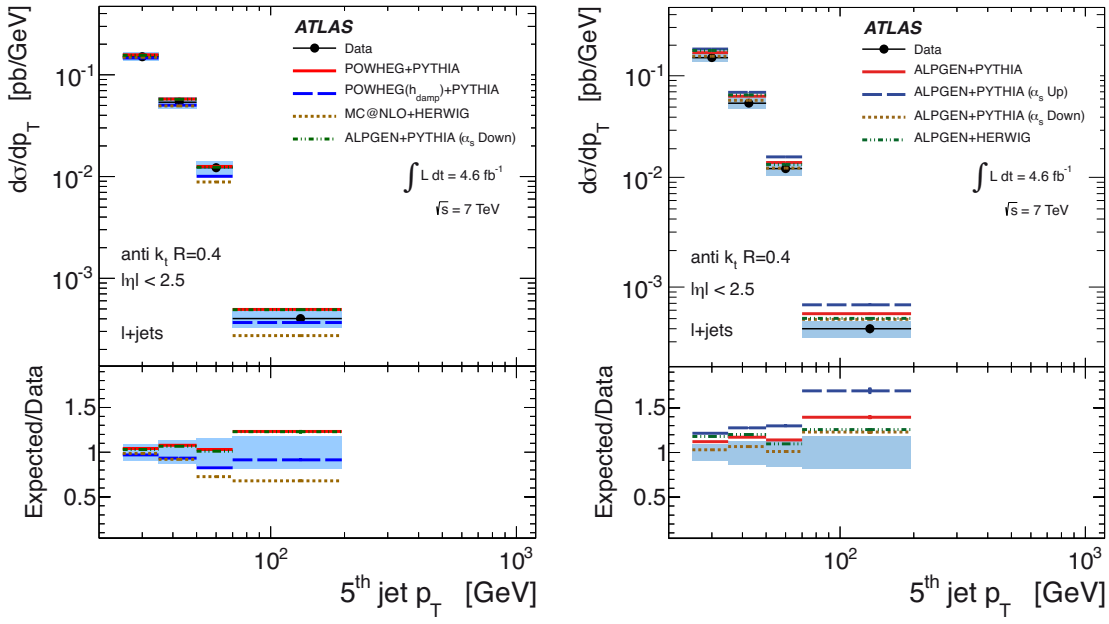

(a) (b)

Figure 10. The $t\bar{t}$ cross-section as a function of the jet p_{T} for the average of the electron and muon channels for the 5th jet. The data are shown in comparison to (a) POWHEG+PYTHIA, POWHEG(h_{damp})+PYTHIA, MC@NLO+HERWIG and ALPGEN+PYTHIA (α_{S} down) predictions and in comparison to (b) the ALPGEN+PYTHIA, ALPGEN+PYTHIA ISR/FSR variations and ALPGEN+HERWIG. The data points and their corresponding total statistical and systematic uncertainties added in quadrature is shown as a shaded band. The MC predictions are shown with their statistical uncertainty.

of the uncertainty band or above the data. Only POWHEG with reduced hard radiation is able to describe both observables consistently with high accuracy.

The present measurements provide important tests of higher-order QCD effects in $t\bar{t}$ production at the LHC. They provide important inputs for MC developments, in particular for the recent developments of NLO QCD calculations of $t\bar{t}$+jets matched to parton-shower algorithms as discussed in [68]. An improved understanding in this area is highly important for searches for new particles or new interactions.

Acknowledgments

We thank CERN for the very successful operation of the LHC, as well as the support staff from our institutions without whom ATLAS could not be operated efficiently.

We acknowledge the support of ANPCyT, Argentina; YerPhI, Armenia; ARC, Australia; BMWFW and FWF, Austria; ANAS, Azerbaijan; SSTC, Belarus; CNPq and FAPESP, Brazil; NSERC, NRC and CFI, Canada; CERN; CONICYT, Chile; CAS, MOST and NSFC, China; COLCIENCIAS, Colombia; MSMT CR, MPO CR and VSC CR, Czech Republic; DNRF, DNSRC and Lundbeck Foundation, Denmark; EPLANET, ERC and NSRF, European Union; IN2P3-CNRS, CEA-DSM/IRFU, France; GNSF, Georgia;

JHEP01(2015)020

BMBF, DFG, HGF, MPG and AvH Foundation, Germany; GSRT and NSRF, Greece; ISF, MINERVA, GIF, I-CORE and Benoziyo Center, Israel; INFN, Italy; MEXT and JSPS, Japan; CNRST, Morocco; FOM and NWO, Netherlands; BRF and RCN, Norway; MNiSW and NCN, Poland; GRICES and FCT, Portugal; MNE/IFA, Romania; MES of Russia and ROSATOM, Russian Federation; JINR; MSTD, Serbia; MSSR, Slovakia; ARRS and MIZŠ, Slovenia; DST/NRF, South Africa; MINECO, Spain; SRC and Wallenberg Foundation, Sweden; SER, SNSF and Cantons of Bern and Geneva, Switzerland; NSC, Taiwan; TAEK, Turkey; STFC, the Royal Society and Leverhulme Trust, United Kingdom; DOE and NSF, United States of America.

The crucial computing support from all WLCG partners is acknowledged gratefully, in particular from CERN and the ATLAS Tier-1 facilities at TRIUMF (Canada), NDGF (Denmark, Norway, Sweden), CC-IN2P3 (France), KIT/GridKA (Germany), INFN-CNAF (Italy), NL-T1 (Netherlands), PIC (Spain), ASGC (Taiwan), RAL (U.K.) and BNL (U.S.A.) and in the Tier-2 facilities worldwide.

JHEP01(2015)020

A Reconstruction-level results

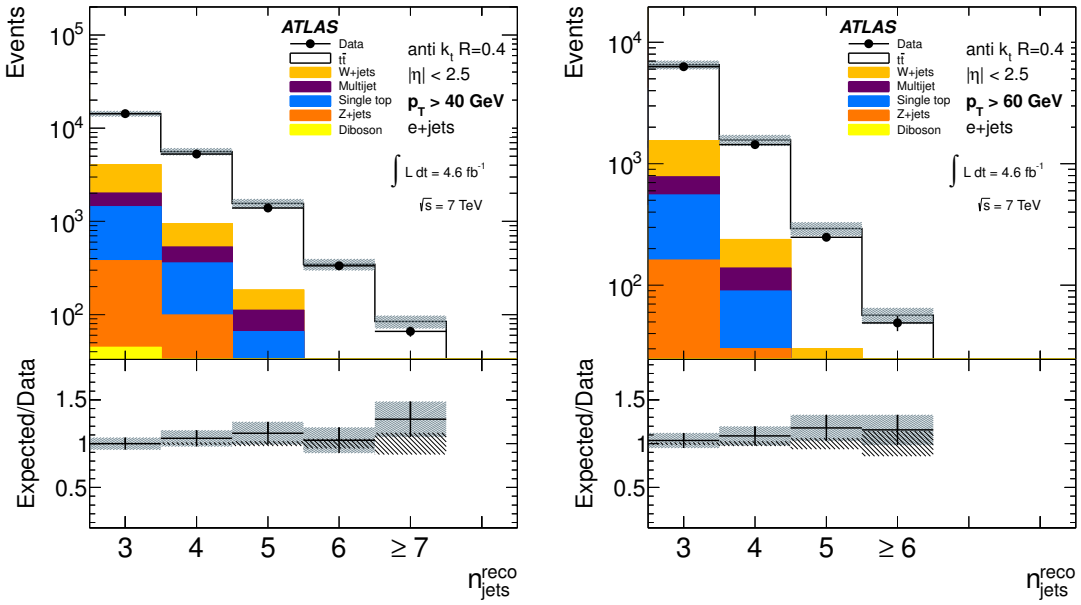

(a) $e+$jets, $p_{\mathrm{T}} > 40$ GeV

(b) $e+$jets, $p_{\mathrm{T}} > 60$ GeV

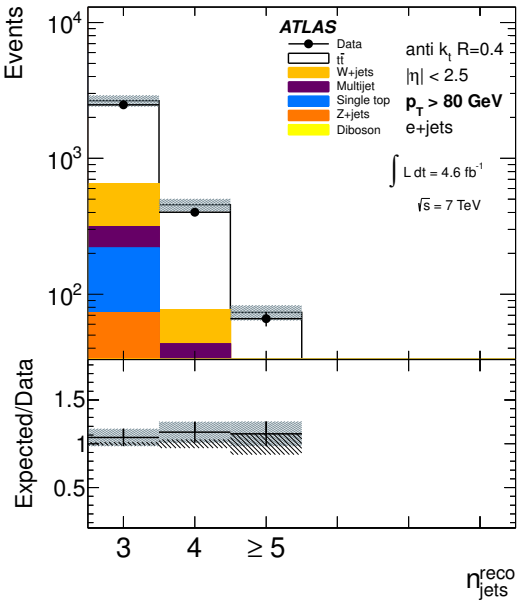

(c) $e+$jets, $p_{\mathrm{T}} > 80$ GeV

Figure 11. The reconstructed jet multiplicities in the electron ($e+$jets) channel for the jet p_{T} thresholds (a) 40, (b) 60, and (c) 80 GeV. The data are compared to the sum of the $t\bar{t}$ POWHEG+PYTHIA MC signal prediction and the background models. The shaded bands show the total systematic and statistical uncertainties on the combined signal and background estimate. The errors bar on the black points and the hatched area in the ratio, show the statistical uncertainty on the data measurements.

JHEP01(2015)020

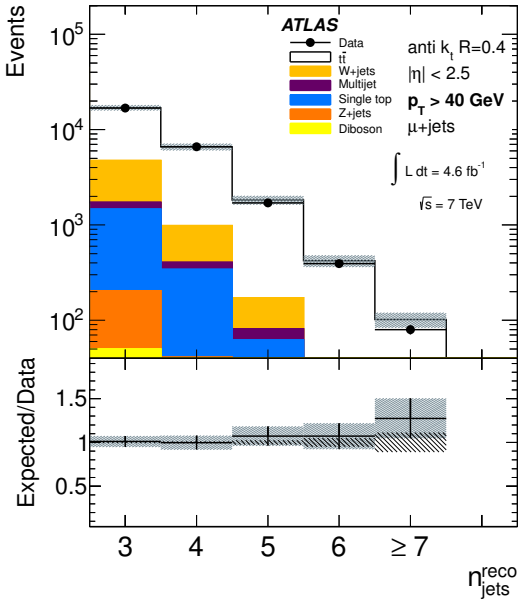

(a) $\mu+$jets, $p_{\mathrm{T}} > 40$ GeV

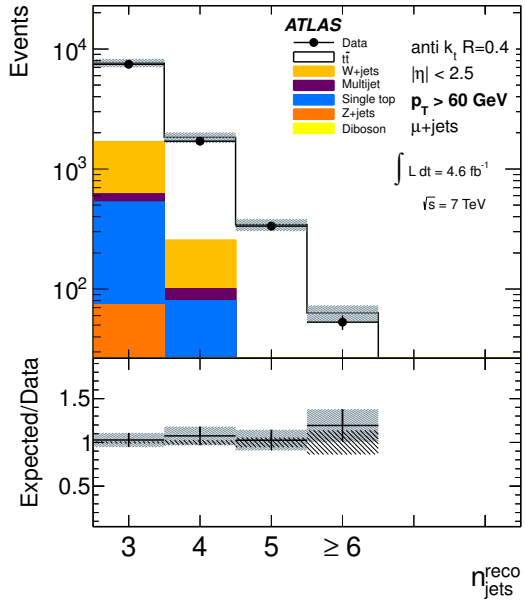

(b) $\mu+$jets, $p_{\mathrm{T}} > 60$ GeV

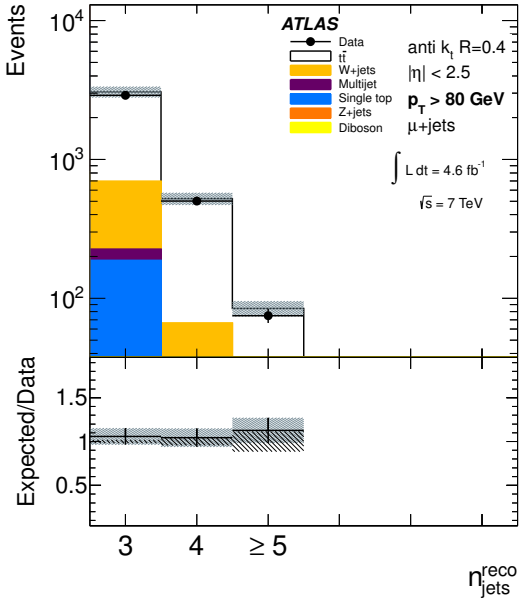

(c) $\mu+$jets, $p_{\mathrm{T}} > 80$ GeV

Figure 12. The reconstructed jet multiplicities in the muon (μ + jets) channel for the jet p_{T} thresholds (a) 40, (b) 60, and (c) 80 GeV. The data are compared to the sum of the $t\bar{t}$ POWHEG+PYTHIA MC signal prediction and the background models. The shaded bands show the total systematic and statistical uncertainties on the combined signal and background estimate. The errors bar on the black points and the hatched area in the ratio, show the statistical uncertainty on the data measurements.

JHEP01(2015)020

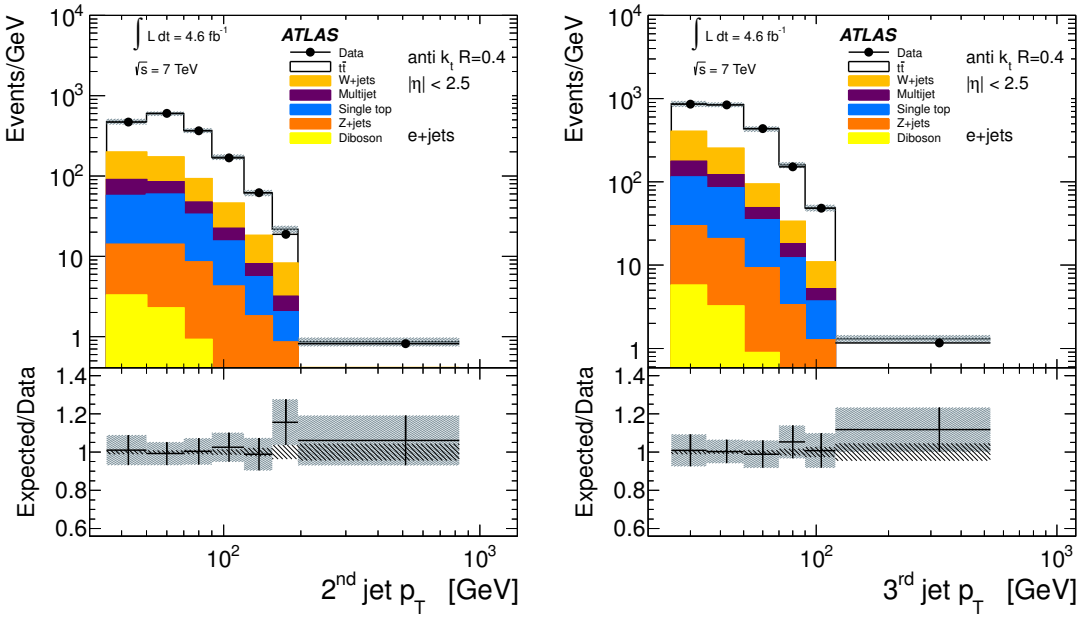

(a) $e+\text{jets}$, $p_{\mathrm{T}} > 25$ GeV, 2^{nd} jet

(b) $e+\text{jets}$, $p_{\mathrm{T}} > 25$ GeV, 3^{rd} jet

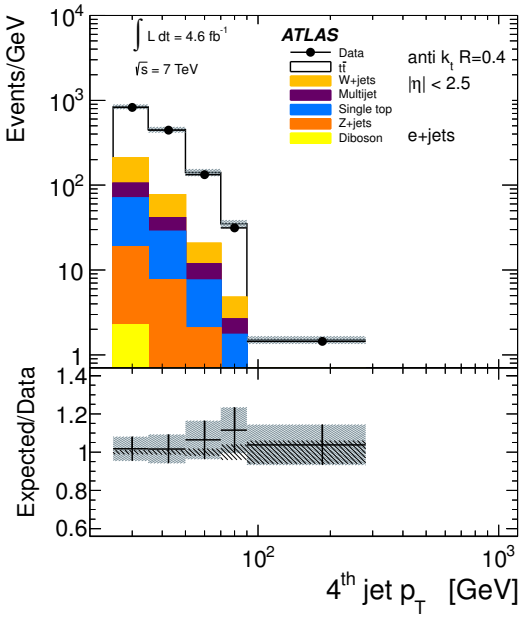

(c) $e+\text{jets}$, $p_{\mathrm{T}} > 25$ GeV, 4^{th} jet

Figure 13. The reconstructed jet p_{T} for the 2^{nd} (a), 3^{th} (b) and 4^{th} (c) jets in the electron ($e+\text{jets}$) channel. The data are compared to the sum of the $t\bar{t}$ POWHEG+PYTHIA MC signal prediction and the background models. The shaded bands show the total systematic and statistical uncertainties on the combined signal and background estimate. The errors bar on the black points and the hatched area in the ratio, show the statistical uncertainty on the data measurements.

JHEP01(2015)020

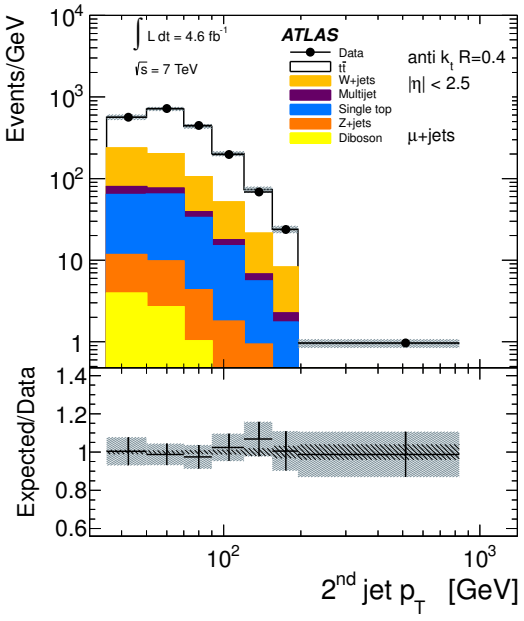

(a) $\mu+$jets, $p_{\mathrm{T}} > 25$ GeV, 2^{nd} jet

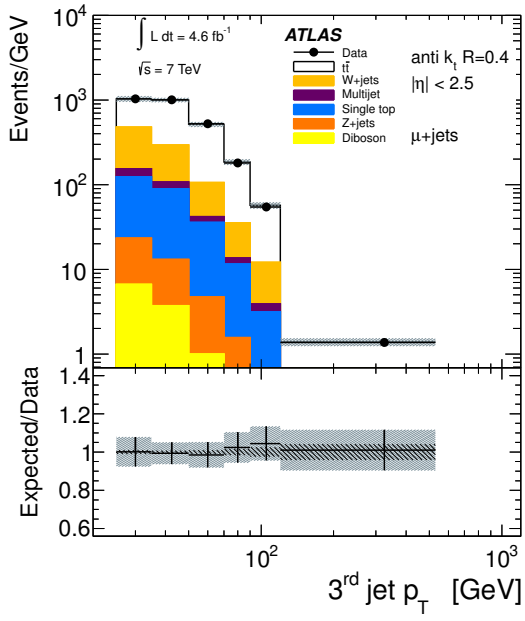

(b) $\mu+$jets, $p_{\mathrm{T}} > 25$ GeV, 3^{rd} jet

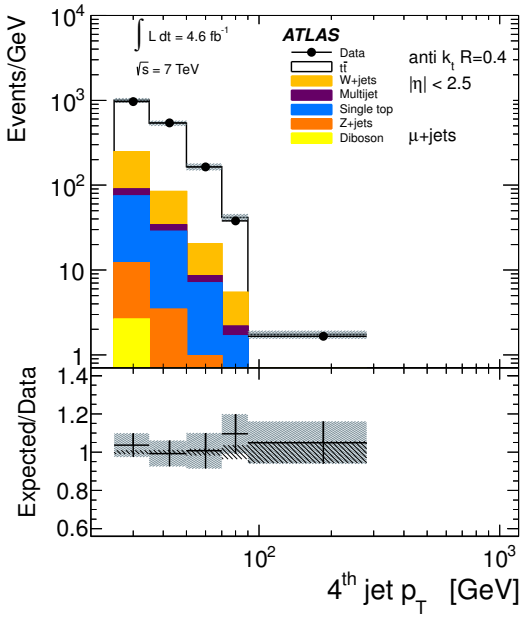

(c) $\mu+$jets, $p_{\mathrm{T}} > 25$ GeV, 4^{th} jet

Figure 14. The reconstructed jet p_{T} for the 2^{nd} (a), 3^{th} (b) and 4^{th} (c) jets in the muon ($\mu+$ jets) channel. The data are compared to the sum of the $t\bar{t}$ POWHEG+PYTHIA MC signal prediction and the background models. The shaded bands show the total systematic and statistical uncertainties on the combined signal and background estimate. The errors bar on the black points and the hatched area in the ratio, show the statistical uncertainty on the data measurements.

JHEP01(2015)020

B Global correction factors

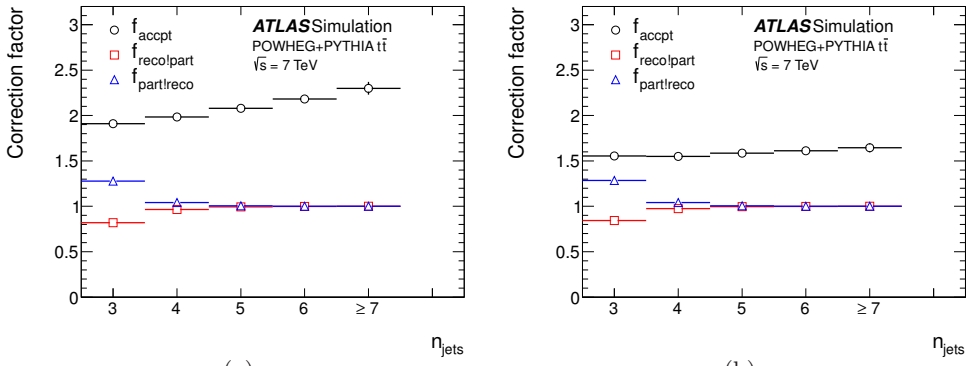

Figure 15. Global correction factors used in the unfolding of jets with $p_{\mathrm{T}} > 40$ GeV to particle level in the electron (a) and muon (b) channel as described in the text and in eq. (7.1). The axis label n_{jets} refers to the number of particle-level jets for $f_{\mathrm{part!reco}}$ and to the number of reconstructed jets in the case of f_{accpt} and $f_{\mathrm{reco!part}}$.

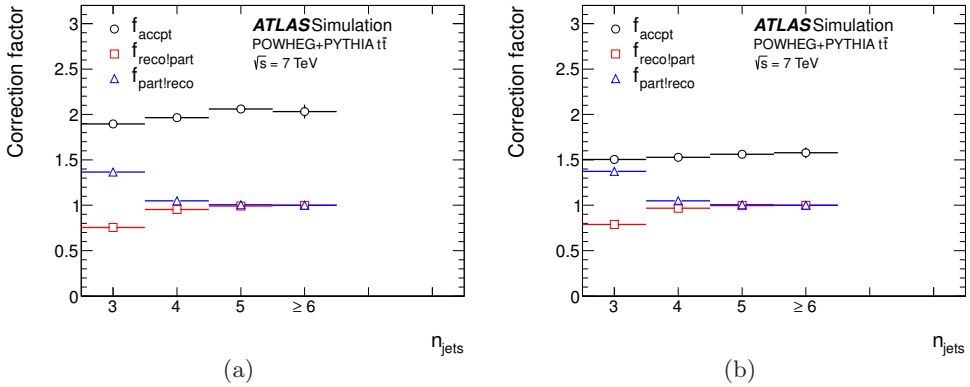

Figure 16. Global correction factors used in the unfolding of jets with $p_{\mathrm{T}} > 60$ GeV to particle level in the electron (a) and muon (b) channel as described in the text and in eq. (7.1). The axis label n_{jets} refers to the number of particle-level jets for $f_{\mathrm{part!reco}}$ and to the number of reconstructed jets in the case of f_{accpt} and $f_{\mathrm{reco!part}}$.

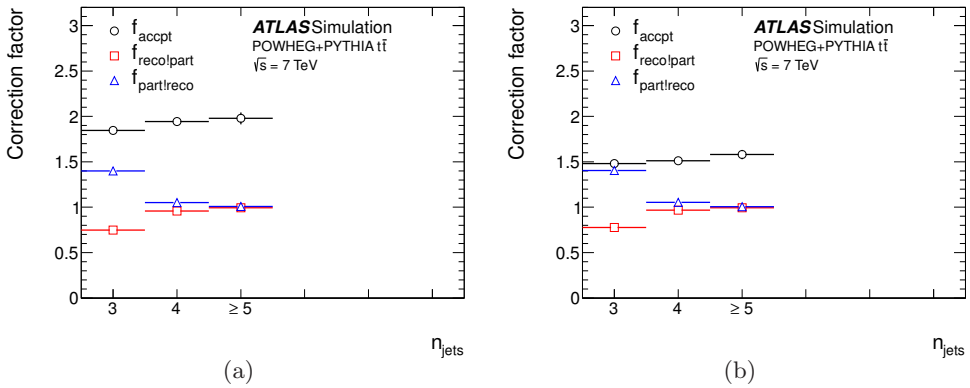

Figure 17. Global correction factors used in the unfolding of jets with $p_{\mathrm{T}} > 80$ GeV to particle level in the electron (a) and muon (b) channel as described in the text and in eq. (7.1). The axis label n_{jets} refers to the number of particle-level jets for $f_{\mathrm{part!reco}}$ and to the number of reconstructed jets in the case of f_{accpt} and $f_{\mathrm{reco!part}}$.

JHEP01(2015)020

C Tables of results with systematic uncertainties

$\frac{d\sigma}{dn_{\text{jets}}}$ [%] / n_{jets}	3	4	5	6	7	≥ 8
MC statistics	0.5	0.5	0.9	1.8	2.0	3.4
PDF	1.2	0.8	2.4	3.8	5.0	5.2
MC generator	0.9	0.5	0.7	1.6	1.5	2.2
Fragmentation	2.5	0.3	0.6	2.5	6.5	8.1
ISR/FSR	2.9	2.8	1.4	2.6	3.5	5.5
Colour reconnection	1.4	0.2	0.2	3.5	4.0	4.4
ℓ resolution & efficiency	0.3	0.3	0.4	0.4	0.3	0.7
$E_{\text{T}}^{\text{miss}}$ cell-out	0.2	0.2	0.2	0.1	0.4	0.4
b-quark tagging efficiency	4.3	3.8	3.5	3.6	3.4	3.6
Additional interactions	0.1	0.1	0.1	0.1	0.4	0.2
Jet reconstruction efficiency	0.0	0.0	0.0	0.2	0.1	0.3
Jet energy resolution	1.2	0.7	1.2	2.9	4.0	8.8
b-quark jets (JES)	0.1	1.0	1.3	1.4	1.4	1.7
Close by jets (JES)	2.4	1.2	3.9	5.9	9.6	14.5
Effective detector NP set 1 (JES)	0.6	0.5	1.3	1.7	2.3	3.2
Effective detector NP set 2 (JES)	0.0	0.0	0.1	0.2	0.2	0.5
Effective mixed NP set 1 (JES)	0.0	0.0	0.1	0.2	0.2	0.4
Effective mixed NP set 2 (JES)	0.3	0.2	0.5	0.8	0.8	1.7
Effective model NP set 1 (JES)	1.7	1.1	3.2	4.3	5.9	9.4
Effective model NP set 2 (JES)	0.1	0.0	0.1	0.2	0.2	0.5
Effective model NP set 3 (JES)	0.1	0.0	0.1	0.1	0.0	0.3
Effective model NP set 4 (JES)	0.0	0.0	0.1	0.1	0.1	0.4
Effective stat. NP set 1 (JES)	1.0	0.6	1.8	2.4	3.3	5.7
Effective stat. NP set 2 (JES)	0.0	0.0	0.0	0.0	0.0	0.0
Effective stat. NP set 3 (JES)	0.1	0.1	0.2	0.3	0.3	1.0
η-intercalibration (JES)	1.2	0.8	2.2	3.1	4.3	6.4
η-intercalibration statistics (JES)	0.4	0.3	0.7	1.1	1.4	2.3
Flavour composition (JES)	0.6	0.8	1.0	1.8	2.9	2.2
Flavour response (JES)	1.9	0.3	2.0	5.7	10.3	7.2
Additional interactions μ (JES)	0.1	0.3	0.3	0.3	0.4	1.4
Additional interactions N_{PV} (JES)	0.2	0.1	0.2	0.5	0.8	2.4
Relative non-closure (JES)	0.3	0.2	0.6	0.8	0.9	1.6
Single particle high-p_{T} (JES)	0.0	0.0	0.0	0.0	0.0	0.0
Jet vertex fraction efficiency	0.4	0.3	0.3	0.4	0.7	1.5
W+jets normalisation	5.2	1.9	1.6	0.9	0.6	0.9
W+jets heavy/light flavour	9.7	2.5	0.5	0.2	0.6	0.7
Multijet normalisation	1.4	0.4	0.3	0.6	0.5	2.3
Multijet shape	0.2	0.3	0.3	0.3	0.2	0.4
Small backgrounds	6.0	3.0	3.1	1.5	2.3	4.3
Luminosity	1.8	1.8	1.8	1.8	1.8	1.8
Total systematic uncertainty	14.7	7.3	9.0	13.6	20.5	25.3
Statistical uncertainty	1.4	1.3	2.2	4.0	4.4	10.2
Cross-section [pb]	4.34e+00	3.76e+00	1.72e+00	6.11e-01	1.61e-01	4.25e-02

Table 5. Relative uncertainties on the final differential cross-section after the e/μ channel combination, for the jet multiplicity using a 25 GeV jet p_{T} threshold. The uncertainties are shown as a percentage of the expected $t\bar{t}$ signal. The energy scale uncertainty (JES) is shown for each JES nuisance parameter (NP). The effective NP are obtained by combining a total of 54 detector, detector and model ("mixed"), modelling and statistical NPs. An uncertainty value of 0.0 implies that the uncertainty is below 0.05.

JHEP01(2015)020

$\frac{d\sigma}{dn_{\text{jets}}}$ [%] / n_{jets}	3	4	5	6	≥ 7
MC statistics	0.5	0.9	2.0	2.2	4.8
PDF	0.2	1.9	1.6	3.1	2.0
MC generator	1.1	0.7	0.2	0.9	5.6
Fragmentation	1.3	0.9	0.2	2.2	2.8
ISR/FSR	2.9	4.1	0.3	6.3	6.0
Colour reconnection	0.6	0.5	1.1	1.5	2.0
ℓ resolution & efficiency	0.3	0.4	0.5	0.5	0.9
$E_{\text{T}}^{\text{miss}}$ cell-out	0.2	0.2	0.4	0.1	0.9
b-quark tagging efficiency	3.9	3.7	3.8	3.1	4.2
Additional interactions	0.1	0.1	0.2	0.1	0.6
Jet reconstruction efficiency	0.0	0.0	0.0	0.0	0.1
Jet energy resolution	0.7	0.1	1.1	3.4	2.8
b-quark jets (JES)	1.4	2.5	2.5	2.9	3.0
Close by jets (JES)	0.7	4.6	7.0	10.8	14.8
Effective detector NP set 1 (JES)	0.4	1.7	2.3	3.1	3.5
Effective detector NP set 2 (JES)	0.1	0.1	0.1	0.3	0.7
Effective mixed NP set 1 (JES)	0.1	0.1	0.1	0.3	0.7
Effective mixed NP set 2 (JES)	0.1	0.3	0.4	0.7	0.7
Effective model NP set 1 (JES)	0.4	1.9	2.7	3.6	4.8
Effective model NP set 2 (JES)	0.1	0.3	0.5	0.7	1.0
Effective model NP set 3 (JES)	0.2	0.5	0.7	1.0	1.2
Effective model NP set 4 (JES)	0.1	0.1	0.2	0.4	0.7
Effective stat. NP set 1 (JES)	0.2	0.7	1.1	1.8	2.1
Effective stat. NP set 2 (JES)	0.1	0.1	0.2	0.3	0.8
Effective stat. NP set 3 (JES)	0.1	0.4	0.6	0.9	1.0
η-intercalibration (JES)	0.5	2.1	3.4	5.1	4.5
η-intercalibration statistics (JES)	0.1	0.5	0.8	1.1	1.4
Flavour composition (JES)	0.2	1.0	1.6	2.0	1.0
Flavour response (JES)	0.5	1.2	3.9	5.5	2.7
Additional interactions μ (JES)	0.1	0.1	0.3	0.3	1.0
Additional interactions N_{PV} (JES)	0.0	0.2	0.5	0.8	0.8
Relative non-closure (JES)	0.1	0.2	0.6	0.7	1.2
Single particle high-p_{T} (JES)	0.0	0.0	0.0	0.0	0.0
Jet vertex fraction efficiency	0.2	0.3	0.5	1.3	1.8
W+jets normalisation	2.4	1.5	1.1	0.4	1.1
W+jets heavy/light flavour	4.0	1.2	0.6	0.4	0.6
Multijet normalisation	0.5	0.4	0.6	0.3	1.0
Multijet shape	0.1	0.3	0.4	0.4	0.9
Small backgrounds	3.2	2.2	2.1	2.2	5.2
Luminosity	1.8	1.8	1.8	1.8	1.8
Total systematic uncertainty	8.2	9.5	11.5	17.6	21.9
Statistical uncertainty	1.2	2.2	4.5	5.1	13.1
Cross-section [pb]	4.31e+00	2.00e+00	5.29e-01	1.26e-01	2.36e-02

Table 6. Relative uncertainties on the final differential cross-section after the e/μ channel combination, for the jet multiplicity using a 40 GeV jet p_{T} threshold. The uncertainties are shown as a percentage of the expected $t\bar{t}$ signal. The energy scale uncertainty (JES) is shown for each JES nuisance parameter (NP). The effective NP are obtained by combining a total of 54 detector, detector and model ("mixed"), modelling and statistical NPs. An uncertainty value of 0.0 implies that the uncertainty is below 0.05.

JHEP01(2015)020

$\frac{d\sigma}{dn_{\text{jets}}}$ [%] / n_{jets}	3	4	5	≥ 6
MC statistics	0.8	1.2	2.8	5.9
PDF	0.6	2.1	0.8	0.8
MC generator	1.1	0.7	0.5	4.4
Fragmentation	1.2	1.1	0.4	4.1
ISR/FSR	4.9	5.3	7.4	14.6
Colour reconnection	0.4	1.4	4.2	3.1
ℓ resolution & efficiency	0.3	0.4	0.3	0.5
$E_{\text{T}}^{\text{miss}}$ cell-out	0.1	0.3	0.3	0.4
b-quark tagging efficiency	4.3	4.3	4.3	5.1
Additional interactions	0.1	0.2	0.3	0.6
Jet reconstruction efficiency	0.0	0.0	0.0	0.2
Jet energy resolution	0.1	0.9	3.0	0.8
b-quark jets (JES)	2.9	3.5	3.0	4.5
Close by jets (JES)	3.0	6.0	7.4	10.5
Effective detector NP set 1 (JES)	1.9	3.1	3.5	5.1
Effective detector NP set 2 (JES)	0.1	0.2	0.3	0.4
Effective mixed NP set 1 (JES)	0.1	0.2	0.4	0.4
Effective mixed NP set 2 (JES)	0.2	0.3	0.4	0.7
Effective model NP set 1 (JES)	1.2	1.8	2.0	4.0
Effective model NP set 2 (JES)	0.5	0.8	1.0	1.5
Effective model NP set 3 (JES)	0.7	1.0	1.3	1.8
Effective model NP set 4 (JES)	0.1	0.2	0.3	0.4
Effective stat. NP set 1 (JES)	0.2	0.4	0.4	1.1
Effective stat. NP set 2 (JES)	0.2	0.2	0.4	0.7
Effective stat. NP set 3 (JES)	0.5	0.7	0.9	1.5
η-intercalibration (JES)	2.0	3.2	4.4	5.9
η-intercalibration statistics (JES)	0.4	0.6	0.7	1.3
Flavour composition (JES)	0.8	1.4	1.8	1.7
Flavour response (JES)	0.4	2.4	3.7	2.7
Additional interactions μ (JES)	0.1	0.3	0.4	1.8
Additional interactions N_{PV} (JES)	0.2	0.3	0.7	1.0
Relative non-closure (JES)	0.3	0.5	0.8	1.1
Single particle high-p_{T} (JES)	0.0	0.0	0.0	0.0
Jet vertex fraction efficiency	0.1	0.7	0.6	1.0
W+jets normalisation	2.3	1.2	0.3	0.3
W+jets heavy/light flavour	3.0	1.3	0.0	0.0
Multijet normalisation	0.4	0.6	0.4	0.1
Multijet shape	0.2	0.3	0.2	0.4
Small backgrounds	3.0	3.4	2.6	4.0
Luminosity	1.8	1.8	1.8	1.8
Total systematic uncertainty	10.0	12.6	15.6	24.0
Statistical uncertainty	1.8	2.8	6.3	14.5
Cross-section [pb]	1.99e+00	4.95e-01	1.04e-01	1.72e-02

Table 7. Relative uncertainties on the final differential cross-section after the e/μ channel combination, for the jet multiplicity using a 60 GeV jet p_{T} threshold. The uncertainties are shown as a percentage of the expected $t\bar{t}$ signal. The energy scale uncertainty (JES) is shown for each JES nuisance parameter (NP). The effective NP are obtained by combining a total of 54 detector, detector and model ("mixed"), modelling and statistical NPs. An uncertainty value of 0.0 implies that the uncertainty is below 0.05.

JHEP01(2015)020

$\frac{d\sigma}{dn_{\text{jets}}}$ [%] / n_{jets}	3	4	≥ 5
MC statistics	0.9	2.3	4.7
PDF	0.7	2.4	2.2
MC generator	1.3	1.2	8.7
Fragmentation	2.2	2.7	7.8
ISR/FSR	6.5	7.1	16.3
Colour reconnection	1.0	2.5	3.4
ℓ resolution & efficiency	0.3	0.3	0.8
$E_{\text{T}}^{\text{miss}}$ cell-out	0.1	0.3	0.6
b-quark tagging efficiency	5.2	4.9	6.2
Additional interactions	0.1	0.2	0.4
Jet reconstruction efficiency	0.0	0.0	0.1
Jet energy resolution	1.3	0.6	1.6
b-quark jets (JES)	3.8	4.2	3.8
Close by jets (JES)	2.8	4.3	6.5
Effective detector NP set 1 (JES)	2.5	3.5	4.8
Effective detector NP set 2 (JES)	0.2	0.4	0.4
Effective mixed NP set 1 (JES)	0.2	0.4	0.7
Effective mixed NP set 2 (JES)	0.2	0.5	0.6
Effective model NP set 1 (JES)	1.1	1.8	2.4
Effective model NP set 2 (JES)	0.8	1.4	1.7
Effective model NP set 3 (JES)	0.9	1.5	1.8
Effective model NP set 4 (JES)	0.1	0.2	0.2
Effective stat. NP set 1 (JES)	0.1	0.3	0.3
Effective stat. NP set 2 (JES)	0.2	0.4	0.6
Effective stat. NP set 3 (JES)	0.6	1.1	1.4
η-intercalibration (JES)	2.4	3.1	4.2
η-intercalibration statistics (JES)	0.4	0.8	1.0
Flavour composition (JES)	1.0	1.4	1.6
Flavour response (JES)	1.0	2.1	3.1
Additional interactions μ (JES)	0.3	0.2	1.2
Additional interactions N_{PV} (JES)	0.3	0.4	0.4
Relative non-closure (JES)	0.2	0.6	0.6
Single particle high-p_{T} (JES)	0.0	0.0	0.0
Jet vertex fraction efficiency	0.5	0.6	1.7
W+jets normalisation	2.1	1.0	0.4
W+jets heavy/light flavour	3.4	1.1	0.6
Multijet normalisation	0.6	0.6	0.1
Multijet shape	0.2	0.2	0.7
Small backgrounds	4.4	4.2	4.7
Luminosity	1.8	1.8	1.8
Total systematic uncertainty	12.6	14.1	25.3
Statistical uncertainty	2.2	5.3	12.4
Cross-section [pb]	7.55e-01	1.49e-01	2.46e-02

Table 8. Relative uncertainties on the final differential cross-section after the e/μ channel combination, for the jet multiplicity using a 80 GeV jet p_{T} threshold. The uncertainties are shown as a percentage of the expected $t\bar{t}$ signal. The energy scale uncertainty (JES) is shown for each JES nuisance parameter (NP). The effective NP are obtained by combining a total of 54 detector, detector and model ("mixed"), modelling and statistical NPs. An uncertainty value of 0.0 implies that the uncertainty is below 0.05.

JHEP01(2015)020

$\frac{d\sigma}{dp_{\mathrm{T,jet}}}$ [%] / $p_{\mathrm{T,jet}}$ [GeV]	[50-70]	[70-90]	[90-120]	[120-155]	[155-195]	[195-235]	[235-280]	[280-1030]
MC statistics	0.9	0.6	0.6	0.7	1.0	1.6	2.1	2.7
PDF	0.3	0.1	0.1	0.1	0.1	0.3	0.1	0.5
MC generator	1.4	0.5	0.3	1.3	0.5	0.6	1.0	0.8
Fragmentation	0.9	0.8	0.7	1.0	0.7	0.3	0.8	1.2
ISR/FSR	1.2	1.5	3.0	3.6	5.4	2.3	3.4	3.1
Colour reconnection	0.8	0.1	0.1	0.3	0.6	1.1	0.9	1.6
ℓ resolution & efficiency	1.3	1.4	1.4	1.3	1.3	1.3	1.3	1.3
$E_{\mathrm{T}}^{\mathrm{miss}}$ cell-out	0.3	0.2	0.1	0.1	0.1	0.1	0.1	0.2
b-quark tagging efficiency	3.7	3.7	4.4	5.6	7.4	7.1	6.2	5.6
Additional interactions	0.2	0.1	0.1	0.1	0.1	0.1	0.1	0.1
Jet reconstruction efficiency	0.0	0.0	0.0	0.0	0.0	0.1	0.0	0.0
Jet energy resolution	2.3	1.6	0.6	1.2	1.9	1.3	2.7	1.3
b-quark jets (JES)	4.6	0.7	2.1	3.5	3.8	3.2	3.1	2.0
Close by jets (JES)	2.9	1.7	2.0	1.4	1.4	1.6	1.7	1.5
Effective detector NP set 1 (JES)	3.0	0.6	0.9	1.7	2.2	2.9	3.3	2.9
Effective detector NP set 2 (JES)	0.2	0.0	0.2	0.1	0.1	0.1	0.3	0.1
Effective mixed NP set 1 (JES)	0.2	0.1	0.1	0.1	0.2	0.3	0.8	1.1
Effective mixed NP set 2 (JES)	0.1	0.1	0.2	0.2	0.1	0.1	0.2	0.2
Effective model NP set 1 (JES)	0.7	0.7	1.2	1.1	0.9	0.7	0.6	0.2
Effective model NP set 2 (JES)	1.1	0.3	0.2	0.4	0.6	0.8	1.1	0.8
Effective model NP set 3 (JES)	1.2	0.3	0.3	0.6	0.8	0.6	0.4	0.1
Effective model NP set 4 (JES)	0.0	0.0	0.1	0.0	0.3	0.4	0.5	0.2
Effective stat. NP set 1 (JES)	0.7	0.6	0.4	0.3	0.1	0.1	0.1	0.2
Effective stat. NP set 2 (JES)	0.3	0.0	0.1	0.1	0.2	0.2	0.4	0.3
Effective stat. NP set 3 (JES)	0.8	0.1	0.2	0.3	0.6	0.6	0.8	0.4
η-intercalibration (JES)	2.4	0.2	1.1	1.4	1.9	2.4	2.5	1.5
η-intercalibration statistics (JES)	0.4	0.1	0.3	0.3	0.4	0.3	0.4	0.2
Flavour composition (JES)	0.7	0.3	0.6	0.7	0.6	0.9	1.1	1.2
Flavour response (JES)	0.5	0.0	0.3	0.4	0.5	0.9	1.0	1.3
Additional interactions μ (JES)	0.4	0.1	0.1	0.1	0.2	0.3	0.5	0.2
Additional interactions N_{PV} (JES)	0.3	0.0	0.2	0.1	0.2	0.4	0.2	0.1
Relative non-closure (JES)	0.2	0.1	0.1	0.2	0.5	0.7	0.5	0.2
Single particle high-p_{T} (JES)	0.0	0.0	0.0	0.0	0.0	0.0	0.0	0.0
Jet vertex fraction efficiency	1.4	1.5	1.5	1.6	1.7	1.8	2.0	2.2
W+jets normalisation	3.2	2.1	1.8	1.9	2.6	3.3	3.8	4.7
W+jets heavy/light flavour	6.1	3.6	3.1	3.7	5.1	5.9	6.9	7.0
Multijet normalisation	1.5	0.6	0.4	0.8	1.1	1.0	1.7	1.6
Multijet shape	0.5	0.1	0.1	0.1	0.1	0.1	0.3	0.4
Small backgrounds	2.0	1.3	1.1	1.4	1.7	2.2	3.0	2.6
Luminosity	1.8	1.8	1.8	1.8	1.8	1.8	1.8	1.8
Total systematic uncertainty	11.7	7.2	8.1	10.0	12.8	12.4	13.6	13.0
Statistical uncertainty	2.2	1.4	1.4	1.5	2.4	3.7	5.6	5.9
Cross-section [pb/GeV]	7.86e-02	1.28e-01	1.00e-01	5.12e-02	1.96e-02	8.72e-03	3.63e-03	2.02e-04

Table 9. Relative uncertainties on the final differential cross-section after the e/μ channel combination, for the leading jet. The uncertainties are shown as a percentage of the expected $t\bar{t}$ signal. The energy scale uncertainty (JES) is shown for each JES nuisance parameter (NP). The effective NP are obtained by combining a total of 54 detector, detector and model ("mixed"), modelling and statistical NPs. An uncertainty value of 0.0 implies that the uncertainty is below 0.05.

JHEP01(2015)020

$\frac{d\sigma}{dp_{\mathrm{T,jet}}}$ [%] / $p_{\mathrm{T,jet}}$ [GeV]	[35-50]	[50-70]	[70-90]	[90-120]	[120-155]	[155-195]	[195-830]
MC statistics	0.9	0.5	0.8	0.8	1.1	2.0	2.7
PDF	0.4	0.0	0.2	0.3	0.3	0.5	0.3
MC generator	1.1	0.1	0.7	0.5	1.0	0.6	1.4
Fragmentation	0.9	1.0	0.7	0.0	1.5	1.7	1.0
ISR/FSR	0.9	2.9	2.8	3.8	4.4	2.5	2.3
Colour reconnection	0.5	0.2	0.4	0.3	0.4	0.4	0.9
ℓ resolution & efficiency	1.3	1.4	1.5	1.3	1.3	1.3	1.3
$E_{\mathrm{T}}^{\mathrm{miss}}$ cell-out	0.2	0.2	0.2	0.1	0.2	0.1	0.4
b-quark tagging efficiency	4.4	4.1	4.3	5.4	7.5	9.3	6.9
Additional interactions	0.1	0.1	0.1	0.0	0.1	0.1	0.3
Jet reconstruction efficiency	0.1	0.0	0.0	0.0	0.0	0.0	0.0
Jet energy resolution	1.2	1.0	0.1	0.7	0.4	2.5	1.4
b-quark jets (JES)	3.3	0.2	2.6	3.3	4.2	4.9	5.0
Close by jets (JES)	5.1	1.6	3.6	2.2	1.2	1.9	2.0
Effective detector NP set 1 (JES)	2.3	0.4	1.5	2.0	2.4	3.4	3.8
Effective detector NP set 2 (JES)	0.2	0.0	0.1	0.2	0.1	0.1	0.2
Effective mixed NP set 1 (JES)	0.1	0.0	0.1	0.1	0.1	0.4	0.8
Effective mixed NP set 2 (JES)	0.1	0.1	0.2	0.2	0.2	0.1	0.1
Effective model NP set 1 (JES)	0.6	0.8	1.2	1.2	0.9	1.0	0.2
Effective model NP set 2 (JES)	0.9	0.3	0.4	0.6	0.7	1.1	1.0
Effective model NP set 3 (JES)	1.1	0.3	0.5	0.7	0.9	1.2	0.4
Effective model NP set 4 (JES)	0.2	0.1	0.1	0.0	0.1	0.5	0.4
Effective stat. NP set 1 (JES)	0.5	0.6	0.3	0.2	0.1	0.2	0.3
Effective stat. NP set 2 (JES)	0.3	0.0	0.1	0.2	0.2	0.4	0.3
Effective stat. NP set 3 (JES)	0.7	0.1	0.4	0.5	0.5	1.1	0.6
η-intercalibration (JES)	2.4	0.4	1.8	1.8	2.1	2.6	2.3
η-intercalibration statistics (JES)	0.3	0.2	0.3	0.4	0.4	0.5	0.2
Flavour composition (JES)	0.7	0.3	0.7	0.7	0.7	0.9	0.8
Flavour response (JES)	0.8	0.1	0.4	0.6	0.7	1.1	1.1
Additional interactions μ (JES)	0.2	0.2	0.1	0.1	0.2	0.4	0.1
Additional interactions N_{PV} (JES)	0.1	0.0	0.1	0.2	0.3	0.5	0.1
Relative non-closure (JES)	0.3	0.1	0.3	0.2	0.4	0.7	0.4
Single particle high-p_{T} (JES)	0.0	0.0	0.0	0.0	0.0	0.0	0.0
Jet vertex fraction efficiency	1.6	1.4	1.6	1.7	1.7	2.0	2.3
W+jets normalisation	4.3	2.0	1.7	1.9	2.4	3.3	6.2
W+jets heavy/light flavour	8.1	3.7	2.6	3.2	4.3	6.3	8.3
Multijet normalisation	1.6	0.6	0.3	0.5	1.0	1.3	1.7
Multijet shape	0.6	0.0	0.2	0.1	0.1	0.2	0.4
Small backgrounds	2.5	1.3	1.1	1.4	1.9	2.7	3.8
Luminosity	1.8	1.8	1.8	1.8	1.8	1.8	1.8
Total systematic uncertainty	13.4	7.7	8.7	9.7	12.3	15.2	15.9
Statistical uncertainty	2.2	1.1	1.6	1.8	2.8	5.0	7.0
Cross-section [pb/GeV]	1.14e-01	1.89e-01	1.23e-01	5.14e-02	1.72e-02	5.32e-03	2.01e-04

Table 10. Relative uncertainties on the final differential cross-section after the e/μ channel combination, for the 2nd jet. The uncertainties are shown as a percentage of the expected $t\bar{t}$ signal. The energy scale uncertainty (JES) is shown for each JES nuisance parameter (NP). The effective NP are obtained by combining a total of 54 detector, detector and model ("mixed"), modelling and statistical NPs. An uncertainty value of 0.0 implies that the uncertainty is below 0.05.

JHEP01(2015)020

$\frac{d\sigma}{dp_{\mathrm{T,jet}}}$ [%] / $p_{\mathrm{T,jet}}$ [GeV]	[25-35]	[35-50]	[50-70]	[70-90]	[90-120]	[120-530]
MC statistics	0.8	0.4	0.8	1.0	1.6	2.2
PDF	0.4	0.1	0.3	0.5	0.2	0.4
MC generator	1.2	0.5	0.2	0.6	0.3	1.0
Fragmentation	1.3	0.8	0.6	0.1	0.1	0.4
ISR/FSR	2.5	3.1	3.2	2.1	4.8	4.8
Colour reconnection	0.5	0.6	0.0	0.5	0.8	0.9
ℓ resolution & efficiency	1.3	1.3	1.7	1.4	1.4	1.4
$E_{\mathrm{T}}^{\mathrm{miss}}$ cell-out	0.2	0.2	0.1	0.2	0.1	0.3
b-quark tagging efficiency	5.0	4.4	4.6	5.3	6.5	8.3
Additional interactions	0.1	0.1	0.1	0.1	0.1	0.2
Jet reconstruction efficiency	0.1	0.0	0.0	0.0	0.0	0.1
Jet energy resolution	0.2	0.9	0.4	0.7	1.5	0.8
b-quark jets (JES)	1.6	0.2	2.5	3.3	3.8	4.9
Close by jets (JES)	4.5	0.4	4.5	4.6	2.2	2.0
Effective detector NP set 1 (JES)	1.3	0.4	1.3	2.6	2.7	4.3
Effective detector NP set 2 (JES)	0.1	0.0	0.1	0.2	0.2	0.1
Effective mixed NP set 1 (JES)	0.1	0.0	0.1	0.2	0.2	0.5
Effective mixed NP set 2 (JES)	0.1	0.1	0.2	0.3	0.2	0.2
Effective model NP set 1 (JES)	0.8	0.7	1.4	1.4	1.2	1.1
Effective model NP set 2 (JES)	0.5	0.3	0.3	0.8	0.9	1.3
Effective model NP set 3 (JES)	0.6	0.3	0.5	1.0	1.0	1.3
Effective model NP set 4 (JES)	0.2	0.0	0.2	0.1	0.0	0.5
Effective stat. NP set 1 (JES)	0.1	0.6	0.5	0.2	0.1	0.1
Effective stat. NP set 2 (JES)	0.2	0.1	0.2	0.3	0.2	0.4
Effective stat. NP set 3 (JES)	0.3	0.2	0.4	0.6	0.7	1.0
η-intercalibration (JES)	1.8	0.1	2.0	2.7	2.4	2.9
η-intercalibration statistics (JES)	0.3	0.1	0.4	0.5	0.5	0.7
Flavour composition (JES)	0.6	0.1	0.7	1.2	1.1	1.4
Flavour response (JES)	1.5	0.1	0.7	1.0	1.1	1.7
Additional interactions μ (JES)	0.1	0.2	0.0	0.0	0.2	0.3
Additional interactions N_{PV} (JES)	0.1	0.1	0.2	0.4	0.2	0.4
Relative non-closure (JES)	0.0	0.1	0.3	0.4	0.2	0.6
Single particle high-p_{T} (JES)	0.0	0.0	0.0	0.0	0.0	0.0
Jet vertex fraction efficiency	1.7	1.4	1.6	1.8	1.8	2.2
W+jets normalisation	5.3	2.1	1.4	1.4	2.1	2.4
W+jets heavy/light flavour	10.2	3.9	1.7	2.1	3.1	3.8
Multijet normalisation	1.7	0.8	0.3	0.4	0.4	1.4
Multijet shape	0.7	0.0	0.3	0.2	0.2	0.2
Small backgrounds	2.9	1.4	0.9	1.1	1.4	2.7
Luminosity	1.8	1.8	1.8	1.8	1.8	1.8
Total systematic uncertainty	14.9	7.9	9.2	10.2	11.7	14.5
Statistical uncertainty	2.0	1.0	1.5	2.2	3.6	5.3
Cross-section [pb/GeV]	1.92e-01	2.60e-01	1.50e-01	4.94e-02	1.47e-02	3.58e-04

Table 11. Relative uncertainties on the final differential cross-section after the e/μ channel combination, for the 3rd jet. The uncertainties are shown as a percentage of the expected $t\bar{t}$ signal. The energy scale uncertainty (JES) is shown for each JES nuisance parameter (NP). The effective NP are obtained by combining a total of 54 detector, detector and model ("mixed"), modelling and statistical NPs. An uncertainty value of 0.0 implies that the uncertainty is below 0.05.

JHEP01(2015)020

$\frac{d\sigma}{dp_{\mathrm{T,jet}}}$ [%] / $p_{\mathrm{T,jet}}$ [GeV]	[25-35]	[35-50]	[50-70]	[70-90]	[90-280]
MC statistics	0.6	0.7	1.0	1.8	3.7
PDF	0.1	0.1	0.5	0.7	0.4
MC generator	1.0	0.3	0.8	1.5	0.8
Fragmentation	0.5	0.2	0.2	0.4	1.8
ISR/FSR	1.6	3.7	2.0	6.3	5.7
Colour reconnection	0.2	0.7	0.3	1.2	2.0
ℓ resolution & efficiency	1.3	1.5	1.3	1.4	1.5
$E_{\mathrm{T}}^{\mathrm{miss}}$ cell-out	0.2	0.2	0.1	0.3	0.1
b-quark tagging efficiency	4.6	4.4	4.8	5.4	7.0
Additional interactions	0.1	0.1	0.0	0.2	0.1
Jet reconstruction efficiency	0.1	0.0	0.0	0.0	0.0
Jet energy resolution	0.2	0.0	0.5	1.4	0.6
b-quark jets (JES)	0.1	1.6	3.2	3.8	4.5
Close by jets (JES)	0.9	4.2	7.5	5.5	2.9
Effective detector NP set 1 (JES)	0.2	1.0	2.5	3.6	3.7
Effective detector NP set 2 (JES)	0.0	0.1	0.3	0.3	0.4
Effective mixed NP set 1 (JES)	0.0	0.1	0.2	0.3	0.5
Effective mixed NP set 2 (JES)	0.3	0.4	0.3	0.3	0.3
Effective model NP set 1 (JES)	1.5	2.2	2.1	1.7	1.5
Effective model NP set 2 (JES)	0.4	0.1	0.7	1.2	1.3
Effective model NP set 3 (JES)	0.5	0.2	0.9	1.4	1.5
Effective model NP set 4 (JES)	0.1	0.1	0.3	0.1	0.2
Effective stat. NP set 1 (JES)	1.1	1.2	0.6	0.1	0.2
Effective stat. NP set 2 (JES)	0.2	0.1	0.3	0.3	0.5
Effective stat. NP set 3 (JES)	0.2	0.2	0.7	1.0	1.0
η-intercalibration (JES)	0.3	1.8	3.2	3.6	3.0
η-intercalibration statistics (JES)	0.3	0.5	0.7	0.7	0.7
Flavour composition (JES)	0.7	0.8	1.4	1.4	1.6
Flavour response (JES)	0.7	1.8	2.4	2.1	2.5
Additional interactions μ (JES)	0.3	0.0	0.1	0.5	0.2
Additional interactions N_{PV} (JES)	0.1	0.3	0.3	0.5	0.7
Relative non-closure (JES)	0.4	0.2	0.6	0.5	0.5
Single particle high-p_{T} (JES)	0.0	0.0	0.0	0.0	0.0
Jet vertex fraction efficiency	1.6	1.6	1.9	2.1	2.2
W+jets normalisation	2.1	1.3	0.8	1.1	1.0
W+jets heavy/light flavour	3.2	1.4	1.0	1.2	1.2
Multijet normalisation	0.7	0.2	0.3	0.6	1.2
Multijet shape	0.2	0.3	0.3	0.3	0.5
Small backgrounds	1.4	0.8	1.0	1.3	2.4
Luminosity	1.8	1.8	1.8	1.8	1.8
Total systematic uncertainty	7.7	9.1	11.9	13.5	14.0
Statistical uncertainty	1.3	1.4	2.2	4.2	6.5
Cross-section [pb/GeV]	2.62e-01	1.65e-01	4.92e-02	1.10e-02	5.27e-04

Table 12. Relative uncertainties on the final differential cross-section after the e/μ channel combination, for the 4th jet. The uncertainties are shown as a percentage of the expected $t\bar{t}$ signal. The energy scale uncertainty (JES) is shown for each JES nuisance parameter (NP). The effective NP are obtained by combining a total of 54 detector, detector and model ("mixed"), modelling and statistical NPs. An uncertainty value of 0.0 implies that the uncertainty is below 0.05.

JHEP01(2015)020

$\frac{d\sigma}{dp_{\mathrm{T,jet}}}$ [%] / $p_{\mathrm{T,jet}}$ [GeV]	[25-35]	[35-50]	[50-70]	[70-195]
MC statistics	1.0	1.0	2.1	3.8
PDF	0.1	0.4	0.6	0.4
MC generator	0.4	0.3	1.1	1.8
Fragmentation	0.1	2.1	0.2	0.7
ISR/FSR	2.9	3.9	1.6	6.5
Colour reconnection	0.7	1.4	1.5	4.0
ℓ resolution & efficiency	1.6	1.3	1.3	1.4
$E_{\mathrm{T}}^{\mathrm{miss}}$ cell-out	0.1	0.2	0.4	0.4
b-quark tagging efficiency	4.5	4.5	4.4	6.2
Additional interactions	0.1	0.1	0.2	0.2
Jet reconstruction efficiency	0.1	0.0	0.0	0.1
Jet energy resolution	1.8	0.6	1.8	1.4
b-quark jets (JES)	0.6	2.2	3.3	3.8
Close by jets (JES)	2.3	7.2	9.7	5.1
Effective detector NP set 1 (JES)	0.7	2.0	3.6	4.1
Effective detector NP set 2 (JES)	0.1	0.2	0.3	0.3
Effective mixed NP set 1 (JES)	0.1	0.2	0.2	0.3
Effective mixed NP set 2 (JES)	0.5	0.6	0.4	0.3
Effective model NP set 1 (JES)	3.5	3.0	2.6	1.9
Effective model NP set 2 (JES)	0.5	0.3	1.0	1.4
Effective model NP set 3 (JES)	0.5	0.5	1.2	1.7
Effective model NP set 4 (JES)	0.0	0.3	0.3	0.1
Effective stat. NP set 1 (JES)	2.2	1.5	0.6	0.5
Effective stat. NP set 2 (JES)	0.1	0.2	0.3	0.4
Effective stat. NP set 3 (JES)	0.1	0.5	1.0	0.9
η-intercalibration (JES)	1.5	3.2	4.2	4.1
η-intercalibration statistics (JES)	0.7	0.8	0.8	0.5
Flavour composition (JES)	0.9	1.5	1.6	1.6
Flavour response (JES)	2.5	4.3	3.7	2.9
Additional interactions μ (JES)	0.3	0.1	0.5	0.5
Additional interactions N_{PV} (JES)	0.3	0.3	0.5	0.9
Relative non-closure (JES)	0.6	0.3	0.8	0.4
Single particle high-p_{T} (JES)	0.0	0.0	0.0	0.0
Jet vertex fraction efficiency	1.8	1.9	2.2	2.4
W+jets normalisation	1.9	0.7	0.4	0.5
W+jets heavy/light flavour	1.5	0.9	0.3	0.4
Multijet normalisation	0.3	0.3	0.4	0.3
Multijet shape	0.3	0.3	0.3	0.5
Small backgrounds	0.8	0.9	1.1	1.7
Luminosity	1.8	1.8	1.8	1.8
Total systematic uncertainty	9.1	12.9	14.6	15.2
Statistical uncertainty	1.8	2.1	4.3	9.5
Cross-section [pb/GeV]	1.51e-01	5.38e-02	1.22e-02	4.00e-04

Table 13. Relative uncertainties on the final differential cross-section after the e/μ channel combination, for the 5th jet. The uncertainties are shown as a percentage of the expected $t\bar{t}$ signal. The energy scale uncertainty (JES) is shown for each JES nuisance parameter (NP). The effective NP are obtained by combining a total of 54 detector, detector and model ("mixed"), modelling and statistical NPs. An uncertainty value of 0.0 implies that the uncertainty is below 0.05.

JHEP01(2015)020

References

[1] L. Evans and P. Bryant, *LHC machine*, 2008 *JINST* **3** S08001 [INSPIRE].

[2] ATLAS collaboration, *Measurement of the top quark mass with the template method in the $t\bar{t} \to$ lepton + jets channel using ATLAS data*, *Eur. Phys. J.* **C 72** (2012) 2046 [arXiv:1203.5755] [INSPIRE].

[3] ATLAS collaboration, *Multi-channel search for squarks and gluinos in $\sqrt{s} = 7$ TeV pp collisions with the ATLAS detector*, *Eur. Phys. J.* **C 73** (2013) 2362 [arXiv:1212.6149] [INSPIRE].

[4] M.L. Mangano, *Standard Model backgrounds to supersymmetry searches*, *Eur. Phys. J.* **C 59** (2009) 373 [arXiv:0809.1567] [INSPIRE].

[5] ATLAS collaboration, *Study of jets produced in association with a W boson in pp collisions at $\sqrt{s} = 7$ TeV with the ATLAS detector*, *Phys. Rev.* **D 85** (2012) 092002 [arXiv:1201.1276] [INSPIRE].

[6] ATLAS collaboration, *Measurement of the production cross section for Z/γ^* in association with jets in pp collisions at $\sqrt{s} = 7$ TeV with the ATLAS detector*, *Phys. Rev.* **D 85** (2012) 032009 [arXiv:1111.2690] [INSPIRE].

[7] D0 collaboration, V.M. Abazov et al., *Measurements of differential cross sections of Z/γ^*+ jets $+X$ events in proton anti-proton collisions at $\sqrt{s} = 1.96$ TeV*, *Phys. Lett.* **B 678** (2009) 45 [arXiv:0903.1748] [INSPIRE].

[8] D0 collaboration, V.M. Abazov et al., *Studies of W boson plus jets production in $p\bar{p}$ collisions at $\sqrt{s} = 1.96$ TeV*, *Phys. Rev.* **D 88** (2013) 092001 [arXiv:1302.6508] [INSPIRE].

[9] CDF collaboration, T. Aaltonen et al., *Measurement of inclusive jet cross sections in $Z/gamma^*(\to e^+e^-)+$ jets production in pp collisions at $\sqrt{s} = 1.96$ TeV*, *Phys. Rev. Lett.* **100** (2008) 103001 [arXiv:0711.3717] [INSPIRE].

[10] CDF collaboration, T. Aaltonen et al., *Measurement of the cross section for W^- boson production in association with jets in $p\bar{p}$ collisions at $\sqrt{s} = 1.96$ TeV*, *Phys. Rev.* **D 77** (2008) 011108 [arXiv:0711.4044] [INSPIRE].

[11] CMS collaboration, *Measurement of jet multiplicity distributions in $t\bar{t}$ production in pp collisions at $\sqrt{s} = 7$ TeV*, *Eur. Phys. J.* **C 74** (2014) 3014 [arXiv:1404.3171] [INSPIRE].

[12] ATLAS collaboration, *Measurement of $t\bar{t}$ production with a veto on additional central jet activity in pp collisions at $\sqrt{s} = 7$ TeV using the ATLAS detector*, *Eur. Phys. J.* **C 72** (2012) 2043 [arXiv:1203.5015] [INSPIRE].

[13] M.L. Mangano, M. Moretti, F. Piccinini and M. Treccani, *Matching matrix elements and shower evolution for top-quark production in hadronic collisions*, *JHEP* **01** (2007) 013 [hep-ph/0611129] [INSPIRE].

[14] R. Corke and T. Sjöstrand, *Multiparton interactions with an x-dependent proton size*, *JHEP* **05** (2011) 009 [arXiv:1101.5953] [INSPIRE].

JHEP01(2015)020

[15] ATLAS collaboration, *Measurements of top quark pair relative differential cross-sections with ATLAS in pp collisions at $\sqrt{s} = 7$ TeV*, *Eur. Phys. J.* **C 73** (2013) 2261 [arXiv:1207.5644] [INSPIRE].

[16] CMS collaboration, *Measurement of differential top-quark pair production cross sections in pp colisions at $\sqrt{s} = 7$ TeV*, *Eur. Phys. J.* **C 73** (2013) 2339 [arXiv:1211.2220] [INSPIRE].

[17] ATLAS collaboration, *Improved luminosity determination in pp collisions at $\sqrt{s} = 7$ TeV using the ATLAS detector at the LHC*, *Eur. Phys. J.* **C 73** (2013) 2518 [arXiv:1302.4393] [INSPIRE].

[18] ATLAS collaboration, *Measurement of the top quark pair production cross-section with ATLAS in the single lepton channel*, *Phys. Lett.* **B 711** (2012) 244 [arXiv:1201.1889] [INSPIRE].

[19] ATLAS collaboration, *The ATLAS experiment at the CERN Large Hadron Collider*, 2008 *JINST* **3** S08003 [INSPIRE].

[20] ATLAS collaboration, *Electron reconstruction and identification efficiency measurements with the ATLAS detector using the 2011 LHC proton-proton collision data*, *Eur. Phys. J.* **C 74** (2014) 2941 [arXiv:1404.2240] [INSPIRE].

[21] ATLAS collaboration, *Muon reconstruction efficiency and momentum resolution of the ATLAS experiment in proton-proton collisions at $\sqrt{s} = 7$ TeV in 2010*, *Eur. Phys. J.* **C 74** (2014) 3034 [arXiv:1404.4562] [INSPIRE].

[22] W. Lampl et al., *Calorimeter clustering algorithms: description and performance*, ATL-LARG-PUB-2008-002 (2008).

[23] M. Cacciari, G.P. Salam and G. Soyez, *The anti-k_t jet clustering algorithm*, *JHEP* **04** (2008) 063 [arXiv:0802.1189] [INSPIRE].

[24] ATLAS collaboration, *Jet energy measurement and its systematic uncertainty in proton-proton collisions at $\sqrt{s} = 7$ TeV with the ATLAS detector*, arXiv:1406.0076 [INSPIRE].

[25] ATLAS collaboration, *Jet energy measurement with the ATLAS detector in proton-proton collisions at $\sqrt{s} = 7$ TeV*, *Eur. Phys. J.* **C 73** (2013) 2304 [arXiv:1112.6426] [INSPIRE].

[26] ATLAS collaboration, *Performance of missing transverse momentum reconstruction in proton-proton collisions at 7 TeV with ATLAS*, *Eur. Phys. J.* **C 72** (2012) 1844 [arXiv:1108.5602] [INSPIRE].

[27] ATLAS collaboration, *Commissioning of the ATLAS high-performance b-tagging algorithms in the 7 TeV collision data*, ATLAS-CONF-2011-102 (2011).

[28] ATLAS collaboration, *Measurement of the top quark-pair production cross section with ATLAS in pp collisions at $\sqrt{s} = 7$ TeV*, *Eur. Phys. J.* **C 71** (2011) 1577 [arXiv:1012.1792] [INSPIRE].

[29] M.L. Mangano, M. Moretti, F. Piccinini, R. Pittau and A.D. Polosa, *ALPGEN, a generator for hard multiparton processes in hadronic collisions*, *JHEP* **07** (2003) 001 [hep-ph/0206293] [INSPIRE].

[30] S. Frixione and B.R. Webber, *Matching NLO QCD computations and parton shower simulations*, *JHEP* **06** (2002) 029 [hep-ph/0204244] [INSPIRE].

JHEP01(2015)020

[31] S. Alioli, P. Nason, C. Oleari and E. Re, *A general framework for implementing NLO calculations in shower Monte Carlo programs: the POWHEG BOX*, *JHEP* **06** (2010) 043 [arXiv:1002.2581] [INSPIRE].

[32] D. Stump et al., *Inclusive jet production, parton distributions and the search for new physics*, *JHEP* **10** (2003) 046 [hep-ph/0303013] [INSPIRE].

[33] G. Corcella et al., *HERWIG 6.5 release note*, hep-ph/0210213 [INSPIRE].

[34] J.M. Butterworth, J.R. Forshaw and M.H. Seymour, *Multiparton interactions in photoproduction at HERA*, *Z. Phys.* **C 72** (1996) 637 [hep-ph/9601371] [INSPIRE].

[35] ATLAS collaboration, *First tuning of HERWIG/JIMMY to ATLAS data*, ATL-PHYS-PUB-2010-014 (2010).

[36] H.-L. Lai et al., *New parton distributions for collider physics*, *Phys. Rev.* **D 82** (2010) 074024 [arXiv:1007.2241] [INSPIRE].

[37] T. Sjöstrand, S. Mrenna and P.Z. Skands, *PYTHIA 6.4 physics and manual*, *JHEP* **05** (2006) 026 [hep-ph/0603175] [INSPIRE].

[38] P.Z. Skands, *Tuning Monte Carlo generators: the Perugia tunes*, *Phys. Rev.* **D 82** (2010) 074018 [arXiv:1005.3457] [INSPIRE].

[39] CTEQ collaboration, H.L. Lai et al., *Global QCD analysis of parton structure of the nucleon: CTEQ5 parton distributions*, *Eur. Phys. J.* **C 12** (2000) 375 [hep-ph/9903282] [INSPIRE].

[40] B. Cooper et al., *Importance of a consistent choice of α_s in the matching of ALPGEN and PYTHIA*, *Eur. Phys. J.* **C 72** (2012) 2078 [arXiv:1109.5295] [INSPIRE].

[41] ATLAS collaboration, *Monte Carlo generator comparisons to ATLAS measurements constraining QCD radiation in top anti-top final states*, ATL-PHYS-PUB-2013-005 (2013).

[42] ATLAS collaboration, *Comparison of Monte Carlo generator predictions for gap fraction and jet multiplicity observables in top-antitop events*, ATL-PHYS-PUB-2014-005 (2014).

[43] M. Czakon, P. Fiedler and A. Mitov, *Total top-quark pair-production cross section at hadron colliders through $O(\alpha_S^4)$*, *Phys. Rev. Lett.* **110** (2013) 252004 [arXiv:1303.6254] [INSPIRE].

[44] M. Czakon and A. Mitov, *NNLO corrections to top pair production at hadron colliders: the quark-gluon reaction*, *JHEP* **01** (2013) 080 [arXiv:1210.6832] [INSPIRE].

[45] M. Czakon and A. Mitov, *NNLO corrections to top-pair production at hadron colliders: the all-fermionic scattering channels*, *JHEP* **12** (2012) 054 [arXiv:1207.0236] [INSPIRE].

[46] P. Bärnreuther, M. Czakon and A. Mitov, *Percent level precision physics at the Tevatron: first genuine NNLO QCD corrections to $q\bar{q} \to t\bar{t} + X$*, *Phys. Rev. Lett.* **109** (2012) 132001 [arXiv:1204.5201] [INSPIRE].

[47] M. Cacciari, M. Czakon, M. Mangano, A. Mitov and P. Nason, *Top-pair production at hadron colliders with next-to-next-to-leading logarithmic soft-gluon resummation*, *Phys. Lett.* **B 710** (2012) 612 [arXiv:1111.5869] [INSPIRE].

[48] M. Czakon and A. Mitov, *Top++: a program for the calculation of the top-pair cross-section at hadron colliders*, *Comput. Phys. Commun.* **185** (2014) 2930 [arXiv:1112.5675] [INSPIRE].

[49] M. Botje et al., *The PDF4LHC working group interim recommendations*, arXiv:1101.0538 [INSPIRE].

JHEP01(2015)020

[50] A.D. Martin, W.J. Stirling, R.S. Thorne and G. Watt, *Parton distributions for the LHC*, *Eur. Phys. J.* **C 63** (2009) 189 [arXiv:0901.0002] [INSPIRE].

[51] A.D. Martin, W.J. Stirling, R.S. Thorne and G. Watt, *Uncertainties on α_s in global PDF analyses and implications for predicted hadronic cross sections*, *Eur. Phys. J.* **C 64** (2009) 653 [arXiv:0905.3531] [INSPIRE].

[52] J. Gao et al., *CT10 next-to-next-to-leading order global analysis of QCD*, *Phys. Rev.* **D 89** (2014) 033009 [arXiv:1302.6246] [INSPIRE].

[53] R.D. Ball et al., *Parton distributions with LHC data*, *Nucl. Phys.* **B 867** (2013) 244 [arXiv:1207.1303] [INSPIRE].

[54] M. Aliev et al., *HATHOR: HAdronic Top and Heavy quarks crOss section calculatoR*, *Comput. Phys. Commun.* **182** (2011) 1034 [arXiv:1007.1327] [INSPIRE].

[55] B.P. Kersevan and E. Richter-Was, *The Monte Carlo event generator AcerMC versions 2.0 to 3.8 with interfaces to PYTHIA 6.4, HERWIG 6.5 and ARIADNE 4.1*, *Comput. Phys. Commun.* **184** (2013) 919 [hep-ph/0405247] [INSPIRE].

[56] N. Kidonakis, *Next-to-next-to-leading-order collinear and soft gluon corrections for t-channel single top quark production*, *Phys. Rev.* **D 83** (2012) 091503 [arXiv:1003.2792] [INSPIRE].

[57] N. Kidonakis, *NNLL resummation for s-channel single top quark production*, *Phys. Rev.* **D 81** (2010) 054028 [arXiv:1001.5034] [INSPIRE].

[58] N. Kidonakis, *Two-loop soft anomalous dimensions for single top quark associated production with a W^- or H^-*, *Phys. Rev.* **D 82** (2010) 054018 [arXiv:1005.4451] [INSPIRE].

[59] J.M. Campbell and R.K. Ellis, *An update on vector boson pair production at hadron colliders*, *Phys. Rev.* **D 60** (1999) 113006 [hep-ph/9905386] [INSPIRE].

[60] GEANT4 collaboration, S. Agostinelli et al., *GEANT4 — A simulation toolkit*, *Nucl. Instrum. Meth.* **A 506** (2003) 250 [INSPIRE].

[61] ATLAS collaboration, *The ATLAS simulation infrastructure*, *Eur. Phys. J.* **C 70** (2010) 823 [arXiv:1005.4568] [INSPIRE].

[62] ATLAS collaboration, *Measurement of the b-tag efficiency in a sample of jets containing muons with $5\,fb^{-1}$ of data from the ATLAS detector*, ATLAS-CONF-2012-043 (2012).

[63] ATLAS collaboration, *Measurement of the mistag rate of b-tagging algorithms with $5\,fb^{-1}$ of data collected by the atlas detector*, ATLAS-CONF-2012-040 (2012).

[64] G. D'Agostini, *A multidimensional unfolding method based on Bayes' theorem*, *Nucl. Instrum. Meth.* **A 362** (1995) 487 [INSPIRE].

[65] A. Valassi, *Combining correlated measurements of several different physical quantities*, *Nucl. Instrum. Meth.* **A 500** (2003) 391 [INSPIRE].

[66] L. Lyons, D. Gibaut and P. Clifford, *How to combine correlated estimates of a single physical quantity*, *Nucl. Instrum. Meth.* **A 270** (1988) 110 [INSPIRE].

[67] H1 collaboration, F.D. Aaron et al., *Measurement of the inclusive ep scattering cross section at low Q^2 and x at HERA*, *Eur. Phys. J.* **C 63** (2009) 625 [arXiv:0904.0929] [INSPIRE].

[68] L. Lönnblad and S. Prestel, *Merging multi-leg NLO matrix elements with parton showers*, *JHEP* **03** (2013) 166 [arXiv:1211.7278] [INSPIRE].

JHEP01(2015)020

The ATLAS collaboration

G. Aad[84], B. Abbott[112], J. Abdallah[152], S. Abdel Khalek[116], O. Abdinov[11], R. Aben[106], B. Abi[113], M. Abolins[89], O.S. AbouZeid[159], H. Abramowicz[154], H. Abreu[153], R. Abreu[30], Y. Abulaiti[147a,147b], B.S. Acharya[165a,165b,a], L. Adamczyk[38a], D.L. Adams[25], J. Adelman[177], S. Adomeit[99], T. Adye[130], T. Agatonovic-Jovin[13a], J.A. Aguilar-Saavedra[125a,125f], M. Agustoni[17], S.P. Ahlen[22], F. Ahmadov[64,b], G. Aielli[134a,134b], H. Akerstedt[147a,147b], T.P.A. Åkesson[80], G. Akimoto[156], A.V. Akimov[95], G.L. Alberghi[20a,20b], J. Albert[170], S. Albrand[55], M.J. Alconada Verzini[70], M. Aleksa[30], I.N. Aleksandrov[64], C. Alexa[26a], G. Alexander[154], G. Alexandre[49], T. Alexopoulos[10], M. Alhroob[165a,165c], G. Alimonti[90a], L. Alio[84], J. Alison[31], B.M.M. Allbrooke[18], L.J. Allison[71], P.P. Allport[73], J. Almond[83], A. Aloisio[103a,103b], A. Alonso[36], F. Alonso[70], C. Alpigiani[75], A. Altheimer[35], B. Alvarez Gonzalez[89], M.G. Alviggi[103a,103b], K. Amako[65], Y. Amaral Coutinho[24a], C. Amelung[23], D. Amidei[88], S.P. Amor Dos Santos[125a,125c], A. Amorim[125a,125b], S. Amoroso[48], N. Amram[154], G. Amundsen[23], C. Anastopoulos[140], L.S. Ancu[49], N. Andari[30], T. Andeen[35], C.F. Anders[58b], G. Anders[30], K.J. Anderson[31], A. Andreazza[90a,90b], V. Andrei[58a], X.S. Anduaga[70], S. Angelidakis[9], I. Angelozzi[106], P. Anger[44], A. Angerami[35], F. Anghinolfi[30], A.V. Anisenkov[108], N. Anjos[125a], A. Annovi[47], A. Antonaki[9], M. Antonelli[47], A. Antonov[97], J. Antos[145b], F. Anulli[133a], M. Aoki[65], L. Aperio Bella[18], R. Apolle[119,c], G. Arabidze[89], I. Aracena[144], Y. Arai[65], J.P. Araque[125a], A.T.H. Arce[45], J-F. Arguin[94], S. Argyropoulos[42], M. Arik[19a], A.J. Armbruster[30], O. Arnaez[30], V. Arnal[81], H. Arnold[48], M. Arratia[28], O. Arslan[21], A. Artamonov[96], G. Artoni[23], S. Asai[156], N. Asbah[42], A. Ashkenazi[154], B. Åsman[147a,147b], L. Asquith[6], K. Assamagan[25], R. Astalos[145a], M. Atkinson[166], N.B. Atlay[142], B. Auerbach[6], K. Augsten[127], M. Aurousseau[146b], G. Avolio[30], G. Azuelos[94,d], Y. Azuma[156], M.A. Baak[30], A. Baas[58a], C. Bacci[135a,135b], H. Bachacou[137], K. Bachas[155], M. Backes[30], M. Backhaus[30], J. Backus Mayes[144], E. Badescu[26a], P. Bagiacchi[133a,133b], P. Bagnaia[133a,133b], Y. Bai[33a], T. Bain[35], J.T. Baines[130], O.K. Baker[177], P. Balek[128], F. Balli[137], E. Banas[39], Sw. Banerjee[174], A.A.E. Bannoura[176], V. Bansal[170], H.S. Bansil[18], L. Barak[173], S.P. Baranov[95], E.L. Barberio[87], D. Barberis[50a,50b], M. Barbero[84], T. Barillari[100], M. Barisonzi[176], T. Barklow[144], N. Barlow[28], B.M. Barnett[130], R.M. Barnett[15], Z. Barnovska[5], A. Baroncelli[135a], G. Barone[49], A.J. Barr[119], F. Barreiro[81], J. Barreiro Guimarães da Costa[57], R. Bartoldus[144], A.E. Barton[71], P. Bartos[145a], V. Bartsch[150], A. Bassalat[116], A. Basye[166], R.L. Bates[53], L. Batkova[145a], J.R. Batley[28], M. Battaglia[138], M. Battistin[30], F. Bauer[137], H.S. Bawa[144,e], T. Beau[79], P.H. Beauchemin[162], R. Beccherle[123a,123b], P. Bechtle[21], H.P. Beck[17], K. Becker[176], S. Becker[99], M. Beckingham[171], C. Becot[116], A.J. Beddall[19c], A. Beddall[19c], S. Bedikian[177], V.A. Bednyakov[64], C.P. Bee[149], L.J. Beemster[106], T.A. Beermann[176], M. Begel[25], K. Behr[119], C. Belanger-Champagne[86], P.J. Bell[49], W.H. Bell[49], G. Bella[154], L. Bellagamba[20a], A. Bellerive[29], M. Bellomo[85], K. Belotskiy[97], O. Beltramello[30], O. Benary[154], D. Benchekroun[136a], K. Bendtz[147a,147b], N. Benekos[166], Y. Benhammou[154], E. Benhar Noccioli[49], J.A. Benitez Garcia[160b], D.P. Benjamin[45], J.R. Bensinger[23], K. Benslama[131], S. Bentvelsen[106], D. Berge[106], E. Bergeaas Kuutmann[16], N. Berger[5], F. Berghaus[170], J. Beringer[15], C. Bernard[22], P. Bernat[77], C. Bernius[78], F.U. Bernlochner[170], T. Berry[76], P. Berta[128], C. Bertella[84], G. Bertoli[147a,147b], F. Bertolucci[123a,123b], D. Bertsche[112], M.I. Besana[90a], G.J. Besjes[105], O. Bessidskaia[147a,147b], M.F. Bessner[42], N. Besson[137], C. Betancourt[48], S. Bethke[100], W. Bhimji[46], R.M. Bianchi[124], L. Bianchini[23], M. Bianco[30], O. Biebel[99], S.P. Bieniek[77], K. Bierwagen[54], J. Biesiada[15], M. Biglietti[135a], J. Bilbao De Mendizabal[49], H. Bilokon[47], M. Bindi[54], S. Binet[116], A. Bingul[19c], C. Bini[133a,133b], C.W. Black[151], J.E. Black[144], K.M. Black[22], D. Blackburn[139], R.E. Blair[6], J.-B. Blanchard[137], T. Blazek[145a], I. Bloch[42], C. Blocker[23], W. Blum[82,*], U. Blumenschein[54], G.J. Bobbink[106], V.S. Bobrovnikov[108], S.S. Bocchetta[80], A. Bocci[45], C. Bock[99], C.R. Boddy[119], M. Boehler[48], T.T. Boek[176], J.A. Bogaerts[30], A.G. Bogdanchikov[108], A. Bogouch[91,*], C. Bohm[147a], J. Bohm[126], V. Boisvert[76], T. Bold[38a], V. Boldea[26a], A.S. Boldyrev[98], M. Bomben[79], M. Bona[75], M. Boonekamp[137], A. Borisov[129], G. Borissov[71], M. Borri[83], S. Borroni[42], J. Bortfeldt[99], V. Bortolotto[135a,135b], K. Bos[106], D. Boscherini[20a], M. Bosman[12],

JHEP01(2015)020

H. Boterenbrood[106], J. Boudreau[124], J. Bouffard[2], E.V. Bouhova-Thacker[71], D. Boumediene[34], C. Bourdarios[116], N. Bousson[113], S. Boutouil[136d], A. Boveia[31], J. Boyd[30], I.R. Boyko[64], J. Bracinik[18], A. Brandt[8], G. Brandt[15], O. Brandt[58a], U. Bratzler[157], B. Brau[85], J.E. Brau[115], H.M. Braun[176,*], S.F. Brazzale[165a,165c], B. Brelier[159], K. Brendlinger[121], A.J. Brennan[87], R. Brenner[167], S. Bressler[173], K. Bristow[146c], T.M. Bristow[46], D. Britton[53], F.M. Brochu[28], I. Brock[21], R. Brock[89], C. Bromberg[89], J. Bronner[100], G. Brooijmans[35], T. Brooks[76], W.K. Brooks[32b], J. Brosamer[15], E. Brost[115], J. Brown[55], P.A. Bruckman de Renstrom[39], D. Bruncko[145b], R. Bruneliere[48], S. Brunet[60], A. Bruni[20a], G. Bruni[20a], M. Bruschi[20a], L. Bryngemark[80], T. Buanes[14], Q. Buat[143], F. Bucci[49], P. Buchholz[142], R.M. Buckingham[119], A.G. Buckley[53], S.I. Buda[26a], I.A. Budagov[64], F. Buehrer[48], L. Bugge[118], M.K. Bugge[118], O. Bulekov[97], A.C. Bundock[73], H. Burckhart[30], S. Burdin[73], B. Burghgrave[107], S. Burke[130], I. Burmeister[43], E. Busato[34], D. Büscher[48], V. Büscher[82], P. Bussey[53], C.P. Buszello[167], B. Butler[57], J.M. Butler[22], A.I. Butt[3], C.M. Buttar[53], J.M. Butterworth[77], P. Butti[106], W. Buttinger[28], A. Buzatu[53], M. Byszewski[10], S. Cabrera Urbán[168], D. Caforio[20a,20b], O. Cakir[4a], P. Calafiura[15], A. Calandri[137], G. Calderini[79], P. Calfayan[99], R. Calkins[107], L.P. Caloba[24a], D. Calvet[34], S. Calvet[34], R. Camacho Toro[49], S. Camarda[42], D. Cameron[118], L.M. Caminada[15], R. Caminal Armadans[12], S. Campana[30], M. Campanelli[77], A. Campoverde[149], V. Canale[103a,103b], A. Canepa[160a], M. Cano Bret[75], J. Cantero[81], R. Cantrill[76], T. Cao[40], M.D.M. Capeans Garrido[30], I. Caprini[26a], M. Caprini[26a], M. Capua[37a,37b], R. Caputo[82], R. Cardarelli[134a], T. Carli[30], G. Carlino[103a], L. Carminati[90a,90b], S. Caron[105], E. Carquin[32a], G.D. Carrillo-Montoya[146c], J.R. Carter[28], J. Carvalho[125a,125c], D. Casadei[77], M.P. Casado[12], M. Casolino[12], E. Castaneda-Miranda[146b], A. Castelli[106], V. Castillo Gimenez[168], N.F. Castro[125a], P. Catastini[57], A. Catinaccio[30], J.R. Catmore[118], A. Cattai[30], G. Cattani[134a,134b], S. Caughron[89], V. Cavaliere[166], D. Cavalli[90a], M. Cavalli-Sforza[12], V. Cavasinni[123a,123b], F. Ceradini[135a,135b], B. Cerio[45], K. Cerny[128], A.S. Cerqueira[24b], A. Cerri[150], L. Cerrito[75], F. Cerutti[15], M. Cerv[30], A. Cervelli[17], S.A. Cetin[19b], A. Chafaq[136a], D. Chakraborty[107], I. Chalupkova[128], P. Chang[166], B. Chapleau[86], J.D. Chapman[28], D. Charfeddine[116], D.G. Charlton[18], C.C. Chau[159], C.A. Chavez Barajas[150], S. Cheatham[86], A. Chegwidden[89], S. Chekanov[6], S.V. Chekulaev[160a], G.A. Chelkov[64,f], M.A. Chelstowska[88], C. Chen[63], H. Chen[25], K. Chen[149], L. Chen[33d,g], S. Chen[33c], X. Chen[146c], Y. Chen[35], H.C. Cheng[88], Y. Cheng[31], A. Cheplakov[64], R. Cherkaoui El Moursli[136e], V. Chernyatin[25,*], E. Cheu[7], L. Chevalier[137], V. Chiarella[47], G. Chiefari[103a,103b], J.T. Childers[6], A. Chilingarov[71], G. Chiodini[72a], A.S. Chisholm[18], R.T. Chislett[77], A. Chitan[26a], M.V. Chizhov[64], S. Chouridou[9], B.K.B. Chow[99], D. Chromek-Burckhart[30], M.L. Chu[152], J. Chudoba[126], J.J. Chwastowski[39], L. Chytka[114], G. Ciapetti[133a,133b], A.K. Ciftci[4a], R. Ciftci[4a], D. Cinca[53], V. Cindro[74], A. Ciocio[15], P. Cirkovic[13b], Z.H. Citron[173], M. Citterio[90a], M. Ciubancan[26a], A. Clark[49], P.J. Clark[46], R.N. Clarke[15], W. Cleland[124], J.C. Clemens[84], C. Clement[147a,147b], Y. Coadou[84], M. Cobal[165a,165c], A. Coccaro[139], J. Cochran[63], L. Coffey[23], J.G. Cogan[144], J. Coggeshall[166], B. Cole[35], S. Cole[107], A.P. Colijn[106], J. Collot[55], T. Colombo[58c], G. Colon[85], G. Compostella[100], P. Conde Muiño[125a,125b], E. Coniavitis[48], M.C. Conidi[12], S.H. Connell[146b], I.A. Connelly[76], S.M. Consonni[90a,90b], V. Consorti[48], S. Constantinescu[26a], C. Conta[120a,120b], G. Conti[57], F. Conventi[103a,h], M. Cooke[15], B.D. Cooper[77], A.M. Cooper-Sarkar[119], N.J. Cooper-Smith[76], K. Copic[15], T. Cornelissen[176], M. Corradi[20a], F. Corriveau[86,i], A. Corso-Radu[164], A. Cortes-Gonzalez[12], G. Cortiana[100], G. Costa[90a], M.J. Costa[168], D. Costanzo[140], D. Côté[8], G. Cottin[28], G. Cowan[76], B.E. Cox[83], K. Cranmer[109], G. Cree[29], S. Crépé-Renaudin[55], F. Crescioli[79], W.A. Cribbs[147a,147b], M. Crispin Ortuzar[119], M. Cristinziani[21], V. Croft[105], G. Crosetti[37a,37b], C.-M. Cuciuc[26a], T. Cuhadar Donszelmann[140], J. Cummings[177], M. Curatolo[47], C. Cuthbert[151], H. Czirr[142], P. Czodrowski[3], Z. Czyczula[177], S. D'Auria[53], M. D'Onofrio[73], M.J. Da Cunha Sargedas De Sousa[125a,125b], C. Da Via[83], W. Dabrowski[38a], A. Dafinca[119], T. Dai[88], O. Dale[14], F. Dallaire[94], C. Dallapiccola[85], M. Dam[36], A.C. Daniells[18], M. Dano Hoffmann[137], V. Dao[105], G. Darbo[50a], S. Darmora[8], J.A. Dassoulas[42], A. Dattagupta[60], W. Davey[21], C. David[170], T. Davidek[128], E. Davies[119,c], M. Davies[154], O. Davignon[79],

JHEP01(2015)020

A.R. Davison[77], P. Davison[77], Y. Davygora[58a], E. Dawe[143], I. Dawson[140], R.K. Daya-Ishmukhametova[85], K. De[8], R. de Asmundis[103a], S. De Castro[20a,20b], S. De Cecco[79], N. De Groot[105], P. de Jong[106], H. De la Torre[81], F. De Lorenzi[63], L. De Nooij[106], D. De Pedis[133a], A. De Salvo[133a], U. De Sanctis[165a,165b], A. De Santo[150], J.B. De Vivie De Regie[116], W.J. Dearnaley[71], R. Debbe[25], C. Debenedetti[138], B. Dechenaux[55], D.V. Dedovich[64], I. Deigaard[106], J. Del Peso[81], T. Del Prete[123a,123b], F. Deliot[137], C.M. Delitzsch[49], M. Deliyergiyev[74], A. Dell'Acqua[30], L. Dell'Asta[22], M. Dell'Orso[123a,123b], M. Della Pietra[103a,h], D. della Volpe[49], M. Delmastro[5], P.A. Delsart[55], C. Deluca[106], S. Demers[177], M. Demichev[64], A. Demilly[79], S.P. Denisov[129], D. Derendarz[39], J.E. Derkaoui[136d], F. Derue[79], P. Dervan[73], K. Desch[21], C. Deterre[42], P.O. Deviveiros[106], A. Dewhurst[130], S. Dhaliwal[106], A. Di Ciaccio[134a,134b], L. Di Ciaccio[5], A. Di Domenico[133a,133b], C. Di Donato[103a,103b], A. Di Girolamo[30], B. Di Girolamo[30], A. Di Mattia[153], B. Di Micco[135a,135b], R. Di Nardo[47], A. Di Simone[48], R. Di Sipio[20a,20b], D. Di Valentino[29], F.A. Dias[46], M.A. Diaz[32a], E.B. Diehl[88], J. Dietrich[42], T.A. Dietzsch[58a], S. Diglio[84], A. Dimitrievska[13a], J. Dingfelder[21], C. Dionisi[133a,133b], P. Dita[26a], S. Dita[26a], F. Dittus[30], F. Djama[84], T. Djobava[51b], M.A.B. do Vale[24c], A. Do Valle Wemans[125a,125g], T.K.O. Doan[5], D. Dobos[30], C. Doglioni[49], T. Doherty[53], T. Dohmae[156], J. Dolejsi[128], Z. Dolezal[128], B.A. Dolgoshein[97,*], M. Donadelli[24d], S. Donati[123a,123b], P. Dondero[120a,120b], J. Donini[34], J. Dopke[130], A. Doria[103a], M.T. Dova[70], A.T. Doyle[53], M. Dris[10], J. Dubbert[88], S. Dube[15], E. Dubreuil[34], E. Duchovni[173], G. Duckeck[99], O.A. Ducu[26a], D. Duda[176], A. Dudarev[30], F. Dudziak[63], L. Duflot[116], L. Duguid[76], M. Dührssen[30], M. Dunford[58a], H. Duran Yildiz[4a], M. Düren[52], A. Durglishvili[51b], M. Dwuznik[38a], M. Dyndal[38a], J. Ebke[99], W. Edson[2], N.C. Edwards[46], W. Ehrenfeld[21], T. Eifert[144], G. Eigen[14], K. Einsweiler[15], T. Ekelof[167], M. El Kacimi[136c], M. Ellert[167], S. Elles[5], F. Ellinghaus[82], N. Ellis[30], J. Elmsheuser[99], M. Elsing[30], D. Emeliyanov[130], Y. Enari[156], O.C. Endner[82], M. Endo[117], R. Engelmann[149], J. Erdmann[177], A. Ereditato[17], D. Eriksson[147a], G. Ernis[176], J. Ernst[2], M. Ernst[25], J. Ernwein[137], D. Errede[166], S. Errede[166], E. Ertel[82], M. Escalier[116], H. Esch[43], C. Escobar[124], B. Esposito[47], A.I. Etienvre[137], E. Etzion[154], H. Evans[60], A. Ezhilov[122], L. Fabbri[20a,20b], G. Facini[31], R.M. Fakhrutdinov[129], S. Falciano[133a], R.J. Falla[77], J. Faltova[128], Y. Fang[33a], M. Fanti[90a,90b], A. Farbin[8], A. Farilla[135a], T. Farooque[12], S. Farrell[164], S.M. Farrington[171], P. Farthouat[30], F. Fassi[168], P. Fassnacht[30], D. Fassouliotis[9], A. Favareto[50a,50b], L. Fayard[116], P. Federic[145a], O.L. Fedin[122,j], W. Fedorko[169], M. Fehling-Kaschek[48], S. Feigl[30], L. Feligioni[84], C. Feng[33d], E.J. Feng[6], H. Feng[88], A.B. Fenyuk[129], S. Fernandez Perez[30], S. Ferrag[53], J. Ferrando[53], A. Ferrari[167], P. Ferrari[106], R. Ferrari[120a], D.E. Ferreira de Lima[53], A. Ferrer[168], D. Ferrere[49], C. Ferretti[88], A. Ferretto Parodi[50a,50b], M. Fiascaris[31], F. Fiedler[82], A. Filipčič[74], M. Filipuzzi[42], F. Filthaut[105], M. Fincke-Keeler[170], K.D. Finelli[151], M.C.N. Fiolhais[125a,125c], L. Fiorini[168], A. Firan[40], A. Fischer[2], J. Fischer[176], W.C. Fisher[89], E.A. Fitzgerald[23], M. Flechl[48], I. Fleck[142], P. Fleischmann[88], S. Fleischmann[176], G.T. Fletcher[140], G. Fletcher[75], T. Flick[176], A. Floderus[80], L.R. Flores Castillo[174,k], A.C. Florez Bustos[160b], M.J. Flowerdew[100], A. Formica[137], A. Forti[83], D. Fortin[160a], D. Fournier[116], H. Fox[71], S. Fracchia[12], P. Francavilla[79], M. Franchini[20a,20b], S. Franchino[30], D. Francis[30], M. Franklin[57], S. Franz[61], M. Fraternali[120a,120b], S.T. French[28], C. Friedrich[42], F. Friedrich[44], D. Froidevaux[30], J.A. Frost[28], C. Fukunaga[157], E. Fullana Torregrosa[82], B.G. Fulsom[144], J. Fuster[168], C. Gabaldon[55], O. Gabizon[173], A. Gabrielli[20a,20b], A. Gabrielli[133a,133b], S. Gadatsch[106], S. Gadomski[49], G. Gagliardi[50a,50b], P. Gagnon[60], C. Galea[105], B. Galhardo[125a,125c], E.J. Gallas[119], V. Gallo[17], B.J. Gallop[130], P. Gallus[127], G. Galster[36], K.K. Gan[110], R.P. Gandrajula[62], J. Gao[33b,g], Y.S. Gao[144,e], F.M. Garay Walls[46], F. Garberson[177], C. García[168], J.E. García Navarro[168], M. Garcia-Sciveres[15], R.W. Gardner[31], N. Garelli[144], V. Garonne[30], C. Gatti[47], G. Gaudio[120a], B. Gaur[142], L. Gauthier[94], P. Gauzzi[133a,133b], I.L. Gavrilenko[95], C. Gay[169], G. Gaycken[21], E.N. Gazis[10], P. Ge[33d], Z. Gecse[169], C.N.P. Gee[130], D.A.A. Geerts[106], Ch. Geich-Gimbel[21], K. Gellerstedt[147a,147b], C. Gemme[50a], A. Gemmell[53], M.H. Genest[55], S. Gentile[133a,133b], M. George[54], S. George[76], D. Gerbaudo[164], A. Gershon[154], H. Ghazlane[136b], N. Ghodbane[34],

JHEP01(2015)020

B. Giacobbe[20a], S. Giagu[133a,133b], V. Giangiobbe[12], P. Giannetti[123a,123b], F. Gianotti[30], B. Gibbard[25], S.M. Gibson[76], M. Gilchriese[15], T.P.S. Gillam[28], D. Gillberg[30], G. Gilles[34], D.M. Gingrich[3,d], N. Giokaris[9], M.P. Giordani[165a,165c], R. Giordano[103a,103b], F.M. Giorgi[20a], F.M. Giorgi[16], P.F. Giraud[137], D. Giugni[90a], C. Giuliani[48], M. Giulini[58b], B.K. Gjelsten[118], S. Gkaitatzis[155], I. Gkialas[155,l], L.K. Gladilin[98], C. Glasman[81], J. Glatzer[30], P.C.F. Glaysher[46], A. Glazov[42], G.L. Glonti[64], M. Goblirsch-Kolb[100], J.R. Goddard[75], J. Godfrey[143], J. Godlewski[30], C. Goeringer[82], S. Goldfarb[88], T. Golling[177], D. Golubkov[129], A. Gomes[125a,125b,125d], L.S. Gomez Fajardo[42], R. Gonçalo[125a], J. Goncalves Pinto Firmino Da Costa[137], L. Gonella[21], S. González de la Hoz[168], G. Gonzalez Parra[12], S. Gonzalez-Sevilla[49], L. Goossens[30], P.A. Gorbounov[96], H.A. Gordon[25], I. Gorelov[104], B. Gorini[30], E. Gorini[72a,72b], A. Gorišek[74], E. Gornicki[39], A.T. Goshaw[6], C. Gössling[43], M.I. Gostkin[64], M. Gouighri[136a], D. Goujdami[136c], M.P. Goulette[49], A.G. Goussiou[139], C. Goy[5], S. Gozpinar[23], H.M.X. Grabas[137], L. Graber[54], I. Grabowska-Bold[38a], P. Grafström[20a,20b], K-J. Grahn[42], J. Gramling[49], E. Gramstad[118], S. Grancagnolo[16], V. Grassi[149], V. Gratchev[122], H.M. Gray[30], E. Graziani[135a], O.G. Grebenyuk[122], Z.D. Greenwood[78,m], K. Gregersen[77], I.M. Gregor[42], P. Grenier[144], J. Griffiths[8], A.A. Grillo[138], K. Grimm[71], S. Grinstein[12,n], Ph. Gris[34], Y.V. Grishkevich[98], J.-F. Grivaz[116], J.P. Grohs[44], A. Grohsjean[42], E. Gross[173], J. Grosse-Knetter[54], G.C. Grossi[134a,134b], J. Groth-Jensen[173], Z.J. Grout[150], L. Guan[33b], F. Guescini[49], D. Guest[177], O. Gueta[154], C. Guicheney[34], E. Guido[50a,50b], T. Guillemin[116], S. Guindon[2], U. Gul[53], C. Gumpert[44], J. Gunther[127], J. Guo[35], S. Gupta[119], P. Gutierrez[112], N.G. Gutierrez Ortiz[53], C. Gutschow[77], N. Guttman[154], C. Guyot[137], C. Gwenlan[119], C.B. Gwilliam[73], A. Haas[109], C. Haber[15], H.K. Hadavand[8], N. Haddad[136e], P. Haefner[21], S. Hageböck[21], Z. Hajduk[39], H. Hakobyan[178], M. Haleem[42], D. Hall[119], G. Halladjian[89], K. Hamacher[176], P. Hamal[114], K. Hamano[170], M. Hamer[54], A. Hamilton[146a], S. Hamilton[162], P.G. Hamnett[42], L. Han[33b], K. Hanagaki[117], K. Hanawa[156], M. Hance[15], P. Hanke[58a], R. Hanna[137], J.B. Hansen[36], J.D. Hansen[36], P.H. Hansen[36], K. Hara[161], A.S. Hard[174], T. Harenberg[176], F. Hariri[116], S. Harkusha[91], D. Harper[88], R.D. Harrington[46], O.M. Harris[139], P.F. Harrison[171], F. Hartjes[106], S. Hasegawa[102], Y. Hasegawa[141], A. Hasib[112], S. Hassani[137], S. Haug[17], M. Hauschild[30], R. Hauser[89], M. Havranek[126], C.M. Hawkes[18], R.J. Hawkings[30], A.D. Hawkins[80], T. Hayashi[161], D. Hayden[89], C.P. Hays[119], H.S. Hayward[73], S.J. Haywood[130], S.J. Head[18], T. Heck[82], V. Hedberg[80], L. Heelan[8], S. Heim[121], T. Heim[176], B. Heinemann[15], L. Heinrich[109], J. Hejbal[126], L. Helary[22], C. Heller[99], M. Heller[30], S. Hellman[147a,147b], D. Hellmich[21], C. Helsens[30], J. Henderson[119], R.C.W. Henderson[71], Y. Heng[174], C. Hengler[42], A. Henrichs[177], A.M. Henriques Correia[30], S. Henrot-Versille[116], C. Hensel[54], G.H. Herbert[16], Y. Hernández Jiménez[168], R. Herrberg-Schubert[16], G. Herten[48], R. Hertenberger[99], L. Hervas[30], G.G. Hesketh[77], N.P. Hessey[106], R. Hickling[75], E. Higón-Rodriguez[168], E. Hill[170], J.C. Hill[28], K.H. Hiller[42], S. Hillert[21], S.J. Hillier[18], I. Hinchliffe[15], E. Hines[121], M. Hirose[158], D. Hirschbuehl[176], J. Hobbs[149], N. Hod[106], M.C. Hodgkinson[140], P. Hodgson[140], A. Hoecker[30], M.R. Hoeferkamp[104], J. Hoffman[40], D. Hoffmann[84], J.I. Hofmann[58a], M. Hohlfeld[82], T.R. Holmes[15], T.M. Hong[121], L. Hooft van Huysduynen[109], J-Y. Hostachy[55], S. Hou[152], A. Hoummada[136a], J. Howard[119], J. Howarth[42], M. Hrabovsky[114], I. Hristova[16], J. Hrivnac[116], T. Hryn'ova[5], C. Hsu[146c], P.J. Hsu[82], S.-C. Hsu[139], D. Hu[35], X. Hu[25], Y. Huang[42], Z. Hubacek[30], F. Hubaut[84], F. Huegging[21], T.B. Huffman[119], E.W. Hughes[35], G. Hughes[71], M. Huhtinen[30], T.A. Hülsing[82], M. Hurwitz[15], N. Huseynov[64,b], J. Huston[89], J. Huth[57], G. Iacobucci[49], G. Iakovidis[10], I. Ibragimov[142], L. Iconomidou-Fayard[116], E. Ideal[177], P. Iengo[103a], O. Igonkina[106], T. Iizawa[172], Y. Ikegami[65], K. Ikematsu[142], M. Ikeno[65], Y. Ilchenko[31,o], D. Iliadis[155], N. Ilic[159], Y. Inamaru[66], T. Ince[100], P. Ioannou[9], M. Iodice[135a], K. Iordanidou[9], V. Ippolito[57], A. Irles Quiles[168], C. Isaksson[167], M. Ishino[67], M. Ishitsuka[158], R. Ishmukhametov[110], C. Issever[119], S. Istin[19a], J.M. Iturbe Ponce[83], R. Iuppa[134a,134b], J. Ivarsson[80], W. Iwanski[39], H. Iwasaki[65], J.M. Izen[41], V. Izzo[103a], B. Jackson[121], M. Jackson[73], P. Jackson[1], M.R. Jaekel[30], V. Jain[2], K. Jakobs[48], S. Jakobsen[30], T. Jakoubek[126], J. Jakubek[127], D.O. Jamin[152], D.K. Jana[78], E. Jansen[77], H. Jansen[30], J. Janssen[21], M. Janus[171], G. Jarlskog[80], N. Javadov[64,b], T. Javůrek[48],

JHEP01(2015)020

L. Jeanty[15], J. Jejelava[51a,p], G.-Y. Jeng[151], D. Jennens[87], P. Jenni[48,q], J. Jentzsch[43], C. Jeske[171], S. Jézéquel[5], H. Ji[174], W. Ji[82], J. Jia[149], Y. Jiang[33b], M. Jimenez Belenguer[42], S. Jin[33a], A. Jinaru[26a], O. Jinnouchi[158], M.D. Joergensen[36], K.E. Johansson[147a,147b], P. Johansson[140], K.A. Johns[7], K. Jon-And[147a,147b], G. Jones[171], R.W.L. Jones[71], T.J. Jones[73], J. Jongmanns[58a], P.M. Jorge[125a,125b], K.D. Joshi[83], J. Jovicevic[148], X. Ju[174], C.A. Jung[43], R.M. Jungst[30], P. Jussel[61], A. Juste Rozas[12,n], M. Kaci[168], A. Kaczmarska[39], M. Kado[116], H. Kagan[110], M. Kagan[144], E. Kajomovitz[45], C.W. Kalderon[119], S. Kama[40], A. Kamenshchikov[129], N. Kanaya[156], M. Kaneda[30], S. Kaneti[28], V.A. Kantserov[97], J. Kanzaki[65], B. Kaplan[109], A. Kapliy[31], D. Kar[53], K. Karakostas[10], N. Karastathis[10], M. Karnevskiy[82], S.N. Karpov[64], Z.M. Karpova[64], K. Karthik[109], V. Kartvelishvili[71], A.N. Karyukhin[129], L. Kashif[174], G. Kasieczka[58b], R.D. Kass[110], A. Kastanas[14], Y. Kataoka[156], A. Katre[49], J. Katzy[42], V. Kaushik[7], K. Kawagoe[69], T. Kawamoto[156], G. Kawamura[54], S. Kazama[156], V.F. Kazanin[108], M.Y. Kazarinov[64], R. Keeler[170], R. Kehoe[40], M. Keil[54], J.S. Keller[42], J.J. Kempster[76], H. Keoshkerian[5], O. Kepka[126], B.P. Kerševan[74], S. Kersten[176], K. Kessoku[156], J. Keung[159], F. Khalil-zada[11], H. Khandanyan[147a,147b], A. Khanov[113], A. Khodinov[97], A. Khomich[58a], T.J. Khoo[28], G. Khoriauli[21], A. Khoroshilov[176], V. Khovanskiy[96], E. Khramov[64], J. Khubua[51b], H.Y. Kim[8], H. Kim[147a,147b], S.H. Kim[161], N. Kimura[172], O. Kind[16], B.T. King[73], M. King[168], R.S.B. King[119], S.B. King[169], J. Kirk[130], A.E. Kiryunin[100], T. Kishimoto[66], D. Kisielewska[38a], F. Kiss[48], T. Kittelmann[124], K. Kiuchi[161], E. Kladiva[145b], M. Klein[73], U. Klein[73], K. Kleinknecht[82], P. Klimek[147a,147b], A. Klimentov[25], R. Klingenberg[43], J.A. Klinger[83], T. Klioutchnikova[30], P.F. Klok[105], E.-E. Kluge[58a], P. Kluit[106], S. Kluth[100], E. Kneringer[61], E.B.F.G. Knoops[84], A. Knue[53], D. Kobayashi[158], T. Kobayashi[156], M. Kobel[44], M. Kocian[144], P. Kodys[128], P. Koevesarki[21], T. Koffas[29], E. Koffeman[106], L.A. Kogan[119], S. Kohlmann[176], Z. Kohout[127], T. Kohriki[65], T. Koi[144], H. Kolanoski[16], I. Koletsou[5], J. Koll[89], A.A. Komar[95,*], Y. Komori[156], T. Kondo[65], N. Kondrashova[42], K. Köneke[48], A.C. König[105], S. König[82], T. Kono[65,r], R. Konoplich[109,s], N. Konstantinidis[77], R. Kopeliansky[153], S. Koperny[38a], L. Köpke[82], A.K. Kopp[48], K. Korcyl[39], K. Kordas[155], A. Korn[77], A.A. Korol[108,t], I. Korolkov[12], E.V. Korolkova[140], V.A. Korotkov[129], O. Kortner[100], S. Kortner[100], V.V. Kostyukhin[21], V.M. Kotov[64], A. Kotwal[45], C. Kourkoumelis[9], V. Kouskoura[155], A. Koutsman[160a], R. Kowalewski[170], T.Z. Kowalski[38a], W. Kozanecki[137], A.S. Kozhin[129], V. Kral[127], V.A. Kramarenko[98], G. Kramberger[74], D. Krasnopevtsev[97], M.W. Krasny[79], A. Krasznahorkay[30], J.K. Kraus[21], A. Kravchenko[25], S. Kreiss[109], M. Kretz[58c], J. Kretzschmar[73], K. Kreutzfeldt[52], P. Krieger[159], K. Kroeninger[54], H. Kroha[100], J. Kroll[121], J. Kroseberg[21], J. Krstic[13a], U. Kruchonak[64], H. Krüger[21], T. Kruker[17], N. Krumnack[63], Z.V. Krumshteyn[64], A. Kruse[174], M.C. Kruse[45], M. Kruskal[22], T. Kubota[87], S. Kuday[4a], S. Kuehn[48], A. Kugel[58c], A. Kuhl[138], T. Kuhl[42], V. Kukhtin[64], Y. Kulchitsky[91], S. Kuleshov[32b], M. Kuna[133a,133b], J. Kunkle[121], A. Kupco[126], H. Kurashige[66], Y.A. Kurochkin[91], R. Kurumida[66], V. Kus[126], E.S. Kuwertz[148], M. Kuze[158], J. Kvita[114], A. La Rosa[49], L. La Rotonda[37a,37b], C. Lacasta[168], F. Lacava[133a,133b], J. Lacey[29], H. Lacker[16], D. Lacour[79], V.R. Lacuesta[168], E. Ladygin[64], R. Lafaye[5], B. Laforge[79], T. Lagouri[177], S. Lai[48], H. Laier[58a], L. Lambourne[77], S. Lammers[60], C.L. Lampen[7], W. Lampl[7], E. Lançon[137], U. Landgraf[48], M.P.J. Landon[75], V.S. Lang[58a], A.J. Lankford[164], F. Lanni[25], K. Lantzsch[30], S. Laplace[79], C. Lapoire[21], J.F. Laporte[137], T. Lari[90a], M. Lassnig[30], P. Laurelli[47], W. Lavrijsen[15], A.T. Law[138], P. Laycock[73], B.T. Le[55], O. Le Dortz[79], E. Le Guirriec[84], E. Le Menedeu[12], T. LeCompte[6], F. Ledroit-Guillon[55], C.A. Lee[152], H. Lee[106], J.S.H. Lee[117], S.C. Lee[152], L. Lee[177], G. Lefebvre[79], M. Lefebvre[170], F. Legger[99], C. Leggett[15], A. Lehan[73], M. Lehmacher[21], G. Lehmann Miotto[30], X. Lei[7], W.A. Leight[29], A. Leisos[155], A.G. Leister[177], M.A.L. Leite[24d], R. Leitner[128], D. Lellouch[173], B. Lemmer[54], K.J.C. Leney[77], T. Lenz[106], G. Lenzen[176], B. Lenzi[30], R. Leone[7], S. Leone[123a,123b], K. Leonhardt[44], C. Leonidopoulos[46], S. Leontsinis[10], C. Leroy[94], C.G. Lester[28], C.M. Lester[121], M. Levchenko[122], J. Levêque[5], D. Levin[88], L.J. Levinson[173], M. Levy[18], A. Lewis[119], G.H. Lewis[109], A.M. Leyko[21], M. Leyton[41], B. Li[33b,u], B. Li[84], H. Li[149], H.L. Li[31], L. Li[45], L. Li[33e], S. Li[45], Y. Li[33c,v], Z. Liang[138], H. Liao[34], B. Liberti[134a], P. Lichard[30], K. Lie[166], J. Liebal[21], W. Liebig[14], C. Limbach[21], A. Limosani[87],

JHEP01(2015)020

S.C. Lin[152,w], T.H. Lin[82], F. Linde[106], B.E. Lindquist[149], J.T. Linnemann[89], E. Lipeles[121], A. Lipniacka[14], M. Lisovyi[42], T.M. Liss[166], D. Lissauer[25], A. Lister[169], A.M. Litke[138], B. Liu[152], D. Liu[152], J.B. Liu[33b], K. Liu[33b,x], L. Liu[88], M. Liu[45], M. Liu[33b], Y. Liu[33b], M. Livan[120a,120b], S.S.A. Livermore[119], A. Lleres[55], J. Llorente Merino[81], S.L. Lloyd[75], F. Lo Sterzo[152], E. Lobodzinska[42], P. Loch[7], W.S. Lockman[138], T. Loddenkoetter[21], F.K. Loebinger[83], A.E. Loevschall-Jensen[36], A. Loginov[177], C.W. Loh[169], T. Lohse[16], K. Lohwasser[42], M. Lokajicek[126], V.P. Lombardo[5], B.A. Long[22], J.D. Long[88], R.E. Long[71], L. Lopes[125a], D. Lopez Mateos[57], B. Lopez Paredes[140], I. Lopez Paz[12], J. Lorenz[99], N. Lorenzo Martinez[60], M. Losada[163], P. Loscutoff[15], X. Lou[41], A. Lounis[116], J. Love[6], P.A. Love[71], A.J. Lowe[144,e], F. Lu[33a], H.J. Lubatti[139], C. Luci[133a,133b], A. Lucotte[55], F. Luehring[60], W. Lukas[61], L. Luminari[133a], O. Lundberg[147a,147b], B. Lund-Jensen[148], M. Lungwitz[82], D. Lynn[25], R. Lysak[126], E. Lytken[80], H. Ma[25], L.L. Ma[33d], G. Maccarrone[47], A. Macchiolo[100], J. Machado Miguens[125a,125b], D. Macina[30], D. Madaffari[84], R. Madar[48], H.J. Maddocks[71], W.F. Mader[44], A. Madsen[167], M. Maeno[8], T. Maeno[25], E. Magradze[54], K. Mahboubi[48], J. Mahlstedt[106], S. Mahmoud[73], C. Maiani[137], C. Maidantchik[24a], A.A. Maier[100], A. Maio[125a,125b,125d], S. Majewski[115], Y. Makida[65], N. Makovec[116], P. Mal[137,y], B. Malaescu[79], Pa. Malecki[39], V.P. Maleev[122], F. Malek[55], U. Mallik[62], D. Malon[6], C. Malone[144], S. Maltezos[10], V.M. Malyshev[108], S. Malyukov[30], J. Mamuzic[13b], B. Mandelli[30], L. Mandelli[90a], I. Mandić[74], R. Mandrysch[62], J. Maneira[125a,125b], A. Manfredini[100], L. Manhaes de Andrade Filho[24b], J.A. Manjarres Ramos[160b], A. Mann[99], P.M. Manning[138], A. Manousakis-Katsikakis[9], B. Mansoulie[137], R. Mantifel[86], L. Mapelli[30], L. March[168], J.F. Marchand[29], G. Marchiori[79], M. Marcisovsky[126], C.P. Marino[170], M. Marjanovic[13a], C.N. Marques[125a], F. Marroquim[24a], S.P. Marsden[83], Z. Marshall[15], L.F. Marti[17], S. Marti-Garcia[168], B. Martin[30], B. Martin[89], T.A. Martin[171], V.J. Martin[46], B. Martin dit Latour[14], H. Martinez[137], M. Martinez[12,n], S. Martin-Haugh[130], A.C. Martyniuk[77], M. Marx[139], F. Marzano[133a], A. Marzin[30], L. Masetti[82], T. Mashimo[156], R. Mashinistov[95], J. Masik[83], A.L. Maslennikov[108], I. Massa[20a,20b], N. Massol[5], P. Mastrandrea[149], A. Mastroberardino[37a,37b], T. Masubuchi[156], P. Mättig[176], J. Mattmann[82], J. Maurer[26a], S.J. Maxfield[73], D.A. Maximov[108,t], R. Mazini[152], L. Mazzaferro[134a,134b], G. Mc Goldrick[159], S.P. Mc Kee[88], A. McCarn[88], R.L. McCarthy[149], T.G. McCarthy[29], N.A. McCubbin[130], K.W. McFarlane[56,*], J.A. Mcfayden[77], G. Mchedlidze[54], S.J. McMahon[130], R.A. McPherson[170,i], A. Meade[85], J. Mechnich[106], M. Medinnis[42], S. Meehan[31], S. Mehlhase[99], A. Mehta[73], K. Meier[58a], C. Meineck[99], B. Meirose[80], C. Melachrinos[31], B.R. Mellado Garcia[146c], F. Meloni[17], A. Mengarelli[20a,20b], S. Menke[100], E. Meoni[162], K.M. Mercurio[57], S. Mergelmeyer[21], N. Meric[137], P. Mermod[49], L. Merola[103a,103b], C. Meroni[90a], F.S. Merritt[31], H. Merritt[110], A. Messina[30,z], J. Metcalfe[25], A.S. Mete[164], C. Meyer[82], C. Meyer[31], J-P. Meyer[137], J. Meyer[30], R.P. Middleton[130], S. Migas[73], L. Mijović[21], G. Mikenberg[173], M. Mikestikova[126], M. Mikuž[74], A. Milic[30], D.W. Miller[31], C. Mills[46], A. Milov[173], D.A. Milstead[147a,147b], D. Milstein[173], A.A. Minaenko[129], I.A. Minashvili[64], A.I. Mincer[109], B. Mindur[38a], M. Mineev[64], Y. Ming[174], L.M. Mir[12], G. Mirabelli[133a], T. Mitani[172], J. Mitrevski[99], V.A. Mitsou[168], S. Mitsui[65], A. Miucci[49], P.S. Miyagawa[140], J.U. Mjörnmark[80], T. Moa[147a,147b], K. Mochizuki[84], S. Mohapatra[35], W. Mohr[48], S. Molander[147a,147b], R. Moles-Valls[168], K. Mönig[42], C. Monini[55], J. Monk[36], E. Monnier[84], J. Montejo Berlingen[12], F. Monticelli[70], S. Monzani[133a,133b], R.W. Moore[3], A. Moraes[53], N. Morange[62], D. Moreno[82], M. Moreno Llácer[54], P. Morettini[50a], M. Morgenstern[44], M. Morii[57], S. Moritz[82], A.K. Morley[148], G. Mornacchi[30], J.D. Morris[75], L. Morvaj[102], H.G. Moser[100], M. Mosidze[51b], J. Moss[110], K. Motohashi[158], R. Mount[144], E. Mountricha[25], S.V. Mouraviev[95,*], E.J.W. Moyse[85], S. Muanza[84], R.D. Mudd[18], F. Mueller[58a], J. Mueller[124], K. Mueller[21], T. Mueller[28], T. Mueller[82], D. Muenstermann[49], Y. Munwes[154], J.A. Murillo Quijada[18], W.J. Murray[171,130], H. Musheghyan[54], E. Musto[153], A.G. Myagkov[129,aa], M. Myska[127], O. Nackenhorst[54], J. Nadal[54], K. Nagai[61], R. Nagai[158], Y. Nagai[84], K. Nagano[65], A. Nagarkar[110], Y. Nagasaka[59], M. Nagel[100], A.M. Nairz[30], Y. Nakahama[30], K. Nakamura[65], T. Nakamura[156], I. Nakano[111], H. Namasivayam[41], G. Nanava[21], R. Narayan[58b], T. Nattermann[21], T. Naumann[42], G. Navarro[163], R. Nayyar[7], H.A. Neal[88], P.Yu. Nechaeva[95],

JHEP01(2015)020

T.J. Neep[83], P.D. Nef[144], A. Negri[120a,120b], G. Negri[30], M. Negrini[20a], S. Nektarijevic[49], A. Nelson[164], T.K. Nelson[144], S. Nemecek[126], P. Nemethy[109], A.A. Nepomuceno[24a], M. Nessi[30,ab], M.S. Neubauer[166], M. Neumann[176], R.M. Neves[109], P. Nevski[25], P.R. Newman[18], D.H. Nguyen[6], R.B. Nickerson[119], R. Nicolaidou[137], B. Nicquevert[30], J. Nielsen[138], N. Nikiforou[35], A. Nikiforov[16], V. Nikolaenko[129,aa], I. Nikolic-Audit[79], K. Nikolics[49], K. Nikolopoulos[18], P. Nilsson[8], Y. Ninomiya[156], A. Nisati[133a], R. Nisius[100], T. Nobe[158], L. Nodulman[6], M. Nomachi[117], I. Nomidis[155], S. Norberg[112], M. Nordberg[30], S. Nowak[100], M. Nozaki[65], L. Nozka[114], K. Ntekas[10], G. Nunes Hanninger[87], T. Nunnemann[99], E. Nurse[77], F. Nuti[87], B.J. O'Brien[46], F. O'grady[7], D.C. O'Neil[143], V. O'Shea[53], F.G. Oakham[29,d], H. Oberlack[100], T. Obermann[21], J. Ocariz[79], A. Ochi[66], M.I. Ochoa[77], S. Oda[69], S. Odaka[65], H. Ogren[60], A. Oh[83], S.H. Oh[45], C.C. Ohm[30], H. Ohman[167], T. Ohshima[102], W. Okamura[117], H. Okawa[25], Y. Okumura[31], T. Okuyama[156], A. Olariu[26a], A.G. Olchevski[64], S.A. Olivares Pino[46], D. Oliveira Damazio[25], E. Oliver Garcia[168], A. Olszewski[39], J. Olszowska[39], A. Onofre[125a,125e], P.U.E. Onyisi[31,o], C.J. Oram[160a], M.J. Oreglia[31], Y. Oren[154], D. Orestano[135a,135b], N. Orlando[72a,72b], C. Oropeza Barrera[53], R.S. Orr[159], B. Osculati[50a,50b], R. Ospanov[121], G. Otero y Garzon[27], H. Otono[69], M. Ouchrif[136d], E.A. Ouellette[170], F. Ould-Saada[118], A. Ouraou[137], K.P. Oussoren[106], Q. Ouyang[33a], A. Ovcharova[15], M. Owen[83], V.E. Ozcan[19a], N. Ozturk[8], K. Pachal[119], A. Pacheco Pages[12], C. Padilla Aranda[12], M. Pagáčová[48], S. Pagan Griso[15], E. Paganis[140], C. Pahl[100], F. Paige[25], P. Pais[85], K. Pajchel[118], G. Palacino[160b], S. Palestini[30], M. Palka[38b], D. Pallin[34], A. Palma[125a,125b], J.D. Palmer[18], Y.B. Pan[174], E. Panagiotopoulou[10], J.G. Panduro Vazquez[76], P. Pani[106], N. Panikashvili[88], S. Panitkin[25], D. Pantea[26a], L. Paolozzi[134a,134b], Th.D. Papadopoulou[10], K. Papageorgiou[155,l], A. Paramonov[6], D. Paredes Hernandez[34], M.A. Parker[28], F. Parodi[50a,50b], J.A. Parsons[35], U. Parzefall[48], E. Pasqualucci[133a], S. Passaggio[50a], A. Passeri[135a], F. Pastore[135a,135b,*], Fr. Pastore[76], G. Pásztor[29], S. Pataraia[176], N.D. Patel[151], J.R. Pater[83], S. Patricelli[103a,103b], T. Pauly[30], J. Pearce[170], M. Pedersen[118], S. Pedraza Lopez[168], R. Pedro[125a,125b], S.V. Peleganchuk[108], D. Pelikan[167], H. Peng[33b], B. Penning[31], J. Penwell[60], D.V. Perepelitsa[25], E. Perez Codina[160a], M.T. Pérez García-Estañ[168], V. Perez Reale[35], L. Perini[90a,90b], H. Pernegger[30], R. Perrino[72a], R. Peschke[42], V.D. Peshekhonov[64], K. Peters[30], R.F.Y. Peters[83], B.A. Petersen[30], T.C. Petersen[36], E. Petit[42], A. Petridis[147a,147b], C. Petridou[155], E. Petrolo[133a], F. Petrucci[135a,135b], N.E. Pettersson[158], R. Pezoa[32b], P.W. Phillips[130], G. Piacquadio[144], E. Pianori[171], A. Picazio[49], E. Piccaro[75], M. Piccinini[20a,20b], R. Piegaia[27], D.T. Pignotti[110], J.E. Pilcher[31], A.D. Pilkington[77], J. Pina[125a,125b,125d], M. Pinamonti[165a,165c,ac], A. Pinder[119], J.L. Pinfold[3], A. Pingel[36], B. Pinto[125a], S. Pires[79], M. Pitt[173], C. Pizio[90a,90b], L. Plazak[145a], M.-A. Pleier[25], V. Pleskot[128], E. Plotnikova[64], P. Plucinski[147a,147b], S. Poddar[58a], F. Podlyski[34], R. Poettgen[82], L. Poggioli[116], D. Pohl[21], M. Pohl[49], G. Polesello[120a], A. Policicchio[37a,37b], R. Polifka[159], A. Polini[20a], C.S. Pollard[45], V. Polychronakos[25], K. Pommès[30], L. Pontecorvo[133a], B.G. Pope[89], G.A. Popeneciu[26b], D.S. Popovic[13a], A. Poppleton[30], X. Portell Bueso[12], S. Pospisil[127], K. Potamianos[15], I.N. Potrap[64], C.J. Potter[150], C.T. Potter[115], G. Poulard[30], J. Poveda[60], V. Pozdnyakov[64], P. Pralavorio[84], A. Pranko[15], S. Prasad[30], R. Pravahan[8], S. Prell[63], D. Price[83], J. Price[73], L.E. Price[6], D. Prieur[124], M. Primavera[72a], M. Proissl[46], K. Prokofiev[47], F. Prokoshin[32b], E. Protopapadaki[137], S. Protopopescu[25], J. Proudfoot[6], M. Przybycien[38a], H. Przysiezniak[5], E. Ptacek[115], D. Puddu[135a,135b], E. Pueschel[85], D. Puldon[149], M. Purohit[25,ad], P. Puzo[116], J. Qian[88], G. Qin[53], Y. Qin[83], A. Quadt[54], D.R. Quarrie[15], W.B. Quayle[165a,165b], M. Queitsch-Maitland[83], D. Quilty[53], A. Qureshi[160b], V. Radeka[25], V. Radescu[42], S.K. Radhakrishnan[149], P. Radloff[115], P. Rados[87], F. Ragusa[90a,90b], G. Rahal[179], S. Rajagopalan[25], M. Rammensee[30], A.S. Randle-Conde[40], C. Rangel-Smith[167], K. Rao[164], F. Rauscher[99], T.C. Rave[48], T. Ravenscroft[53], M. Raymond[30], A.L. Read[118], N.P. Readioff[73], D.M. Rebuzzi[120a,120b], A. Redelbach[175], G. Redlinger[25], R. Reece[138], K. Reeves[41], L. Rehnisch[16], H. Reisin[27], M. Relich[164], C. Rembser[30], H. Ren[33a], Z.L. Ren[152], A. Renaud[116], M. Rescigno[133a], S. Resconi[90a], O.L. Rezanova[108,t], P. Reznicek[128], R. Rezvani[94], R. Richter[100], M. Ridel[79], P. Rieck[16], J. Rieger[54], M. Rijssenbeek[149], A. Rimoldi[120a,120b], L. Rinaldi[20a], E. Ritsch[61],

JHEP01(2015)020

I. Riu[12], F. Rizatdinova[113], E. Rizvi[75], S.H. Robertson[86,i], A. Robichaud-Veronneau[86], D. Robinson[28], J.E.M. Robinson[83], A. Robson[53], C. Roda[123a,123b], L. Rodrigues[30], S. Roe[30], O. Røhne[118], S. Rolli[162], A. Romaniouk[97], M. Romano[20a,20b], E. Romero Adam[168], N. Rompotis[139], L. Roos[79], E. Ros[168], S. Rosati[133a], K. Rosbach[49], M. Rose[76], P.L. Rosendahl[14], O. Rosenthal[142], V. Rossetti[147a,147b], E. Rossi[103a,103b], L.P. Rossi[50a], R. Rosten[139], M. Rotaru[26a], I. Roth[173], J. Rothberg[139], D. Rousseau[116], C.R. Royon[137], A. Rozanov[84], Y. Rozen[153], X. Ruan[146c], F. Rubbo[12], I. Rubinskiy[42], V.I. Rud[98], C. Rudolph[44], M.S. Rudolph[159], F. Rühr[48], A. Ruiz-Martinez[30], Z. Rurikova[48], N.A. Rusakovich[64], A. Ruschke[99], J.P. Rutherfoord[7], N. Ruthmann[48], Y.F. Ryabov[122], M. Rybar[128], G. Rybkin[116], N.C. Ryder[119], A.F. Saavedra[151], S. Sacerdoti[27], A. Saddique[3], I. Sadeh[154], H.F-W. Sadrozinski[138], R. Sadykov[64], F. Safai Tehrani[133a], H. Sakamoto[156], Y. Sakurai[172], G. Salamanna[135a,135b], A. Salamon[134a], M. Saleem[112], D. Salek[106], P.H. Sales De Bruin[139], D. Salihagic[100], A. Salnikov[144], J. Salt[168], B.M. Salvachua Ferrando[6], D. Salvatore[37a,37b], F. Salvatore[150], A. Salvucci[105], A. Salzburger[30], D. Sampsonidis[155], A. Sanchez[103a,103b], J. Sánchez[168], V. Sanchez Martinez[168], H. Sandaker[14], R.L. Sandbach[75], H.G. Sander[82], M.P. Sanders[99], M. Sandhoff[176], T. Sandoval[28], C. Sandoval[163], R. Sandstroem[100], D.P.C. Sankey[130], A. Sansoni[47], C. Santoni[34], R. Santonico[134a,134b], H. Santos[125a], I. Santoyo Castillo[150], K. Sapp[124], A. Sapronov[64], J.G. Saraiva[125a,125d], B. Sarrazin[21], G. Sartisohn[176], O. Sasaki[65], Y. Sasaki[156], G. Sauvage[5,*], E. Sauvan[5], P. Savard[159,d], D.O. Savu[30], C. Sawyer[119], L. Sawyer[78,m], D.H. Saxon[53], J. Saxon[121], C. Sbarra[20a], A. Sbrizzi[3], T. Scanlon[77], D.A. Scannicchio[164], M. Scarcella[151], V. Scarfone[37a,37b], J. Schaarschmidt[173], P. Schacht[100], D. Schaefer[121], R. Schaefer[42], S. Schaepe[21], S. Schaetzel[58b], U. Schäfer[82], A.C. Schaffer[116], D. Schaile[99], R.D. Schamberger[149], V. Scharf[58a], V.A. Schegelsky[122], D. Scheirich[128], M. Schernau[164], M.I. Scherzer[35], C. Schiavi[50a,50b], J. Schieck[99], C. Schillo[48], M. Schioppa[37a,37b], S. Schlenker[30], E. Schmidt[48], K. Schmieden[30], C. Schmitt[82], C. Schmitt[99], S. Schmitt[58b], B. Schneider[17], Y.J. Schnellbach[73], U. Schnoor[44], L. Schoeffel[137], A. Schoening[58b], B.D. Schoenrock[89], A.L.S. Schorlemmer[54], M. Schott[82], D. Schouten[160a], J. Schovancova[25], S. Schramm[159], M. Schreyer[175], C. Schroeder[82], N. Schuh[82], M.J. Schultens[21], H.-C. Schultz-Coulon[58a], H. Schulz[16], M. Schumacher[48], B.A. Schumm[138], Ph. Schune[137], C. Schwanenberger[83], A. Schwartzman[144], Ph. Schwegler[100], Ph. Schwemling[137], R. Schwienhorst[89], J. Schwindling[137], T. Schwindt[21], M. Schwoerer[5], F.G. Sciacca[17], E. Scifo[116], G. Sciolla[23], W.G. Scott[130], F. Scuri[123a,123b], F. Scutti[21], J. Searcy[88], G. Sedov[42], E. Sedykh[122], S.C. Seidel[104], A. Seiden[138], F. Seifert[127], J.M. Seixas[24a], G. Sekhniaidze[103a], S.J. Sekula[40], K.E. Selbach[46], D.M. Seliverstov[122,*], G. Sellers[73], N. Semprini-Cesari[20a,20b], C. Serfon[30], L. Serin[116], L. Serkin[54], T. Serre[84], R. Seuster[160a], H. Severini[112], T. Sfiligoj[74], F. Sforza[100], A. Sfyrla[30], E. Shabalina[54], M. Shamim[115], L.Y. Shan[33a], R. Shang[166], J.T. Shank[22], M. Shapiro[15], P.B. Shatalov[96], K. Shaw[165a,165b], C.Y. Shehu[150], P. Sherwood[77], L. Shi[152,ae], S. Shimizu[66], C.O. Shimmin[164], M. Shimojima[101], M. Shiyakova[64], A. Shmeleva[95], M.J. Shochet[31], D. Short[119], S. Shrestha[63], E. Shulga[97], M.A. Shupe[7], S. Shushkevich[42], P. Sicho[126], O. Sidiropoulou[155], D. Sidorov[113], A. Sidoti[133a], F. Siegert[44], Dj. Sijacki[13a], J. Silva[125a,125d], Y. Silver[154], D. Silverstein[144], S.B. Silverstein[147a], V. Simak[127], O. Simard[5], Lj. Simic[13a], S. Simion[116], E. Simioni[82], B. Simmons[77], R. Simoniello[90a,90b], M. Simonyan[36], P. Sinervo[159], N.B. Sinev[115], V. Sipica[142], G. Siragusa[175], A. Sircar[78], A.N. Sisakyan[64,*], S.Yu. Sivoklokov[98], J. Sjölin[147a,147b], T.B. Sjursen[14], H.P. Skottowe[57], K.Yu. Skovpen[108], P. Skubic[112], M. Slater[18], T. Slavicek[127], K. Sliwa[162], V. Smakhtin[173], B.H. Smart[46], L. Smestad[14], S.Yu. Smirnov[97], Y. Smirnov[97], L.N. Smirnova[98,af], O. Smirnova[80], K.M. Smith[53], M. Smizanska[71], K. Smolek[127], A.A. Snesarev[95], G. Snidero[75], S. Snyder[25], R. Sobie[170,i], F. Socher[44], A. Soffer[154], D.A. Soh[152,ae], C.A. Solans[30], M. Solar[127], J. Solc[127], E.Yu. Soldatov[97], U. Soldevila[168], E. Solfaroli Camillocci[133a,133b], A.A. Solodkov[129], A. Soloshenko[64], O.V. Solovyanov[129], V. Solovyev[122], P. Sommer[48], H.Y. Song[33b], N. Soni[1], A. Sood[15], A. Sopczak[127], B. Sopko[127], V. Sopko[127], V. Sorin[12], M. Sosebee[8], R. Soualah[165a,165c], P. Soueid[94], A.M. Soukharev[108], D. South[42], S. Spagnolo[72a,72b], F. Spanò[76], W.R. Spearman[57], F. Spettel[100], R. Spighi[20a], G. Spigo[30], M. Spousta[128], T. Spreitzer[159], B. Spurlock[8],

JHEP01(2015)020

R.D. St. Denis[53,*], S. Staerz[44], J. Stahlman[121], R. Stamen[58a], E. Stanecka[39], R.W. Stanek[6], C. Stanescu[135a], M. Stanescu-Bellu[42], M.M. Stanitzki[42], S. Stapnes[118], E.A. Starchenko[129], J. Stark[55], P. Staroba[126], P. Starovoitov[42], R. Staszewski[39], P. Stavina[145a,*], P. Steinberg[25], B. Stelzer[143], H.J. Stelzer[30], O. Stelzer-Chilton[160a], H. Stenzel[52], S. Stern[100], G.A. Stewart[53], J.A. Stillings[21], M.C. Stockton[86], M. Stoebe[86], G. Stoicea[26a], P. Stolte[54], S. Stonjek[100], A.R. Stradling[8], A. Straessner[44], M.E. Stramaglia[17], J. Strandberg[148], S. Strandberg[147a,147b], A. Strandlie[118], E. Strauss[144], M. Strauss[112], P. Strizenec[145b], R. Ströhmer[175], D.M. Strom[115], R. Stroynowski[40], S.A. Stucci[17], B. Stugu[14], N.A. Styles[42], D. Su[144], J. Su[124], HS. Subramania[3], R. Subramaniam[78], A. Succurro[12], Y. Sugaya[117], C. Suhr[107], M. Suk[127], V.V. Sulin[95], S. Sultansoy[4c], T. Sumida[67], X. Sun[33a], J.E. Sundermann[48], K. Suruliz[140], G. Susinno[37a,37b], M.R. Sutton[150], Y. Suzuki[65], M. Svatos[126], S. Swedish[169], M. Swiatlowski[144], I. Sykora[145a], T. Sykora[128], D. Ta[89], C. Taccini[135a,135b], K. Tackmann[42], J. Taenzer[159], A. Taffard[164], R. Tafirout[160a], N. Taiblum[154], Y. Takahashi[102], H. Takai[25], R. Takashima[68], H. Takeda[66], T. Takeshita[141], Y. Takubo[65], M. Talby[84], A.A. Talyshev[108,t], J.Y.C. Tam[175], K.G. Tan[87], J. Tanaka[156], R. Tanaka[116], S. Tanaka[132], S. Tanaka[65], A.J. Tanasijczuk[143], B.B. Tannenwald[110], N. Tannoury[21], S. Tapprogge[82], S. Tarem[153], F. Tarrade[29], G.F. Tartarelli[90a], P. Tas[128], M. Tasevsky[126], T. Tashiro[67], E. Tassi[37a,37b], A. Tavares Delgado[125a,125b], Y. Tayalati[136d], F.E. Taylor[93], G.N. Taylor[87], W. Taylor[160b], F.A. Teischinger[30], M. Teixeira Dias Castanheira[75], P. Teixeira-Dias[76], K.K. Temming[48], H. Ten Kate[30], P.K. Teng[152], J.J. Teoh[117], S. Terada[65], K. Terashi[156], J. Terron[81], S. Terzo[100], M. Testa[47], R.J. Teuscher[159,i], J. Therhaag[21], T. Theveneaux-Pelzer[34], J.P. Thomas[18], J. Thomas-Wilsker[76], E.N. Thompson[35], P.D. Thompson[18], P.D. Thompson[159], A.S. Thompson[53], L.A. Thomsen[36], E. Thomson[121], M. Thomson[28], W.M. Thong[87], R.P. Thun[88,*], F. Tian[35], M.J. Tibbetts[15], V.O. Tikhomirov[95,ag], Yu.A. Tikhonov[108,t], S. Timoshenko[97], E. Tiouchichine[84], P. Tipton[177], S. Tisserant[84], T. Todorov[5], S. Todorova-Nova[128], B. Toggerson[7], J. Tojo[69], S. Tokár[145a], K. Tokushuku[65], K. Tollefson[89], L. Tomlinson[83], M. Tomoto[102], L. Tompkins[31], K. Toms[104], N.D. Topilin[64], E. Torrence[115], H. Torres[143], E. Torró Pastor[168], J. Toth[84,ah], F. Touchard[84], D.R. Tovey[140], H.L. Tran[116], T. Trefzger[175], L. Tremblet[30], A. Tricoli[30], I.M. Trigger[160a], S. Trincaz-Duvoid[79], M.F. Tripiana[12], N. Triplett[25], W. Trischuk[159], B. Trocmé[55], C. Troncon[90a], M. Trottier-McDonald[143], M. Trovatelli[135a,135b], P. True[89], M. Trzebinski[39], A. Trzupek[39], C. Tsarouchas[30], J.C-L. Tseng[119], P.V. Tsiareshka[91], D. Tsionou[137], G. Tsipolitis[10], N. Tsirintanis[9], S. Tsiskaridze[12], V. Tsiskaridze[48], E.G. Tskhadadze[51a], I.I. Tsukerman[96], V. Tsulaia[15], S. Tsuno[65], D. Tsybychev[149], A. Tudorache[26a], V. Tudorache[26a], A.N. Tuna[121], S.A. Tupputi[20a,20b], S. Turchikhin[98,af], D. Turecek[127], I. Turk Cakir[4d], R. Turra[90a,90b], P.M. Tuts[35], A. Tykhonov[49], M. Tylmad[147a,147b], M. Tyndel[130], K. Uchida[21], I. Ueda[156], R. Ueno[29], M. Ughetto[84], M. Ugland[14], M. Uhlenbrock[21], F. Ukegawa[161], G. Unal[30], A. Undrus[25], G. Unel[164], F.C. Ungaro[48], Y. Unno[65], D. Urbaniec[35], P. Urquijo[87], G. Usai[8], A. Usanova[61], L. Vacavant[84], V. Vacek[127], B. Vachon[86], N. Valencic[106], S. Valentinetti[20a,20b], A. Valero[168], L. Valery[34], S. Valkar[128], E. Valladolid Gallego[168], S. Vallecorsa[49], J.A. Valls Ferrer[168], W. Van Den Wollenberg[106], P.C. Van Der Deijl[106], R. van der Geer[106], H. van der Graaf[106], R. Van Der Leeuw[106], D. van der Ster[30], N. van Eldik[30], P. van Gemmeren[6], J. Van Nieuwkoop[143], I. van Vulpen[106], M.C. van Woerden[30], M. Vanadia[133a,133b], W. Vandelli[30], R. Vanguri[121], A. Vaniachine[6], P. Vankov[42], F. Vannucci[79], G. Vardanyan[178], R. Vari[133a], E.W. Varnes[7], T. Varol[85], D. Varouchas[79], A. Vartapetian[8], K.E. Varvell[151], F. Vazeille[34], T. Vazquez Schroeder[54], J. Veatch[7], F. Veloso[125a,125c], S. Veneziano[133a], A. Ventura[72a,72b], D. Ventura[85], M. Venturi[170], N. Venturi[159], A. Venturini[23], V. Vercesi[120a], M. Verducci[133a,133b], W. Verkerke[106], J.C. Vermeulen[106], A. Vest[44], M.C. Vetterli[143,d], O. Viazlo[80], I. Vichou[166], T. Vickey[146c,ai], O.E. Vickey Boeriu[146c], G.H.A. Viehhauser[119], S. Viel[169], R. Vigne[30], M. Villa[20a,20b], M. Villaplana Perez[90a,90b], E. Vilucchi[47], M.G. Vincter[29], V.B. Vinogradov[64], J. Virzi[15], I. Vivarelli[150], F. Vives Vaque[3], S. Vlachos[10], D. Vladoiu[99], M. Vlasak[127], A. Vogel[21], M. Vogel[32a], P. Vokac[127], G. Volpi[123a,123b], M. Volpi[87], H. von der Schmitt[100], H. von Radziewski[48], E. von Toerne[21], V. Vorobel[128], K. Vorobev[97], M. Vos[168], R. Voss[30],

JHEP01(2015)020

J.H. Vossebeld[73], N. Vranjes[137], M. Vranjes Milosavljevic[106], V. Vrba[126], M. Vreeswijk[106], T. Vu Anh[48], R. Vuillermet[30], I. Vukotic[31], Z. Vykydal[127], P. Wagner[21], W. Wagner[176], H. Wahlberg[70], S. Wahrmund[44], J. Wakabayashi[102], J. Walder[71], R. Walker[99], W. Walkowiak[142], R. Wall[177], P. Waller[73], B. Walsh[177], C. Wang[152,aj], C. Wang[45], F. Wang[174], H. Wang[15], H. Wang[40], J. Wang[42], J. Wang[33a], K. Wang[86], R. Wang[104], S.M. Wang[152], T. Wang[21], X. Wang[177], C. Wanotayaroj[115], A. Warburton[86], C.P. Ward[28], D.R. Wardrope[77], M. Warsinsky[48], A. Washbrook[46], C. Wasicki[42], P.M. Watkins[18], A.T. Watson[18], I.J. Watson[151], M.F. Watson[18], G. Watts[139], S. Watts[83], B.M. Waugh[77], S. Webb[83], M.S. Weber[17], S.W. Weber[175], J.S. Webster[31], A.R. Weidberg[119], P. Weigell[100], B. Weinert[60], J. Weingarten[54], C. Weiser[48], H. Weits[106], P.S. Wells[30], T. Wenaus[25], D. Wendland[16], Z. Weng[152,ae], T. Wengler[30], S. Wenig[30], N. Wermes[21], M. Werner[48], P. Werner[30], M. Wessels[58a], J. Wetter[162], K. Whalen[29], A. White[8], M.J. White[1], R. White[32b], S. White[123a,123b], D. Whiteson[164], D. Wicke[176], F.J. Wickens[130], W. Wiedenmann[174], M. Wielers[130], P. Wienemann[21], C. Wiglesworth[36], L.A.M. Wiik-Fuchs[21], P.A. Wijeratne[77], A. Wildauer[100], M.A. Wildt[42,ak], H.G. Wilkens[30], J.Z. Will[99], H.H. Williams[121], S. Williams[28], C. Willis[89], S. Willocq[85], A. Wilson[88], J.A. Wilson[18], I. Wingerter-Seez[5], F. Winklmeier[115], B.T. Winter[21], M. Wittgen[144], T. Wittig[43], J. Wittkowski[99], S.J. Wollstadt[82], M.W. Wolter[39], H. Wolters[125a,125c], B.K. Wosiek[39], J. Wotschack[30], M.J. Woudstra[83], K.W. Wozniak[39], M. Wright[53], M. Wu[55], S.L. Wu[174], X. Wu[49], Y. Wu[88], E. Wulf[35], T.R. Wyatt[83], B.M. Wynne[46], S. Xella[36], M. Xiao[137], D. Xu[33a], L. Xu[33b,al], B. Yabsley[151], S. Yacoob[146b,am], M. Yamada[65], H. Yamaguchi[156], Y. Yamaguchi[117], A. Yamamoto[65], K. Yamamoto[63], S. Yamamoto[156], T. Yamamura[156], T. Yamanaka[156], K. Yamauchi[102], Y. Yamazaki[66], Z. Yan[22], H. Yang[33e], H. Yang[174], U.K. Yang[83], Y. Yang[110], S. Yanush[92], L. Yao[33a], W-M. Yao[15], Y. Yasu[65], E. Yatsenko[42], K.H. Yau Wong[21], J. Ye[40], S. Ye[25], A.L. Yen[57], E. Yildirim[42], M. Yilmaz[4b], R. Yoosoofmiya[124], K. Yorita[172], R. Yoshida[6], K. Yoshihara[156], C. Young[144], C.J.S. Young[30], S. Youssef[22], D.R. Yu[15], J. Yu[8], J.M. Yu[88], J. Yu[113], L. Yuan[66], A. Yurkewicz[107], I. Yusuff[28,an], B. Zabinski[39], R. Zaidan[62], A.M. Zaitsev[129,aa], A. Zaman[149], S. Zambito[23], L. Zanello[133a,133b], D. Zanzi[100], C. Zeitnitz[176], M. Zeman[127], A. Zemla[38a], K. Zengel[23], O. Zenin[129], T. Ženiš[145a], D. Zerwas[116], G. Zevi della Porta[57], D. Zhang[88], F. Zhang[174], H. Zhang[89], J. Zhang[6], L. Zhang[152], X. Zhang[33d], Z. Zhang[116], Z. Zhao[33b], A. Zhemchugov[64], J. Zhong[119], B. Zhou[88], L. Zhou[35], N. Zhou[164], C.G. Zhu[33d], H. Zhu[33a], J. Zhu[88], Y. Zhu[33b], X. Zhuang[33a], K. Zhukov[95], A. Zibell[175], D. Zieminska[60], N.I. Zimine[64], C. Zimmermann[82], R. Zimmermann[21], S. Zimmermann[21], S. Zimmermann[48], Z. Zinonos[54], M. Ziolkowski[142], G. Zobernig[174], A. Zoccoli[20a,20b], M. zur Nedden[16], G. Zurzolo[103a,103b], V. Zutshi[107], L. Zwalinski[30]

[1] Department of Physics, University of Adelaide, Adelaide, Australia
[2] Physics Department, SUNY Albany, Albany NY, United States of America
[3] Department of Physics, University of Alberta, Edmonton AB, Canada
[4] [(a)] Department of Physics, Ankara University, Ankara; [(b)] Department of Physics, Gazi University, Ankara; [(c)] Division of Physics, TOBB University of Economics and Technology, Ankara; [(d)] Turkish Atomic Energy Authority, Ankara, Turkey
[5] LAPP, CNRS/IN2P3 and Université de Savoie, Annecy-le-Vieux, France
[6] High Energy Physics Division, Argonne National Laboratory, Argonne IL, United States of America
[7] Department of Physics, University of Arizona, Tucson AZ, United States of America
[8] Department of Physics, The University of Texas at Arlington, Arlington TX, United States of America
[9] Physics Department, University of Athens, Athens, Greece
[10] Physics Department, National Technical University of Athens, Zografou, Greece
[11] Institute of Physics, Azerbaijan Academy of Sciences, Baku, Azerbaijan
[12] Institut de Física d'Altes Energies and Departament de Física de la Universitat Autònoma de Barcelona, Barcelona, Spain
[13] [(a)] Institute of Physics, University of Belgrade, Belgrade; [(b)] Vinca Institute of Nuclear Sciences, University of Belgrade, Belgrade, Serbia

JHEP01(2015)020

[14] Department for Physics and Technology, University of Bergen, Bergen, Norway
[15] Physics Division, Lawrence Berkeley National Laboratory and University of California, Berkeley CA, United States of America
[16] Department of Physics, Humboldt University, Berlin, Germany
[17] Albert Einstein Center for Fundamental Physics and Laboratory for High Energy Physics, University of Bern, Bern, Switzerland
[18] School of Physics and Astronomy, University of Birmingham, Birmingham, United Kingdom
[19] [(a)] Department of Physics, Bogazici University, Istanbul; [(b)] Department of Physics, Dogus University, Istanbul; [(c)] Department of Physics Engineering, Gaziantep University, Gaziantep, Turkey
[20] [(a)] INFN Sezione di Bologna; [(b)] Dipartimento di Fisica e Astronomia, Università di Bologna, Bologna, Italy
[21] Physikalisches Institut, University of Bonn, Bonn, Germany
[22] Department of Physics, Boston University, Boston MA, United States of America
[23] Department of Physics, Brandeis University, Waltham MA, United States of America
[24] [(a)] Universidade Federal do Rio De Janeiro COPPE/EE/IF, Rio de Janeiro; [(b)] Federal University of Juiz de Fora (UFJF), Juiz de Fora; [(c)] Federal University of Sao Joao del Rei (UFSJ), Sao Joao del Rei; [(d)] Instituto de Fisica, Universidade de Sao Paulo, Sao Paulo, Brazil
[25] Physics Department, Brookhaven National Laboratory, Upton NY, United States of America
[26] [(a)] National Institute of Physics and Nuclear Engineering, Bucharest; [(b)] National Institute for Research and Development of Isotopic and Molecular Technologies, Physics Department, Cluj Napoca; [(c)] University Politehnica Bucharest, Bucharest; [(d)] West University in Timisoara, Timisoara, Romania
[27] Departamento de Física, Universidad de Buenos Aires, Buenos Aires, Argentina
[28] Cavendish Laboratory, University of Cambridge, Cambridge, United Kingdom
[29] Department of Physics, Carleton University, Ottawa ON, Canada
[30] CERN, Geneva, Switzerland
[31] Enrico Fermi Institute, University of Chicago, Chicago IL, United States of America
[32] [(a)] Departamento de Física, Pontificia Universidad Católica de Chile, Santiago; [(b)] Departamento de Física, Universidad Técnica Federico Santa María, Valparaíso, Chile
[33] [(a)] Institute of High Energy Physics, Chinese Academy of Sciences, Beijing; [(b)] Department of Modern Physics, University of Science and Technology of China, Anhui; [(c)] Department of Physics, Nanjing University, Jiangsu; [(d)] School of Physics, Shandong University, Shandong; [(e)] Physics Department, Shanghai Jiao Tong University, Shanghai, China
[34] Laboratoire de Physique Corpusculaire, Clermont Université and Université Blaise Pascal and CNRS/IN2P3, Clermont-Ferrand, France
[35] Nevis Laboratory, Columbia University, Irvington NY, United States of America
[36] Niels Bohr Institute, University of Copenhagen, Kobenhavn, Denmark
[37] [(a)] INFN Gruppo Collegato di Cosenza, Laboratori Nazionali di Frascati; [(b)] Dipartimento di Fisica, Università della Calabria, Rende, Italy
[38] [(a)] AGH University of Science and Technology, Faculty of Physics and Applied Computer Science, Krakow; [(b)] Marian Smoluchowski Institute of Physics, Jagiellonian University, Krakow, Poland
[39] The Henryk Niewodniczanski Institute of Nuclear Physics, Polish Academy of Sciences, Krakow, Poland
[40] Physics Department, Southern Methodist University, Dallas TX, United States of America
[41] Physics Department, University of Texas at Dallas, Richardson TX, United States of America
[42] DESY, Hamburg and Zeuthen, Germany
[43] Institut für Experimentelle Physik IV, Technische Universität Dortmund, Dortmund, Germany
[44] Institut für Kern- und Teilchenphysik, Technische Universität Dresden, Dresden, Germany
[45] Department of Physics, Duke University, Durham NC, United States of America
[46] SUPA - School of Physics and Astronomy, University of Edinburgh, Edinburgh, United Kingdom
[47] INFN Laboratori Nazionali di Frascati, Frascati, Italy

JHEP01(2015)020

[48] Fakultät für Mathematik und Physik, Albert-Ludwigs-Universität, Freiburg, Germany
[49] Section de Physique, Université de Genève, Geneva, Switzerland
[50] [(a)] INFN Sezione di Genova; [(b)] Dipartimento di Fisica, Università di Genova, Genova, Italy
[51] [(a)] E. Andronikashvili Institute of Physics, Iv. Javakhishvili Tbilisi State University, Tbilisi; [(b)] High Energy Physics Institute, Tbilisi State University, Tbilisi, Georgia
[52] II Physikalisches Institut, Justus-Liebig-Universität Giessen, Giessen, Germany
[53] SUPA - School of Physics and Astronomy, University of Glasgow, Glasgow, United Kingdom
[54] II Physikalisches Institut, Georg-August-Universität, Göttingen, Germany
[55] Laboratoire de Physique Subatomique et de Cosmologie, Université Grenoble-Alpes, CNRS/IN2P3, Grenoble, France
[56] Department of Physics, Hampton University, Hampton VA, United States of America
[57] Laboratory for Particle Physics and Cosmology, Harvard University, Cambridge MA, United States of America
[58] [(a)] Kirchhoff-Institut für Physik, Ruprecht-Karls-Universität Heidelberg, Heidelberg; [(b)] Physikalisches Institut, Ruprecht-Karls-Universität Heidelberg, Heidelberg; [(c)] ZITI Institut für technische Informatik, Ruprecht-Karls-Universität Heidelberg, Mannheim, Germany
[59] Faculty of Applied Information Science, Hiroshima Institute of Technology, Hiroshima, Japan
[60] Department of Physics, Indiana University, Bloomington IN, United States of America
[61] Institut für Astro- und Teilchenphysik, Leopold-Franzens-Universität, Innsbruck, Austria
[62] University of Iowa, Iowa City IA, United States of America
[63] Department of Physics and Astronomy, Iowa State University, Ames IA, United States of America
[64] Joint Institute for Nuclear Research, JINR Dubna, Dubna, Russia
[65] KEK, High Energy Accelerator Research Organization, Tsukuba, Japan
[66] Graduate School of Science, Kobe University, Kobe, Japan
[67] Faculty of Science, Kyoto University, Kyoto, Japan
[68] Kyoto University of Education, Kyoto, Japan
[69] Department of Physics, Kyushu University, Fukuoka, Japan
[70] Instituto de Física La Plata, Universidad Nacional de La Plata and CONICET, La Plata, Argentina
[71] Physics Department, Lancaster University, Lancaster, United Kingdom
[72] [(a)] INFN Sezione di Lecce; [(b)] Dipartimento di Matematica e Fisica, Università del Salento, Lecce, Italy
[73] Oliver Lodge Laboratory, University of Liverpool, Liverpool, United Kingdom
[74] Department of Physics, Jožef Stefan Institute and University of Ljubljana, Ljubljana, Slovenia
[75] School of Physics and Astronomy, Queen Mary University of London, London, United Kingdom
[76] Department of Physics, Royal Holloway University of London, Surrey, United Kingdom
[77] Department of Physics and Astronomy, University College London, London, United Kingdom
[78] Louisiana Tech University, Ruston LA, United States of America
[79] Laboratoire de Physique Nucléaire et de Hautes Energies, UPMC and Université Paris-Diderot and CNRS/IN2P3, Paris, France
[80] Fysiska institutionen, Lunds universitet, Lund, Sweden
[81] Departamento de Fisica Teorica C-15, Universidad Autonoma de Madrid, Madrid, Spain
[82] Institut für Physik, Universität Mainz, Mainz, Germany
[83] School of Physics and Astronomy, University of Manchester, Manchester, United Kingdom
[84] CPPM, Aix-Marseille Université and CNRS/IN2P3, Marseille, France
[85] Department of Physics, University of Massachusetts, Amherst MA, United States of America
[86] Department of Physics, McGill University, Montreal QC, Canada
[87] School of Physics, University of Melbourne, Victoria, Australia
[88] Department of Physics, The University of Michigan, Ann Arbor MI, United States of America
[89] Department of Physics and Astronomy, Michigan State University, East Lansing MI, United States of America
[90] [(a)] INFN Sezione di Milano; [(b)] Dipartimento di Fisica, Università di Milano, Milano, Italy
[91] B.I. Stepanov Institute of Physics, National Academy of Sciences of Belarus, Minsk, Republic of Belarus

JHEP01(2015)020

[92] National Scientific and Educational Centre for Particle and High Energy Physics, Minsk, Republic of Belarus
[93] Department of Physics, Massachusetts Institute of Technology, Cambridge MA, United States of America
[94] Group of Particle Physics, University of Montreal, Montreal QC, Canada
[95] P.N. Lebedev Institute of Physics, Academy of Sciences, Moscow, Russia
[96] Institute for Theoretical and Experimental Physics (ITEP), Moscow, Russia
[97] Moscow Engineering and Physics Institute (MEPhI), Moscow, Russia
[98] D.V.Skobeltsyn Institute of Nuclear Physics, M.V.Lomonosov Moscow State University, Moscow, Russia
[99] Fakultät für Physik, Ludwig-Maximilians-Universität München, München, Germany
[100] Max-Planck-Institut für Physik (Werner-Heisenberg-Institut), München, Germany
[101] Nagasaki Institute of Applied Science, Nagasaki, Japan
[102] Graduate School of Science and Kobayashi-Maskawa Institute, Nagoya University, Nagoya, Japan
[103] [(a)] INFN Sezione di Napoli; [(b)] Dipartimento di Fisica, Università di Napoli, Napoli, Italy
[104] Department of Physics and Astronomy, University of New Mexico, Albuquerque NM, United States of America
[105] Institute for Mathematics, Astrophysics and Particle Physics, Radboud University Nijmegen/Nikhef, Nijmegen, Netherlands
[106] Nikhef National Institute for Subatomic Physics and University of Amsterdam, Amsterdam, Netherlands
[107] Department of Physics, Northern Illinois University, DeKalb IL, United States of America
[108] Budker Institute of Nuclear Physics, SB RAS, Novosibirsk, Russia
[109] Department of Physics, New York University, New York NY, United States of America
[110] Ohio State University, Columbus OH, United States of America
[111] Faculty of Science, Okayama University, Okayama, Japan
[112] Homer L. Dodge Department of Physics and Astronomy, University of Oklahoma, Norman OK, United States of America
[113] Department of Physics, Oklahoma State University, Stillwater OK, United States of America
[114] Palacký University, RCPTM, Olomouc, Czech Republic
[115] Center for High Energy Physics, University of Oregon, Eugene OR, United States of America
[116] LAL, Université Paris-Sud and CNRS/IN2P3, Orsay, France
[117] Graduate School of Science, Osaka University, Osaka, Japan
[118] Department of Physics, University of Oslo, Oslo, Norway
[119] Department of Physics, Oxford University, Oxford, United Kingdom
[120] [(a)] INFN Sezione di Pavia; [(b)] Dipartimento di Fisica, Università di Pavia, Pavia, Italy
[121] Department of Physics, University of Pennsylvania, Philadelphia PA, United States of America
[122] Petersburg Nuclear Physics Institute, Gatchina, Russia
[123] [(a)] INFN Sezione di Pisa; [(b)] Dipartimento di Fisica E. Fermi, Università di Pisa, Pisa, Italy
[124] Department of Physics and Astronomy, University of Pittsburgh, Pittsburgh PA, United States of America
[125] [(a)] Laboratorio de Instrumentacao e Fisica Experimental de Particulas - LIP, Lisboa; [(b)] Faculdade de Ciências, Universidade de Lisboa, Lisboa; [(c)] Department of Physics, University of Coimbra, Coimbra; [(d)] Centro de Física Nuclear da Universidade de Lisboa, Lisboa; [(e)] Departamento de Fisica, Universidade do Minho, Braga; [(f)] Departamento de Fisica Teorica y del Cosmos and CAFPE, Universidad de Granada, Granada (Spain); [(g)] Dep Fisica and CEFITEC of Faculdade de Ciencias e Tecnologia, Universidade Nova de Lisboa, Caparica, Portugal
[126] Institute of Physics, Academy of Sciences of the Czech Republic, Praha, Czech Republic
[127] Czech Technical University in Prague, Praha, Czech Republic
[128] Faculty of Mathematics and Physics, Charles University in Prague, Praha, Czech Republic
[129] State Research Center Institute for High Energy Physics, Protvino, Russia
[130] Particle Physics Department, Rutherford Appleton Laboratory, Didcot, United Kingdom

JHEP01(2015)020

[131] Physics Department, University of Regina, Regina SK, Canada
[132] Ritsumeikan University, Kusatsu, Shiga, Japan
[133] [(a)] INFN Sezione di Roma; [(b)] Dipartimento di Fisica, Sapienza Università di Roma, Roma, Italy
[134] [(a)] INFN Sezione di Roma Tor Vergata; [(b)] Dipartimento di Fisica, Università di Roma Tor Vergata, Roma, Italy
[135] [(a)] INFN Sezione di Roma Tre; [(b)] Dipartimento di Matematica e Fisica, Università Roma Tre, Roma, Italy
[136] [(a)] Faculté des Sciences Ain Chock, Réseau Universitaire de Physique des Hautes Energies - Université Hassan II, Casablanca; [(b)] Centre National de l'Energie des Sciences Techniques Nucleaires, Rabat; [(c)] Faculté des Sciences Semlalia, Université Cadi Ayyad, LPHEA-Marrakech; [(d)] Faculté des Sciences, Université Mohamed Premier and LPTPM, Oujda; [(e)] Faculté des sciences, Université Mohammed V-Agdal, Rabat, Morocco
[137] DSM/IRFU (Institut de Recherches sur les Lois Fondamentales de l'Univers), CEA Saclay (Commissariat à l'Energie Atomique et aux Energies Alternatives), Gif-sur-Yvette, France
[138] Santa Cruz Institute for Particle Physics, University of California Santa Cruz, Santa Cruz CA, United States of America
[139] Department of Physics, University of Washington, Seattle WA, United States of America
[140] Department of Physics and Astronomy, University of Sheffield, Sheffield, United Kingdom
[141] Department of Physics, Shinshu University, Nagano, Japan
[142] Fachbereich Physik, Universität Siegen, Siegen, Germany
[143] Department of Physics, Simon Fraser University, Burnaby BC, Canada
[144] SLAC National Accelerator Laboratory, Stanford CA, United States of America
[145] [(a)] Faculty of Mathematics, Physics & Informatics, Comenius University, Bratislava; [(b)] Department of Subnuclear Physics, Institute of Experimental Physics of the Slovak Academy of Sciences, Kosice, Slovak Republic
[146] [(a)] Department of Physics, University of Cape Town, Cape Town; [(b)] Department of Physics, University of Johannesburg, Johannesburg; [(c)] School of Physics, University of the Witwatersrand, Johannesburg, South Africa
[147] [(a)] Department of Physics, Stockholm University; [(b)] The Oskar Klein Centre, Stockholm, Sweden
[148] Physics Department, Royal Institute of Technology, Stockholm, Sweden
[149] Departments of Physics & Astronomy and Chemistry, Stony Brook University, Stony Brook NY, United States of America
[150] Department of Physics and Astronomy, University of Sussex, Brighton, United Kingdom
[151] School of Physics, University of Sydney, Sydney, Australia
[152] Institute of Physics, Academia Sinica, Taipei, Taiwan
[153] Department of Physics, Technion: Israel Institute of Technology, Haifa, Israel
[154] Raymond and Beverly Sackler School of Physics and Astronomy, Tel Aviv University, Tel Aviv, Israel
[155] Department of Physics, Aristotle University of Thessaloniki, Thessaloniki, Greece
[156] International Center for Elementary Particle Physics and Department of Physics, The University of Tokyo, Tokyo, Japan
[157] Graduate School of Science and Technology, Tokyo Metropolitan University, Tokyo, Japan
[158] Department of Physics, Tokyo Institute of Technology, Tokyo, Japan
[159] Department of Physics, University of Toronto, Toronto ON, Canada
[160] [(a)] TRIUMF, Vancouver BC; [(b)] Department of Physics and Astronomy, York University, Toronto ON, Canada
[161] Faculty of Pure and Applied Sciences, University of Tsukuba, Tsukuba, Japan
[162] Department of Physics and Astronomy, Tufts University, Medford MA, United States of America
[163] Centro de Investigaciones, Universidad Antonio Narino, Bogota, Colombia
[164] Department of Physics and Astronomy, University of California Irvine, Irvine CA, United States of America
[165] [(a)] INFN Gruppo Collegato di Udine, Sezione di Trieste, Udine; [(b)] ICTP, Trieste; [(c)] Dipartimento di Chimica, Fisica e Ambiente, Università di Udine, Udine, Italy

JHEP01(2015)020

[166] Department of Physics, University of Illinois, Urbana IL, United States of America
[167] Department of Physics and Astronomy, University of Uppsala, Uppsala, Sweden
[168] Instituto de Física Corpuscular (IFIC) and Departamento de Física Atómica, Molecular y Nuclear and Departamento de Ingeniería Electrónica and Instituto de Microelectrónica de Barcelona (IMB-CNM), University of Valencia and CSIC, Valencia, Spain
[169] Department of Physics, University of British Columbia, Vancouver BC, Canada
[170] Department of Physics and Astronomy, University of Victoria, Victoria BC, Canada
[171] Department of Physics, University of Warwick, Coventry, United Kingdom
[172] Waseda University, Tokyo, Japan
[173] Department of Particle Physics, The Weizmann Institute of Science, Rehovot, Israel
[174] Department of Physics, University of Wisconsin, Madison WI, United States of America
[175] Fakultät für Physik und Astronomie, Julius-Maximilians-Universität, Würzburg, Germany
[176] Fachbereich C Physik, Bergische Universität Wuppertal, Wuppertal, Germany
[177] Department of Physics, Yale University, New Haven CT, United States of America
[178] Yerevan Physics Institute, Yerevan, Armenia
[179] Centre de Calcul de l'Institut National de Physique Nucléaire et de Physique des Particules (IN2P3), Villeurbanne, France

[a] Also at Department of Physics, King's College London, London, United Kingdom
[b] Also at Institute of Physics, Azerbaijan Academy of Sciences, Baku, Azerbaijan
[c] Also at Particle Physics Department, Rutherford Appleton Laboratory, Didcot, United Kingdom
[d] Also at TRIUMF, Vancouver BC, Canada
[e] Also at Department of Physics, California State University, Fresno CA, United States of America
[f] Also at Tomsk State University, Tomsk, Russia
[g] Also at CPPM, Aix-Marseille Université and CNRS/IN2P3, Marseille, France
[h] Also at Università di Napoli Parthenope, Napoli, Italy
[i] Also at Institute of Particle Physics (IPP), Canada
[j] Also at Department of Physics, St. Petersburg State Polytechnical University, St. Petersburg, Russia
[k] Also at Chinese University of Hong Kong, China
[l] Also at Department of Financial and Management Engineering, University of the Aegean, Chios, Greece
[m] Also at Louisiana Tech University, Ruston LA, United States of America
[n] Also at Institucio Catalana de Recerca i Estudis Avancats, ICREA, Barcelona, Spain
[o] Also at Department of Physics, The University of Texas at Austin, Austin TX, United States of America
[p] Also at Institute of Theoretical Physics, Ilia State University, Tbilisi, Georgia
[q] Also at CERN, Geneva, Switzerland
[r] Also at Ochadai Academic Production, Ochanomizu University, Tokyo, Japan
[s] Also at Manhattan College, New York NY, United States of America
[t] Also at Novosibirsk State University, Novosibirsk, Russia
[u] Also at Institute of Physics, Academia Sinica, Taipei, Taiwan
[v] Also at LAL, Université Paris-Sud and CNRS/IN2P3, Orsay, France
[w] Also at Academia Sinica Grid Computing, Institute of Physics, Academia Sinica, Taipei, Taiwan
[x] Also at Laboratoire de Physique Nucléaire et de Hautes Energies, UPMC and Université Paris-Diderot and CNRS/IN2P3, Paris, France
[y] Also at School of Physical Sciences, National Institute of Science Education and Research, Bhubaneswar, India
[z] Also at Dipartimento di Fisica, Sapienza Università di Roma, Roma, Italy
[aa] Also at Moscow Institute of Physics and Technology State University, Dolgoprudny, Russia
[ab] Also at Section de Physique, Université de Genève, Geneva, Switzerland
[ac] Also at International School for Advanced Studies (SISSA), Trieste, Italy

JHEP01(2015)020

[ad] Also at Department of Physics and Astronomy, University of South Carolina, Columbia SC, United States of America
[ae] Also at School of Physics and Engineering, Sun Yat-sen University, Guangzhou, China
[af] Also at Faculty of Physics, M.V.Lomonosov Moscow State University, Moscow, Russia
[ag] Also at Moscow Engineering and Physics Institute (MEPhI), Moscow, Russia
[ah] Also at Institute for Particle and Nuclear Physics, Wigner Research Centre for Physics, Budapest, Hungary
[ai] Also at Department of Physics, Oxford University, Oxford, United Kingdom
[aj] Also at Department of Physics, Nanjing University, Jiangsu, China
[ak] Also at Institut für Experimentalphysik, Universität Hamburg, Hamburg, Germany
[al] Also at Department of Physics, The University of Michigan, Ann Arbor MI, United States of America
[am] Also at Discipline of Physics, University of KwaZulu-Natal, Durban, South Africa
[an] Also at University of Malaya, Department of Physics, Kuala Lumpur, Malaysia
[*] Deceased

JHEP01(2015)020